



UNIVERSIDADE DE BRASÍLIA – UNB
FACULDADE DE TECNOLOGIA / FACULDADE DO GAMA
PROGRAMA DE PÓS-GRADUAÇÃO EM INTEGRIDADE DE MATERIAIS DA ENGENHARIA

DISCRETE WAVELET BASED DAMAGE LOCALIZATION ON BEAM-LIKE STRUCTURES

JOSÉ LEANDRO CARDOSO RIVERA VILA

ORIENTADOR: PROF. DR. JHON NERO VAZ GOULART
COORIENTADOR: PROF. DR. SERGIO HENRIQUE DA SILVA CARNEIRO

UNIVERSIDADE DE BRASÍLIA – UNB
FACULDADE DE TECNOLOGIA / FACULDADE DO GAMA

DISCRETE WAVELET BASED DAMAGE LOCALIZATION ON BEAM-LIKE STRUCTURES

JOSÉ LEANDRO CARDOSO RIVERA VILA

ORIENTADOR: PROF. DR. JHON NERO VAZ GOULART
COORIENTADOR: PROF. DR. SERGIO HENRIQUE DA SILVA CARNEIRO

DISSERTAÇÃO DE MESTRADO EM
INTEGRIDADE DE MATERIAIS DA ENGENHARIA

PUBLICAÇÃO: 105A/2023

BRASÍLIA/DF, NOVEMBRO DE 2023

UNIVERSIDADE DE BRASÍLIA - UNB
FACULDADE DE TECNOLOGIA / FACULDADE DO GAMA
PROGRAMA DE PÓS-GRADUAÇÃO EM INTEGRIDADE DE MATERIAIS DA ENGENHARIA

DISCRETE WAVELET BASED DAMAGE LOCALIZATION ON BEAM-LIKE STRUCTURES

JOSÉ LEANDRO CARDOSO RIVERA VILA

DISSERTAÇÃO DE Mestrado submetida ao Programa de Pós-graduação em Integridade de Materiais da Engenharia da Faculdade de Tecnologia da Universidade de Brasília, como parte dos requisitos necessários para a obtenção do grau de Mestre.

APROVADA POR:

PROF. DR. JHON NERO VAZ GOULART
ORIENTADOR(A) – UNIVERSIDADE DE BRASÍLIA

PROF. DR. SERGIO HENRIQUE DA SILVA CARNEIRO
CO-ORIENTADOR(A) – UNIVERSIDADE DE BRASÍLIA

PROF. DR. GUILHERME FERREIRA GOMES
EXAMINADOR – UNIVERSIDADE FEDERAL DE ITAJUBÁ

PROFA. DRA. MARIA ALZIRA DE ARAÚJO NUNES
EXAMINADORA – UNIVERSIDADE DE BRASÍLIA

RELATÓRIO (ATA) DE DEFESA DE DISSERTAÇÃO ASSINADO ELETRONICAMENTE PELA BANCA AVALIADORA, VIA SISTEMA ELETRÔNICO DE INFORMAÇÕES - SEI, DOCUMENTO 10441930, PROCESSO 23106.112605/2023-64.

BRASÍLIA/DF, NOVEMBRO DE 2023

FICHA CATALOGRÁFICA

VILA, JOSÉ LEANDRO CARDOSO RIVERA

Discrete Wavelet Based Damage Localization on Beam-Like Structures, 2023.
xvii, 134p. 210 x 297 mm (FGA/FT/UnB, Mestre, Integridade de Materiais da Engenharia, 2023).

Dissertação de Mestrado – Universidade de Brasília. Faculdade de Tecnologia.
Faculdade do Gama.

1. Localização de dano

2. Quantificação do dano

3. Structural Health Monitoring

4. Transformada de Wavelet

I. ENC/FT/UnB

II. Título (série)

Referência

Vila, J. L. (2023). Discrete Wavelet Based Damage Localization on Beam-Like Structures. Dissertação de mestrado em integridade de Materiais da Engenharia, Publicação 105A/2023, Programa de Pós-Graduação, Faculdade de Tecnologia, Universidade de Brasília, Brasília, DF, 134p.

Cessão de Direitos

Autor: José Leandro Cardoso Rivera Vila

Título: Discrete Wavelet Based Damage Localization on Beam-Like Structures

Grau: Mestre

Ano: 2023

É concedida à Universidade de Brasília permissão para reproduzir cópias desta dissertação de mestrado e para emprestar ou vender essas cópias somente para propósitos acadêmicos e científicos. O autor reserva outros direitos de publicação e nenhuma parte desta dissertação de mestrado pode ser reproduzida sem a autorização por escrito do autor.

jl.vila@hotmail.com

Brasília, DF – Brasil

ABSTRACT

This research investigates damage detection using Discrete Wavelet Transform (DWT) as the method of analysis on beam-like structures. This kind of structure is found in engineering applications such as bridges, aeronautic fuselages and navy ports. The study proposes indexes for damage localization (d^1 -index) and quantification (d^2 -index). The indexes analyze the displacement and mode shapes data of the beams which are treated with the DWT. Static and dynamic analysis are conducted. The displacement of the beams is obtained with finite elements method (FEM) subjected to static transversal load applied in selected nodes along its length. For the modal analysis, the first five mode shapes are considered. The investigated structures have three support types: simply supported, cantilever and double-clamped. Ahead, the influence of the boundary conditions, the wavelet type and the load application points are also investigated to guarantee the reliability of the method. The influence of the usage of a baseline function, the decomposition level, the wavelet mother type and the damage severity are also aim of the research. Damage is simulated through an elasticity module reduction of one or more elements. Results show great potential to the proposed method based on DWT, once the developed indexes are capable to detect, localize and quantify damage with precision. The approach showed accordance between the localization indexes while for quantification it is noted that the damage severity prediction curves are identified to be very similar independent of the beam and parameters involved.

Keywords: Damage, Localization, Quantification, Structural Health Monitoring, Wavelet Transform.

RESUMO

LOCALIZAÇÃO DE DANO EM ESTRUTURAS DO TIPO VIGA COM BASE EM ONDALETAS DISCRETAS

Esta pesquisa investiga a detecção de dano utilizando a Transformada Discreta de Wavelet (DWT) como método de análise em estruturas do tipo viga. Este tipo de estrutura é encontrada em aplicações da engenharia como pontes, fuselagens aeronáuticas e até portos. O estudo propõe indicadores de dano para localização (d^1 -index) e quantificação (d^2 -index). Os indicadores analisam dados de deslocamento da viga que são tratados com a DWT. Análises estáticas e dinâmicas foram conduzidas. O deslocamento das vigas é obtido através de método de elementos finitos (MEF) submetidos a cargas estáticas transversais aplicadas em pontos selecionados ao longo de seu comprimento. Para a análise Modal, os cinco primeiros modos de vibração são considerados. As estruturas investigadas possuem três tipos de suportes: bi-apoiada, cantilever e bi-engastada. Adiante, a influência das condições de contorno, dos tipos de Wavelet e do ponto de aplicação da carga também são investigados para garantir a confiabilidade do método. A influência do uso de uma função de baseline para comparação, nível de decomposição, tipo de wavelet mãe e severidade do dano também são alvos da pesquisa. O dano simulado é aplicado à estrutura através da redução local do módulo de elasticidade de um ou mais elementos. Os resultados mostram grande potencial para a metodologia proposta com base em DWT, uma vez que os indicadores propostos são capazes de identificar, localizar e quantificar o dano com precisão. A abordagem mostra concordância entre os índices de localização, enquanto para a quantificação, é notado que as curvas de previsão de severidade do dano foram identificadas muito similares independentemente do tipo de viga e parâmetros considerados.

Palavras-chave: Dano, Localização, Quantificação, Structural Health Monitoring, Transformada de Wavelet.

SUMMARY

1	Introduction.....	1
1.1	Motivation	2
1.2	Objectives.....	3
1.2.1	General Objective	3
1.2.2	Specific Objectives.....	3
1.3	Text Organization	4
2	State of the Art.....	5
2.1	Structural Health Monitoring	5
2.2	Damage Detection and Localization	6
2.2.1	Damage Detection and Localization Methods	11
2.2.1.1	MAC Method.....	11
2.2.1.2	Flexibility Change Method.....	12
2.2.1.3	Curvature Method	12
2.2.1.4	Wavelets for Damage Detection	13
2.3	Damage Quantification	19
2.4	Wavelets and SHM	23
3	Theoretical Background.....	26
3.1	Signal Processing for Damage Detection	26
3.1.1	Signal Analysis on the Frequency Domain.....	26
3.1.1.1	Fourier Transform	27
3.1.1.2	Signal Analysis on the Time-Frequency Domain	28
3.2	Wavelet Transform	29
3.2.1	Introduction to Wavelets.....	29
3.2.2	Wavelet Mother Types	34
3.2.3	CWT – Continuous Wavelet Transform.....	36
3.2.4	DWT – Discrete Wavelet Transform.....	37
3.3	Static Analysis	41
3.3.1	Deflection	41
3.3.2	Diagram of Bending Moment and Shear Stress	42
3.3.3	Equation of the Elastic Line.....	43
3.4	Modal Analysis.....	46

3.4.1	Equation of Motion in Free Vibration	47
3.4.1.1	Simply Supported Mode Shape	48
3.4.1.1	Double-Clamped Mode Shape.....	49
3.4.1.1	Cantilever Mode Shape	50
3.4.2	Numerical Model for Natural Frequencies and Mode Shapes	51
4	Methodology	56
4.1	Model Description	56
4.1.1	Static Analysis	57
4.1.2	Modal Analysis	58
4.2	Wavelet Toolbox – MATLAB®	59
4.3	Damage Indicator: d^1 -index and d^2 -index	60
5	Results of Damage Identification and Localization	63
5.1	Model Validation	63
5.2	Static Analysis	66
5.2.1	d^1 -index Damage Detection and Localization.....	66
5.2.1.1	Simply Supported Beam	66
5.2.1.2	Cantilever Beam	70
5.2.1.3	Double-Clamped Beam.....	74
5.2.2	Influence of the Several Parameters of Damage Identification and Localization 76	
5.2.2.1	Baseline and Baseline-Free.....	76
5.2.2.2	Damage Severity	79
5.2.2.3	Decomposition Level.....	80
5.2.2.4	Wavelet Mother Type.....	83
5.2.2.5	Boundary Conditions Influence on the Coefficients Near the Supports.....	85
5.2.2.6	Multiple Damaged Elements	86
5.2.2.7	Distributed Loads	88
5.3	Modal Analysis.....	89
5.3.1	Mode Shapes Analysis.....	89
5.3.1.1	Simply Supported Beam	89
5.3.1.2	Cantilever and Double-Clamped Beams.....	94
6	Results of Damage Quantification	97
6.1	d^2 -index Damage Quantification	97
6.1.1	Concentrated Loads.....	97

6.1.2	Distributed Loads	101
6.1.3	Vibration Mode Shapes	102
6.1.4	Influence of the Beam Material (Elasticity Module)	104
6.1.5	Influence of Other Parameters Investigation	105
7	Conclusion	109
	List of References	111
	Appendix A. Table of maximum deflection	117
	Appendix B. Published Papers	118

LIST OF TABLES

Table 3.1. Simply supported beam natural frequencies and mode shapes. Source: [Paz and Kim, 2019].....	49
Table 3.2. Double-clamped beam natural frequencies and mode shapes. Source: [Paz and Kim, 2019].....	50
Table 3.3. Cantilever beam natural frequencies and mode shapes. Source: [Paz and Kim, 2019].....	51
Table 5.1. Maximum deflection for the analyzed beams.....	64
Table 5.2. Natural frequency for the analyzed beams.....	65
Table 6.1. Squared wavelet coefficients variation $(d_d - d_0)^2$ for a cantilever beam with 5% damage.....	97
Table 6.2. Squared maximum wavelet coefficients variation $(d_{\max} - d_0)^2$ for a cantilever beam with 5% damage.....	98
Table 6.3. d ² -index values $(d_d - d_0)^2 / (d_{\max} - d_0)^2$ for a cantilever beam with 5% damage.....	98
Table 6.4. d ² -index values $(d_d - d_0)^2 / (d_{\max} - d_0)^2$ for a simply supported beam with 5% damage.....	99
Table 6.5. d ² -index values $(d_d - d_0)^2 / (d_{\max} - d_0)^2$ for a double-clamped beam with 5% damage.....	99
Table 6.6. Polynomial degree influence on damage quantification.....	103
Table 6.7. Elasticity Module influence on damage quantification.....	105
Table 6.8. Wavelet Mother influence on damage quantification.....	106
Table 6.9. Decomposition Level influence on damage quantification.....	106
Table 6.10. Load and Damage Localization influence on damage quantification.....	107
Table 6.11. Function Normalization influence on damage quantification.....	107
Table 6.12. Mode shapes influence on damage quantification.....	108

LIST OF FIGURES

Figure 2.1. Structural heal monitoring flowchart.....	6
Figure 2.2. Schematic setup of the steel bridge. Source: [Beskhyroun et al. 2010].....	7
Figure 2.3. Schematic of the cantilever beam with two cuts. Source: [Lopes et al. 2012]....	8
Figure 2.4. Schematic of load and damage positions on the beam. Source: [Palechor et al. 2014].....	9
Figure 2.5. Beam model with a crack utilized by Gillich et al. (2021). Source: [Gillich et al. 2021].....	10
Figure 2.6. Finite element model of the cantilever beam. Modified: [Surace and Ruotolo 1994].....	13
Figure 2.7. (a) Simply supported beam with a crack and subjected to static loading; (b) Plate containing a fissure. Source: [Wang and Deng 1999].....	14
Figure 2.8. Numerical model of the beam using SOLID45 element. Source: [Okafor and Dutta 2000].....	15
Figure 2.9. Monitoring damage analysis with damaged and undamaged DWT coefficients. Source: [Beskhyroun et al. 2010].....	16
Figure 2.10. Approximate frequency content of the discrete wavelet transform (DWT). Source: [Yun et al. 2011].....	17
Figure 2.11. Edge effect analysis with DWT approach. Source: [Gogolewski 2019].....	18
Figure 2.12. Wavelet coefficients for (a) damage localization, and (b) damage quantification, based on deflection profiles. Source: [Umesha et al. 2009].....	20
Figure 2.13. Evaluation of damage, for an interval of 5% to 50%. Source: [Viet and Golinval 2010].....	21
Figure 2.14. Crack depth. Source: [Machado et al. 2017].....	22
Figure 2.15. Damage detection comparison when utilizing (a) FFT and (b) CWT. Source: [Kankanamge et al., 2020].....	23
Figure 2.16. Non-destructive monitoring techniques. Source: [Saranya et al. 2020].....	24
Figure 2.17. Wavelet coefficients of a (a) damaged, and a (b) undamaged beam. Source: [Saranya et al. 2020].....	24
Figure 2.18. Damage detection based on pearson-based mode shape signal. Source: [Saadatmorad et al. 2022].....	25
Figure 3.1. Wavelet Transform. Source: [Misiti and Poggi, 2001].....	29

Figure 3.2. Haar wavelet function. Source: [Misiti and Poggi 2001].....	34
Figure 3.3. Wavelet-Daubechies functions. Source: [Misiti and Poggi 2001].....	35
Figure 3.4. Symlet wavelet function. Source: [Misiti and Poggi 2001].....	35
Figure 3.5. Coiflets wavelet function. Source: [Misiti and Poggi 2001].....	36
Figure 3.6. Wavelets tree for a $j = 3$ level of decomposition for (a) wavelets and (b) wavelets package. Source: [Indrusiak and Moller, 2004].....	39
Figure 3.7. Sketch of DWT transform.....	40
Figure 3.8. Deflection curve of a cantilever beam (a) beam under a punctual load; (b) deflection curve diagram. Source: [Gere, 2009].....	41
Figure 3.9. Diagrams of bending moment and shear stress of a simply supported beam. (a-d) diagram development; (e) shear stress; (f) bending moment. Source: [Beer, 2011].....	42
Figure 3.10. Elastic Line. Source: [Hibbeler, 2010].....	43
Figure 3.11. Boundary conditions for a (a) double-clamped; (b) simply supported; (c) cantilever beam. Adapted from: [Beer, 2011].....	45
Figure 3.12. (a) simply supported beam and it's (b) elements free body diagram. Source: [Paz and Kim, 2019].....	47
Figure 3.13. 2D beam nodes degrees of freedom for x, y and z-axis.....	52
Figure 4.1. Discretized beams models for the finite element method.....	56
Figure 4.2. Finite element beam discretization.....	58
Figure 4.3. "Wavemenu" window - MATLAB.....	60
Figure 4.4. d^1 -index and d^2 -index flowchart for damage detection, localization and quantification.....	62
Figure 5.1. Mode shape comparison for a (b,d,f) theoretical behavior and (a,c,e) numerical obtained results for the simply supported, the cantilever and the double-clamped beams respectively.....	65
Figure 5.2. Beam displacement for the same load applied to different nodes with a (a) undamaged and damaged beams on elements (b) 5; (c) 25; (d) 50; (e) 76; (f) 96.....	67
Figure 5.3. Beam displacement for the same load applied to different damaged elements; load was located on node (a) 5; (b) 97; (c) 25 and (d) 77.....	67
Figure 5.4. Squared difference of $(d_d-d_0)^2$ coefficients of displacement for the same load applied to different damaged elements: (a) 5; (b) 96; (c) 25 and (d) 76.....	68
Figure 5.5. d^1 -index for simply supported beam for different load application point using COIF2, considering the: (a-c) median values; (d-f) box height.....	69

Figure 5.6. Analysis of beam displacement for distinct load application node for a cantilever beam (a) with and (b) without damage.....	70
Figure 5.7. Damage localization for DWT coefficients for a cantilever beam with damage on element 25 for load location on node (a) 25 and (b) 77.....	71
Figure 5.8. Damage localization for DWT coefficients for a cantilever beam with damage on element 25 for load location on nodes (a) 5, (b) 51 and (c) 97.....	72
Figure 5.9. median d^1 -index distribution in a cantilever beam for a fixed damage and different nodes load application (a-e) damage at $e=5, 25, 50, 76$ and 96 , respectively.....	73
Figure 5.10. Analysis of beam displacement for distinct load application node for a double-clamped beam (a) with and (b) without damage.....	74
Figure 5.11. d^1 -index distribution or a damaged double-clamped beam at element 25 for load location of nodes (a) 5; (b) 25; (c) 51; (d) 77 and (e) 97.....	75
Figure 5.12. d^1 -index distribution in a double-clamped beam for a fixed damage and different nodes load application a-e) damage at $e=5, 25, 50, 76$ and 96 , respectively.....	76
Figure 5.13. Double-clamped beam non-baseline ($d_d^2/\max(d_d^2)$) damage localization analysis for damaged elements (a) E5, (b) E25, (c) E50, (d) E76, and (e) E96.....	78
Figure 5.14. Double-clamped beam damage localization for a (a) baseline-free, and a (b) baseline considered simulation.....	78
Figure 5.15. d^1 -index for a simply supported beam at different damage severity (10% up to 50%). (a-b) Median values of d^1 -index for load application at nodes 25 and 77. (c-d) Box height values of d^1 -index for load application at nodes 25 and 77.....	79
Figure 5.16. Test of influence of wavelet decomposition level “ J ” with damage on elements (a) 25 and (b) 76 for a Simply supported Beam; (c) 25 and (d) 76 for a Cantilever Beam; and (e) 25 and (f) 76 for a Double-Clamped Beam.....	81
Figure 5.17. Test of influence of wavelet decomposition level “ J ” with damage on elements (a) 5 and (b) 96 for a Simply supported Beam; (c) 5 and (d) 96 for a Cantilever Beam; and (e) 5 and (f) 96 for a Double-Clamped Beam.....	82
Figure 5.18. Wavelet mother type comparison for a simply supported beam with damage on element 25 for (a) haar, (b) coif2, (c) db5 and (d) sym8.....	83
Figure 5.19. Wavelet mother type comparison for a cantilever beam with damage on element 25 for (a) haar, (b) coif2, (c) db5 and (d) sym8.....	84
Figure 5.20. Wavelet mother type comparison for a double-clamped beam with damage on element 25 for (a) haar, (b) coif2, (c) db5 and (d) sym8.....	84

Figure 5.21. Comparison of boundary conditions influence on the d^1 -index coefficients with damage on elements (a) 5 and (b) 25 for a Simply supported; (c) 5 and (d) 25 for a Cantilever; and (e) 5 and (f) 25 for a Double-Clamped Beam.....	86
Figure 5.22. Damage localization for double-clamped beam with multiple damaged elements. (a) case 1; (b) case 2; (c) case 3; (d) case 4; (e) case5.....	87
Figure 5.23. d^1 -index damage localization for distributed loads for a simply supported beam with damage on elements (a) 25 and (b) 76; and for a cantilever at elements (c) 25 and (d) 76; and for a double-clamped beam at (e) 25 and (f) 76.....	88
Figure 5.24. Simply supported beam (a) 1 st , (b) 2 nd , (c) 3 rd , (d) 4 th , (e) 5 th , mode shapes for a damage severity range from 0% to 50%; (f) 5 th mode shape approximated peak.....	90
Figure 5.25. Simply supported beam (a) 1 st , (b) 2 nd , (c) 3 rd , (d) 4 th , (e) 5 th , mode shapes for five different damaged element locations; (f) 5 th mode shape approximated peak.....	91
Figure 5.26. Damage localization for the Simply supported beam for damaged elements (a) E5, (b) E25, (c) E50, (d) E76, (e) E96.....	92
Figure 5.27. Non-baseline damage localization for the Simply supported beam for damaged elements (a) E5, (b) E25, (c) E50, (d) E76, (e) E96.....	93
Figure 5.28. Vibration mode shapes (a and c) 1 st mode for the cantilever beam. (b and d) 1 nd mode for the double-clamped beam.....	94
Figure 5.29. Damage localization for the Cantilever beam for damaged elements (a) E5, (b) E25, (c) E50, (d) E76, (e) E96.....	95
Figure 5.30. Damage localization for the Double-Clamped beam for damaged elements (a) E5, (b) E25, (c) E50, (d) E76, (e) E96.....	96
Figure 6.1. Relationship of damage severity and d^2 -index for the (a) cantilever, (b) simply supported, and the (c) double-clamped beam, under concentrated loads.....	100
Figure 6.2. Relationship of damage severity and d^2 -index for the (a) cantilever, (b) simply supported, and the (c) double-clamped, under distributed loads.....	101
Figure 6.3. Relationship of damage severity and d^2 -index for the (a) cantilever, (b) simply supported, and the (c) double-clamped beam, from mode shapes.....	102
Figure 6.4. Damage quantification analysis over each type of load or mode shapes for the (a) cantilever, (b) simply supported, and the (c) double-clamped beam.....	104

LIST OF ABBREVIATIONS AND SYMBOLS

BIOR	Biorthogonal
COIF	Coiflets
COMAC	Coordinate Modal Assurance Criterion
CWT	Continuous Wavelet Transform
DBN	Daubechies
DCNN	Deep Convolutional Neural Network
DFT	Discrete Fourier Transform
DOF	Degree of Freedom
DWT	Discrete Wavelet Transform
FEM	Finite Element Method
FFT	Fast Fourier Transform
FT	Fourier Transform
HPF	High Pass Filter
LPF	Low Pass Filter
LSOM	Linear Second Order Matrix
MAC	Modal Assurance Criterion
MDOF	Multiple Degrees of Freedom
RFS	Relative Frequency Shift
PSD	Power Spectral Density
SHM	Structural Health Monitoring
STFT	Short Time Fourier Transform
SYM	Symlet
VTB	Engineering Vibration Toolbox
WFT	Windowed Fourier Transform
WPERI	Wavelet Package Energy Rate Index
WT	Wavelet Transform
<i>a</i>	Scale of the Wavelet
<i>A</i>	Approximation
<i>b</i>	Position of the Wavelet
<i>D</i>	Detail

d^1 -index	Damage localization indicator
d^2 -index	Damage quantification indicator
d_s	Damage Severity
E	Module of Elasticity
$\kappa(x)$	Cross-Section Curvature
f	Frequency
F	Flexibility Matrix
F_Ψ	Pseudo-Frequency of the Wavelet
I	Moment of Area
j	dilatation coefficient
J	Wavelet Decomposition Level
k	translation coefficient
K	Stiffness Matrix
M	Mass Matrix
$M_{(x)}$	Bending Moment
$P_{xx}(f)$	Energy Spectrum
ρ	Mass Density
S	Signal
t	Time Instant
T	Transpose Vector
uy	Displacement
W	Window Function
ω	Natural Frequency
x	Displacement
$x(f)$	Fourier Coefficient
ϕ	Scale Function
Φ	Mode shape of Vibration
Ω	Squared Diagonal Matrix of the natural frequencies

1 INTRODUCTION

Naturally, a beam is under the influence of many forces and stresses. Structural health monitoring (SHM) is used to assure safe operational levels. This monitoring approach is studied by Yang and Huang (2021) and Nick et al. (2021). Beams are found in many engineering applications, from aerospace structures, such as aeronautic fuselages, to civil construction, such as bridges and navy ports.

The Structural Health Monitoring is defined by Farrar and Worden (2007) as a method to observe, monitor, obtain readings, and by these readings, detect, localize, and identify the damage, so to allow a preventive maintenance. A review on this field is made by Sohn et al. (2003).

Rytter (1993) classified SHM in four stages: damage detection, damage localization, damage severity assessment and the determination of the remaining useful life-time.

The analysis is constituted mainly from three stages: data acquisition, which may be through a continuous observation of a structure in periodic intervals of time via sensors attached to the structure, data treatment, and finally the critical analysis with damage indexes.

Meanwhile, a beam is designed to operate under severe load-service regime, regardless of the static or dynamic nature of the load, that can stimulate degradation and sometimes damage. Damage is understood as a level of degradation enough to reduce the beam structural characteristics, hence failing to meet the initial design requirements. SHM exists to monitor the development of such kind of behavior.

In this regard, the Wavelet Transform (WT) technique is of great application. It consists into decoding the signal and treating so it can be easier analyzed, as does the FFT. The wavelets are composed by basic functions which describe a signal in a certain time and frequency domain, (Daubechies, 1992).

Misiti et al. (1996) defined that the Wavelet Transform is based on that any signal can be split into smaller waves, preserving the space and scale.

Wavelets have two main branches: continuous (CWT) and discrete (DWT). Besides, there are two other important concepts: mother wavelets and wavelets

discretization into details and approximations. Some wavelet mother types are daubechies, haar and coiflets. The best suited type depends on the application. Other aspect of wavelets is the discretization of a function or signal into sub-bands of frequency. During these processes, details and approximations are generated.

This research presents a numerical campaign for damage detection, localization and quantification through a discrete wavelet analysis approach, based on displacement data of beam-like structures with elastic behavior. Three types of beams were studied: simply supported, cantilever, and double-clamped. For the analyses, damage is simulated by a percentage reduction on the elasticity module of one or more elements.

Two statistical indexes are proposed for localization (d^1 -index) and quantification (d^2 -index).

1.1 Motivation

Beam-like structures are present on a daily basis on our lives. One must assure its operational safety. A great part of the industry is heavily invested into designing, to calculate tolerable loads and stresses, define work parameters and so on. Although its monitoring and maintenance is of equal importance. Engineers need to guarantee a safe work life for these structures.

There comes SHM, so to establish a monitoring approach to enable predictive and preventive maintenance on these structures and contribute to the safety of the users.

On this field, there are great authors such as Farrar and Worden (2007) and Katunin et al. (2021) whom utilizes the discrete wavelet transform (DWT) along the SHM to develop methods to analyze the data with damage indexes. The DWT stands out from other methods for its ability to describe a signal at the time-frequency domain.

SHM is constituted of four levels: detection, localization, quantification and the determination of the remaining useful life of the structure (Rytter, 1993). In most papers, analysis is presented up to the second level.

This research aims up to the third level.

1.2 Objectives

1.2.1 General Objective

Develop a method for damage detection, localization and quantification with a Discrete Wavelet Transform based on both Static and Modal signals on beam-like structures with elastic behavior.

This approach deals with some parameters which might influence results. This is clarified on the specific objectives section.

1.2.2 Specific Objectives

The following specific objectives can be cited:

- a. damage detection and localization of undamaged elements.
- b. damage quantification of undamaged elements.
- c. investigation of the influence of variables which might influence damage detection, localization and quantification:
 - i. Location of the Load application;
 - ii. Load type (punctual or distributed);
 - iii. Damage element Location;
 - iv. Beam's boundary conditions, regarding the type of supports;
 - v. DWT Level of decomposition;
 - vi. Influence of the Mode shapes for damage detection and localization;
 - vii. Usage of Baseline function or not;
 - viii. Damage severity;
 - ix. Mother Wavelet type;
 - x. The polynomial degree of the quantification function;

1.3 Text Organization

The thesis is composed of six chapters.

Chapter 1 introduces the proposed research theme, as well as some important authors on the field. It also presents the motivation for the study and the objectives.

Chapter 2 presents a review on the state of the art of the theme.

Chapter 3 establishes the necessary theoretical background needed to develop the proposed approach utilized for the numerical campaign, and proposes the two statistical damage indexes for localization (d^1 -index) and quantification (d^2 -index), further described on chapter 4.

Chapter 5 covers the results for d^1 -index, read localization, while Chapter 6, for quantification, d^2 -index.

Chapter 7 organizes the main conclusions observed through the study, and suggests possible future continuation for the research.

2 STATE OF THE ART

This chapter presents relevant research on the field as well as some important contributions to guide the following investigations.

2.1 Structural Health Monitoring

During the last decades, a lot of research has been dedicated to systems of Structure Health Monitoring (SHM), which consists of a method to detect possible changes on physical and geometric properties of a structure from data gathered at two different states: damaged and non-damaged (Grooteman, 2012).

SHM is a process for damage detection and characterization with the basic objective of monitoring structures and guarantee safety standards (Friswell and Penny, 2002). It is a periodic process, with continuous observation and measurements to analyze and determine the state of health of a structure (Farrar and Doebling, 1999).

According to Rytter (1993), a complete and advanced SHM system consists of four levels:

- I) Damage detection;
- II) Damage localization;
- III) Damage severity assessment;
- IV) Remaining useful lifetime determination;

Level I aims to determinate whether the structure is damaged or not while level II considers whether the structure is damaged and the location of the damage. At level III, the detection and location must be quantified in severity and at level IV, the remaining useful life is determined considering the damage.

Damage is understood as any alteration to the structure that may affect its current or future performance. Based on this concept, the identification of damage is made by comparing two states of the structure, a non-damaged one and a damaged structure.

Damage affects the performance of the structure and results in a loss of functionality. SHM serves as an approach to assure structural integrity to a certain engineering case. To monitor the health of structures, diverse methods of damage detection exist.

The SHM flowchart process of analysis is presented in Figure 2.1. It is constituted of three phases, the monitoring which consists in data acquisition, which may be done with sensors distributed through the structure. The second and third phases processes the obtained data and converts it through statistical tools into damage indexes capable of revealing the health state of the analyzed structure, establishing the existence of damage or not, where it is and how much, depending on the SHM levels developed.



Figure 2.1. Structural health monitoring flowchart.

2.2 Damage Detection and Localization

There are many ways to detect damage. This section reviews some methods, as well as some classic publications.

Back in 1992, Kam and Lee (1992) used a modal test data approach to identify cracks. The structure was first discretized into a set of elements and the crack was assumed to be in one of these. The damage on these elements was analyzed with a reduced stiffness model method which uses measured vibration frequencies and mode shapes as a basis for detection. The author used static deflection to gather data from the usual approach of damaged and non-damaged beams.

Further, Kam and his co-author (Kam and Lee, 1992) used a strain energy equilibrium equation to determine the size of a crack. The authors developed a method capable of detecting damage on structures with single cracks, but they resembled that with a few modifications it could serve to detect multiple cracks as well.

Five years later, Salawu (1997) made a review based on an approach to detect damage based on periodical vibration monitoring. The author measured changes of natural frequency. An advantage of this approach is that the global nature of the identified frequencies allows the measurement points to be customized. Although, methods usually require a theoretical model to be computed before physical

measurements. The author then concluded that natural frequencies alone are not enough for unique identification of the damaged region.

Beskyroun et al. (2005) went for another direction. He used a power spectral density approach to develop a damage identification algorithm, which analyzes global characteristics such as natural frequencies itself and others like, mode shapes, modal damping, modal participation factors, impulse response, and others. The algorithm is able to detect damage, predict its location and determine damage extension.

The authors then, Beskyroun et al. (2010), utilized a steel bridge as the experimental setup. The model, disposed on Figure 2.2 consists of two girders and six cross beams. Each cross beam is connected to the girders with four bolts, 2 bolts in each side. The actuator is located at the center of the upper flange of the main girder. The excitation force amplitude is 0.2 kN for both damage and non-damage beams. Frequency of excitation ranged from 0.1 to 400 Hz.

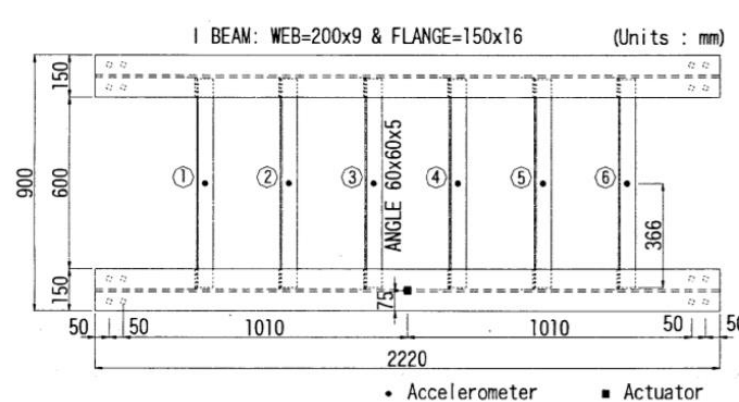


Figure 2.2. Schematic setup of the steel bridge. Source: [Beskyroun et al. 2010].

The main advantages of the Beskyroun et al. (2010) algorithm is the ability to use vibration as an excitation for continuous SHM. Ambient vibration is a natural excitation induced by nature and has the advantage of being inexpensive since no equipment is needed to excite the beam. The method also encompasses the three fields of damage detection: existence, localization and monitoring the damage increase. Also, it has shown better damage identification through PSD than vibration-based damage identification methods. As a downside the accuracy is sometimes reduced when the damage occurs at a node of the used mode shapes.

Lopes et al. (2011), used rotation fields spatial differences to calculate modal curvature fields for detection damage in plates. The study is experimentally and

numerically applied to isotropic and laminated plates. An interferometer is used to measure rotation, while the plate is analyzed with FEM. The author concludes that the Gaussian differentiation is the most adequate to calculate curvature fields. Results show that the Gaussian differentiation is the best suited, since it deals with high frequencies at local levels. The author also noted that the technique deals well with discontinuities at the edges of the structure.

Continuing his research, Lopes et al. (2012) applied his method based on interferometer data acquisition in aluminum beams. The interferometer was used to measure displacement. Cantilever and double-clamped beam boundary conditions were analyzed. Damage is reproduced with small cuts on the beam, as represented on Figure 2.3. The method was validated by a comparison of experimental and numerical results.

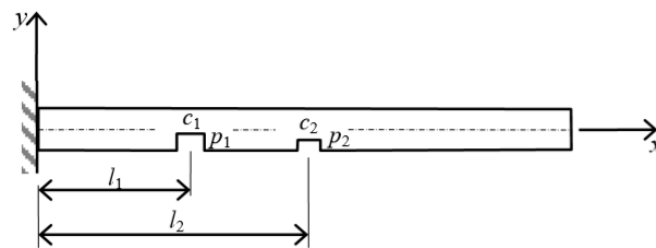


Figure 2.3. Schematic of the cantilever beam with two cuts. Source: [Lopes et al. 2012].

Lopes and his co-authors determined the bending moments and shear forces of static and modal responses for a cantilever and a double-clamped beam. Results based on static forces showed better results than a modal analysis. The bending moment indicator was found to be better suited for damage localization when it is based on rotation fields, since the experimental high frequency noise becomes dominant during the calculation of spatial derivatives.

Palechor et al. (2014) used the wavelet transform (WT) approach as a non-destructive method for damage detection in beams. This method was based on the numerical treatment of experimental data and is better explained the last section of this chapter.

At this section it is important to understand that the damage was simulated through saw cuts in the top and bottom flanges of the beam, like made by Palechor et

al. (2014), see Figure 2.4. From the WT perspective, the authors concluded that usage of Coiflets 2, Symlet 6, Biorthogonal 6.8, Daubechies 10, Daubechies 9, Symlet 3, and Symlet 7 as wave-mother were very efficient in detecting the damage. Further, the author noticed that this method was found very sensitive closed to the boundary conditions, causing discontinuities in the wavelet coefficients.

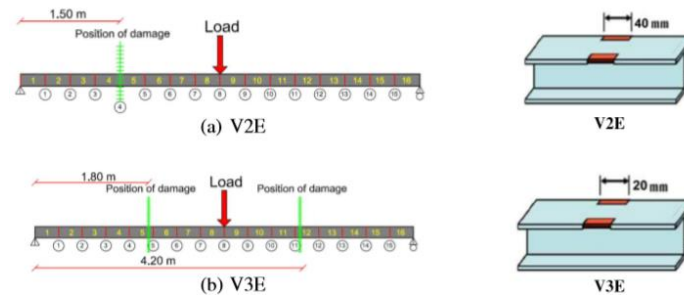


Figure 2.4. Schematic of load and damage positions on the beam. Source: [Palechor et al. 2014].

Continuing the research on structural health monitoring (SHM) and damage detection, authors have been creating and enhancing the existent methods.

In this regard, Gomes et al. (2018) united most successful and recent models and published a review. More than a hundred studies around the theme are reviewed. Gomes et al. (2018) concluded that the greatest challenge on SHM is to adjust the parameters of the chosen method to enhance efficiency in detection and identification, avoiding or, even, reducing, false positives. Some of the investigated methods were the use of mechanical vibrations, natural frequency, mode shapes, no-baseline and hybrid methods.

Yu et al. (2019), carried out a study on a deep learning-based method for damage identification on smart structures. The technique is based on deep convolutional neural networks to identify and localize damages of constructions equipped with smart sensors. The proposed technique is to extract high-level features from raw data features via a multi-layer fusion to satisfy any damage identification objective. Experimental data was obtained on a scaled building model equipped with adaptive smart isolators subjected to the seismic loads. Loads and excitations are generated with a shaking table that can generate horizontal random and seismic excitations. The DCNN-based (Deep Convolutional Neural Network) method was used

to validate the analysis of vibrations. Results showed a great generalization capacity and higher accuracy than most machine learning methods. The study aims to develop a model to predict the health condition of real smart structures.

Gillich et al. (2021) studied damage detection for multiple cracks through a simplified method based on a relative frequency shift (RFS) index. This indicator involved the square of modal curvatures of a non-damaged and deflection from damaged and non-damaged beams. The authors, with superposition calculation, observed that when cracks are too close to each other the method is not capable of detecting damage. In other words, the method limitation happens because it reads the beam segment between the two cracks as only one. Note that this distance between the cracks is infinitesimally small.

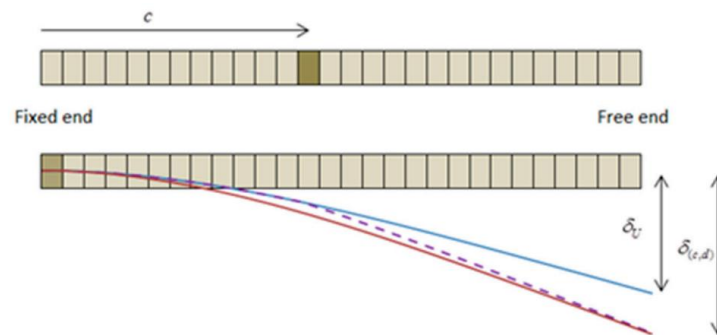


Figure 2.5. Beam model with a crack utilized by Gillich et al. (2021). Source: [Gillich et al. 2021].

More recently damage detection modes have been used for design optimization. An et al. (2022) used a model of uncertainty based on mode shapes to try to define the minimum possible number of vibration sensors in order to have a reliable method. The number of mode shapes was determined based on the sum of modal fractions. The author then developed an MKE-index (modal kinetic energy) to narrow the design. Through the campaign, An and his co-authors observed that the usage of a Gaussian process recession method, alongside with MAC – Modal Assurance Criterion, the minimum calculations were achieved.

2.2.1 Damage Detection and Localization Methods

There are many methods of damage detection. They generally permeate between static and dynamic analysis. Doebling et al. (1998) classified the dynamic methods as the most common. Dynamic methods are based in dynamic measurements, being one of the most important techniques for damage assessment in bridges. It is worth to mention: MAC (Modal Assurance Criterion), Flexibility change, Curvature, and Wavelet Transform methods. Such methods are recognized as the most promising tools for damage detection in beams (Salgado et al., 2006).

A big part on damage detection is concerned to vibration monitoring, based on the assumption that structural damage causes variation on the structure key-parameters, changing the dynamic parameters of the structure (natural frequencies, mode shapes, damping ratio). However, these alterations are often too small to measure and further identify damage.

2.2.1.1 MAC Method

In damage detection, the simplest method is the MAC, it indicates the degree of correlation between two modes and varies from 0 to 1. For a MAC equal to 0 it represents that there is no correlation while equal to 1 it represents a perfect correlation. If the displacements at node i of a set of mode shapes are identical, then the MAC value is 1 for this node. In contrast, when we have a disturbance generated by the damage, the displacements at node i will be different for the set of mode shapes. The deviation from a MAC of 1, can be interpreted as an indication of damage to the structure.

Allemang (2003) described the method equation and its development. He also defined it as a statistical indicator, with a purpose of providing a consistency measurement (degree of linearity) between estimates of a modal vector. Then, the author defined as a scalar constant which relates linearity degree between modal vectors. The complete equation is shown by Allemang (2003) in his work. Following the modal vector, two branches exist: MAC Zero, where the modal assurance criterion has a value near zero indicating that the modal vectors are not consistent, and MAC

Unity, where the modal assurance criterion has a value near unity leading to consistent modal vectors. MAC Zero fails might occur due to a non-stationary system, noises and specific modal parameters.

2.2.1.2 Flexibility Change Method

Pandey et al. (1991) proposed a method to identify and locate damage using the modal parameters of the structure. The method uses a normalized mode shape in relation to mass, stiffness and flexibility matrices. It also compares matrices from intact and damaged structures. Although, the authors stated that the use of mode shapes for damage detection has some drawbacks, as the presence of damage may not significantly influence mode shapes smaller than those usually measured. In addition, signal noise and the choice of sensors used can considerably affect the accuracy of the damage detection procedure (Kim et al., 2003).

2.2.1.3 Curvature Method

The referred technique is based on the curvature of the mode shapes is related to the flexural stiffness of the structure.

Pandey et al. (1991) showed that the curvature of the mode shapes, as the second derivative of the vibration mode, is more sensitive to damage than the vibration mode itself. The author stated that damage is detected through the highest peaks presented on a function between the modal curvature of a damaged and a non-damaged beam. Meanwhile, Farrar and Jauregui (1997) found that this method is only able to detect two or three points and that the method is unlikely to be as successful for detecting larger regions of damage.

Alvandi and Cremona (2006) formulated this curvature method with the introduction of damage or a crack in the structure is simulated with a stiffness reduction (EI) at the damaged region and hence, the magnitude of curvature in the section will increase. These alterations can be used to damage detection. Still, a stiffness reduction associated with damage leads to an increase in curvature. Further, an

estimation of the extent of damage can be obtained by measuring the amount of change in the mode shapes curvatures.

2.2.1.4 Wavelets for Damage Detection

Surace e Ruotolo (1994) were the first ones to study damage detection with Wavelet Transform (WT). The authors studied a cantilever beam subjected to dynamic loading using a simple finite element model (FEM), as illustrated in Figure 2.6.

At the investigation, a damaged cantilever beam was excited with a punctual load at its free-end. The study has been undertaken by simulating a cracked beam using FEM. Damage was simulated in the beam via thickness (h) reduction, represented in percentages, from 15% up to 45%. The approach adopted a sampling frequency of 6.67 kHz, aiming to avoid numerical errors and aliasing.

The authors, through the method, were able to detect damage at the free-end of the cantilever and detecting the alterations in the dynamic behavior at the crack appearance. Although for lower amounts of damage severity, damage was poorly detected. Crack location was seen influent on the damage localization, although to work it around, the height of the non-stationary signals was used to determine its size.

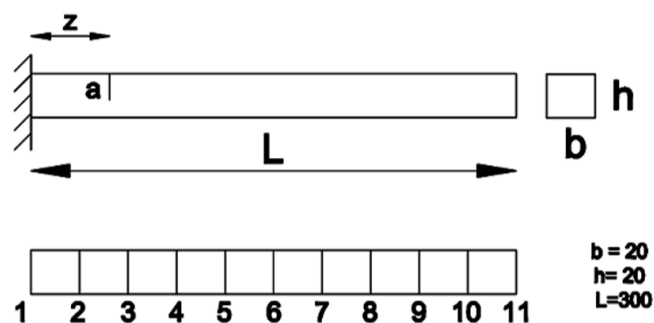


Figure 2.6. Finite element model of the cantilever beam. Modified: [Surace and Ruotolo 1994].

A few years later, Wang and Deng (1999) used WT to detect damage in a simply supported beam with a transverse crack, subjected to a static load (Figure 2.7 (a)). They also investigated damage in a plate containing a crack (Figure 2.7 (b)). The beam

displacement was obtained using the FEM method while the plate response was obtained analytically. Wand and Deng chose Haar as the Mother Wavelet due to it revealing the clearest results. The authors found that wavelet scales equal or superior to 8 were able to detect the perturbed region through a peak of the wavelet coefficient (y-axis) at the location (x-axis). Further, it was observed that damage can create structural distortions and that these can be read with the wavelet transform.

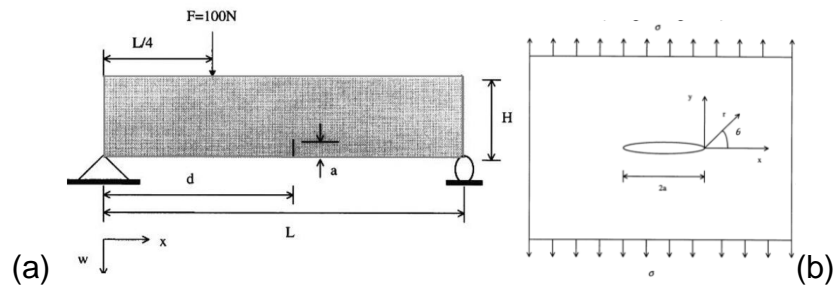


Figure 2.7. (a) Simply supported beam with a crack and subjected to static loading; (b) Plate containing a fissure. Source: [Wang and Deng 1999].

In 2000, Okafor and Dutta (2000) used ANSYS to model a cantilever aluminum beam (Figure 2.8) to obtain the first of six mode shapes for the cases with and without damage. The damage was reproduced by a reduction of the stiffness in a certain element. The damage was localized from the wavelet coefficients, obtained with Daubechies mother wavelet. A correlation between the damage severity and the magnitude of the wavelet coefficients in the damaged region was observed. The authors used both DWT and CWT and observed that the magnitude of the wavelet coefficients is increased as the damage became severe. They also noted that the increase of damage in a certain element, affects the displacement behavior in vicinity. Further, it was also noted that as damage was more severe, wavelet coefficients were also raised proportionally.

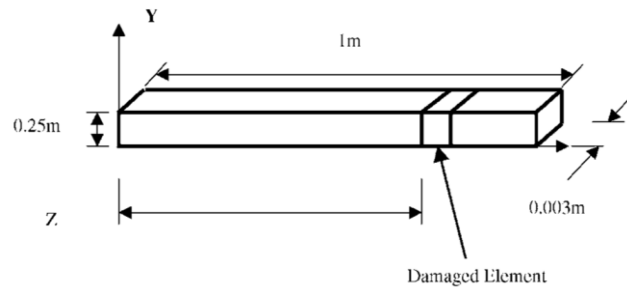


Figure 2.8. Numerical model of the beam using SOLID45 element. Source: [Okafor and Dutta 2000].

Quek et al. (2001) analyzed the WT sensitivity on beams crack detection. The research focused on boundary conditions, crack length and width, and the type of the mother wavelet (Haar and Gabor were considered). The results showed that the continuous wavelet transform is useful for beam damage detection. The authors concluded that the method could also predict the size of a crack along its longitudinal direction. They also stated the sensitivity to the detection profile as a function of the boundary condition. Quek obtained reasonable results with the Haar mother wavelet.

Han et al. (2005) proposed a damage index named as Wavelet Packet Energy Rate Index (WPERI), which works under an arbitrary time-frequency domain. The process of signal decomposition is better explained in chapter 3. Han and co-workers used the method to decompose the signal into wavelet components and then the energy is computed to indicate damage. At first, the approach is simulated on a simply supported beam. The authors were able to find a damage pattern in satisfactory agreement with the tests. Also, they investigated the first eight levels of decomposition and justified the importance of this study, claiming that the use of the lowest decomposition level, which can correctly identify damage, leads to a reduction in usage of computational power.

Estrada (2008) made a comparative study on damage detection methods in bridges, with focus on the WT. The methods were evaluated through three different points: 1D and 2D cracked beams and bridges, experimental tests and dynamic tests on bridges. The author concluded that the effectiveness of the methods depends on factors such as: the number of sensors on the damaged region, the noise level, and the length and severity of the damage.

Grabowska et al. (2008) investigated the ability of each mother wavelet, aside of a comparison of decomposition level and a central frequency analysis of each level, to identify damage. The authors adopted the biorthogonal, coiflets, daubechies, haar, meyer and symlets mother wavelets. Further, Grabowska even exposes a method to determine exactly the size of the discontinuity when both the local coefficients of wavelet transformation and the relative changes of the energy of the reflected signal from the discontinuity indicate the failure size. He also noticed that the approach has allowed the analysis of all frequency bands hidden in a system response while it is also able to examine the time–frequency domain.

Beskyroun et al. (2010) used DWT for damage detection. The author proposed a method using the difference between the DWT decomposition approximation coefficients of two signal series obtained from the operational mode shapes of the undamaged and damaged structures (Figure 2.9). The graphic shows a comparison of damage detection through DWT coefficients (y-axis) from a difference of damaged and undamaged beams. Each channel represents a beam element. Frequency of testes ranged from 1 to 800 Hz. As a negative side, the author could not quantify damage severity, however, they observed that the amplitude levels are higher for the cases of more severe damage, which can represent the damage severity to some extent.

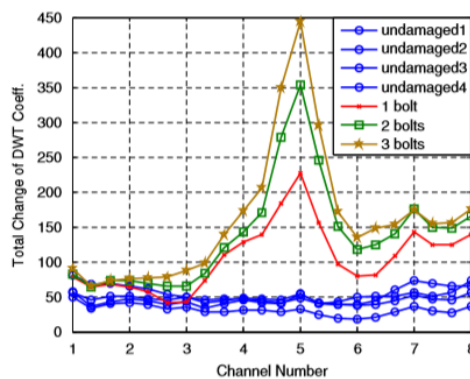


Figure 2.9. Monitoring damage analysis with damaged and undamaged DWT coefficients. Source: [Beskyroun et al. 2010].

Yun et al. (2011) used the DWT to identify damage based on data acquired from wireless smart sensors. The approach uses wavelet entropy to serve as a

signature to detect damage obtained from the sensors. The author used a method of wavelet packet decomposition to see changes which would be difficult to read on other damage detection methods. This decomposition level approach is illustrated on Figure 2.10. The referred image used a 70 Hz cut-off frequency from acceleration measurements which is then split into further sub-bands of frequencies. Yun concluded that the choice of a specific sub-band is important to increase detection reliability. Thus, selecting the sub-band correspondent to the natural frequency when calculating the total energy increases damage specificity.

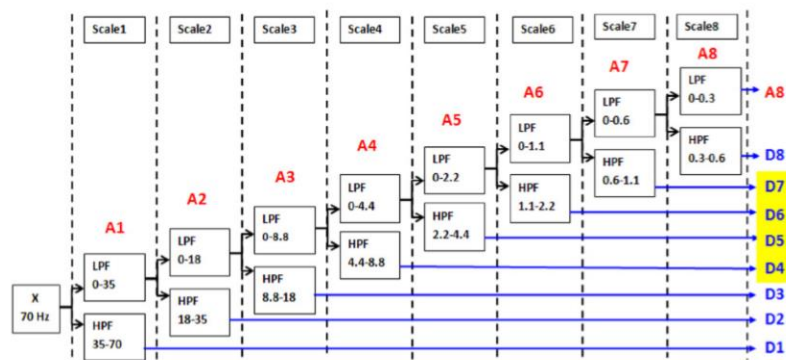


Figure 2.10. Approximate frequency content of the discrete wavelet transform (DWT). Source: [Yun et al. 2011].

Yu et al. (2016) implemented a new approach: the use of a moving load along the beam. This approach gives damage detection an interesting aspect, it proved that the method is able to determine the damage element independent of load location. The author also considered the influence of different damage severity, multiple damage, different sensor locations, load velocity and load magnitude. With the use of the CWT, the authors observed that damage severity does not influence its detection, as well as the number of damaged elements do not influence the reading of each one of these on the beam.

Gogolewski (2019) studied the edge effect. A beam can be constructed through a numerical model by nodes and elements, while each element is constituted by two nodes. The first and the last node of a beam are so called edges. A discrete wavelet

analysis which considers the full length of a beam suffers from what the author determines as the edge effect (Figure 2.11).

The author investigated the behavior of the DWT approach on some surface profiles. The decomposition level was also considered, while the author found the least influence of the effect on the fifth level. Gogolewski remarked that the size of the edge influence depends on the decomposition level. The author also noted that the length of the supports depends on the type of mother wavelet, however the size of the deformation is not equal to this size. Interestingly, the author also concluded that for a certain group of results there is a slight difference between the results obtained on both sides of a beam.

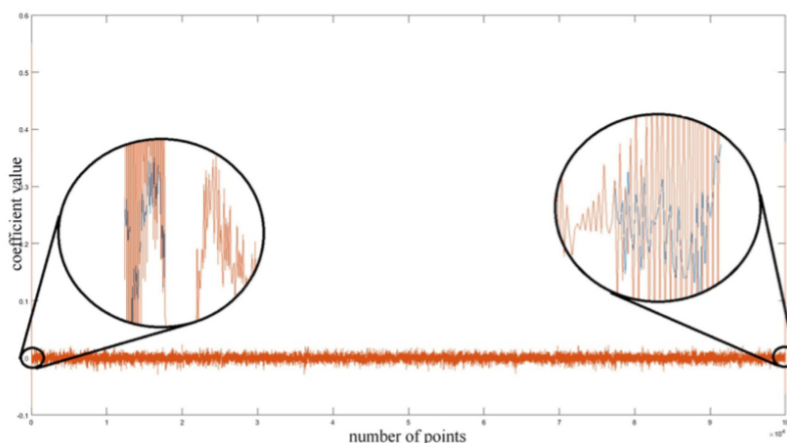


Figure 2.11. Edge effect analysis with DWT approach. Source: [Gogolewski 2019].

Katunin et al. (2021), named this effect as the boundary effect. At this time, the authors presented a new approach for the reduction of this influence, which allows an improved visualization of the resulting maps using the proposed damage identification method. As follows, Katunin and co-workers investigated damage detection with a CWT transform. They stated that the DWT has some disadvantages over the CWT such as compact support or orthogonality and the decrease of the number of available wavelets accordingly. This making the use of CWT approach for 1D and 2D boundary signal treatment more suitable for boundary effect investigation.

2.3 Damage Quantification

As important as the damage detection and localization is the quantification and the prediction of the remaining useful life of the structure (Doebbling et al., 1998). To predict the remaining work-life under safety constraints, it is crucial to quantify damage.

As said in the previous sections, SHM consists of four stages. The first three, deal with detection, localization and quantification, (Han et al., 2005, and Chaupal and Rajendran, 2023). The fourth estimates the remaining useful lifetime of the structure.

Over the decades, diverse methods have been presented to monitor the structures integrity. In this context, numerical techniques are required to identify signs of damage and, moreover, to determine the type of damage and its extent (qualification and quantification).

Han et al. (2005), developed a WPERI-index damage indicator based on a version of the DWT, called WPT (Wavelet Packet Transform). The author used it in a simply supported beam under an impact excitation to identify damage. The author aimed not only to localize but to also quantify. For this, the WPERI-index was calculated from the energy stored in a specific band of frequency subtracted from a damaged and a non-damaged beam. In other words, it is a baseline analysis. Damage was simulated through reducing the stiffness from 10% to 20% in two of four elements of the beam.

The authors, Han et al. (2005), first used FFT and WPD methods to identify damage but without success. The WPERI-index was able to localize damage in a single element. In situations where various elements are subjected to different types of damage simultaneously, the outcomes struggled to quantify the severity of the damage.

Umesha et al. (2009), proposed a method to detect location and also quantify damage in a beam by using beams response of deflection. The measurement of deflection at a specific location on the beam was conducted for different positions of a concentrated load. This recorded static deflection profile served as the input signal for wavelet analysis, specifically using the Symlet wavelet. Damage was identified

through peaks in the wavelet coefficient plots. The authors had issues with these peaks on the near-supports region.

Umesha and co-authors turned it out by using wavelet transform on the deflection measured at another point. They also conducted a study to define parameters for better damage localization and quantification, by varying the damage, location of damage, intensity of load, flexural rigidity, and length of the beam.

Finally, the authors observed that the wavelet coefficients are dependent of these parameters, so it presented through Figure 2.12 the variation of damage quantification, where d/D is the crack depth ratio between the size of the crack and the beams cross-section area, and z/L is the distance of the concentrated load by the length of the beam. Through damage quantification, the author concluded that the wavelet coefficients are directly proportional to the load's magnitude and the square length, while inversely proportional to the crack length and square value of depth.

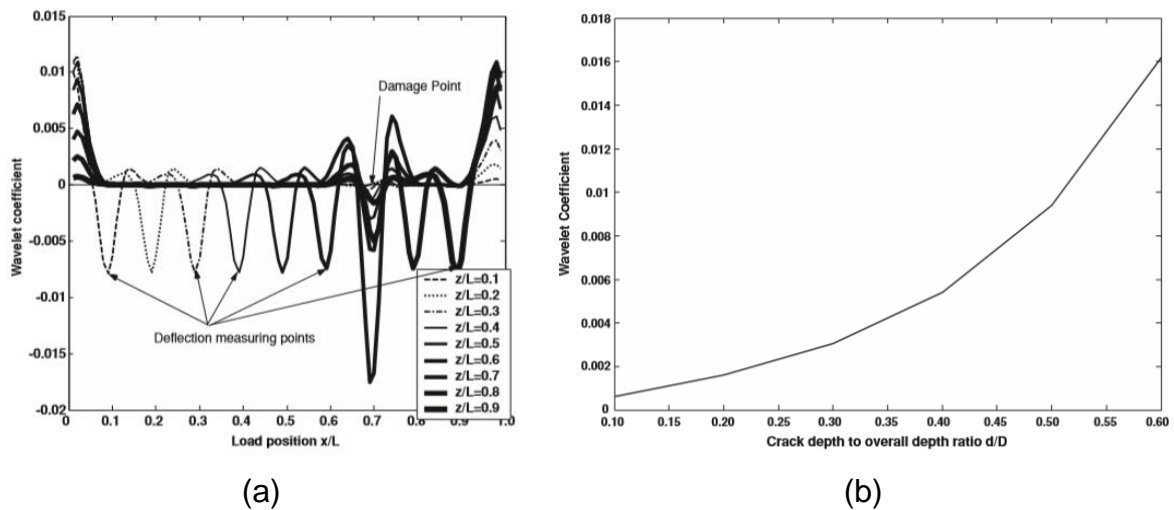


Figure 2.12. Wavelet coefficients for (a) damage localization, and (b) damage quantification, based on deflection profiles. Source: [Umesha et al. 2009].

Viet and Golinval (2010) proposed a damage study based on variations of PCA (principal components analysis) results. The deflection was measured at a particular point for various locations of a concentrated load in the beam. This static deflection profile was used as the input basis for wavelet analysis, specifically using the Symlet wavelet. In the frequency domain, linear-form structures were analysed.

Viet and co-authors objective was not only to detect the presence of damage but also to localize and evaluate it. The frequency response functions measured at different locations on the beam were considered as data for the PCA process. Sensitivities of principal components obtained from PCA to beam parameters were computed and inspected according to the location of sensors.

The variation of the PCA components from the healthy state to the damaged state indicated damage locations. Figure 2.13 presents damage quantification curve from an interval of 5% to 50% damage severity. It showed that the number of iterations needed to process the damage curve are directly proportional to the damage severity.

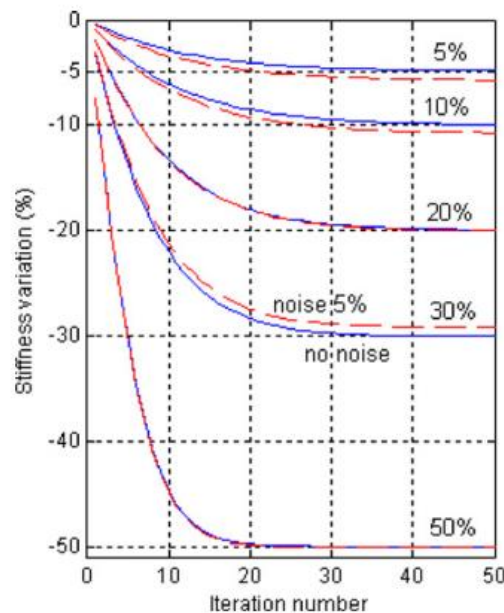


Figure 2.13. Evaluation of damage, for an interval of 5% to 50%. Source: [Viet and Golinval 2010].

Machado et al. (2017) used a spectral approach for damage quantification. The Spectral Element Method (SEM) is a numerical technique based on wave principles that is utilized for modelling structures. Additionally, the SEM has been developed to incorporate the representation of parameters as spatially correlated random fields within its formulation. The authors, presented through Figure 2.14, the results for a specific crack depth versus its flexibility. Investigated polynomial degrees were: 2, 5, 7 and 10. Θ is the crack flexibility coefficient and α is the crack depth coefficient.

The flexibility of a crack did not change significantly for every degree. For crack depth values higher than that, the divergence among curves increased as the degree of the polynomial increased. The authors furthered the investigation by correlating damage quantification and the polynomial degree, stating that the polynomial order is directly proportional to the crack's flexibility.

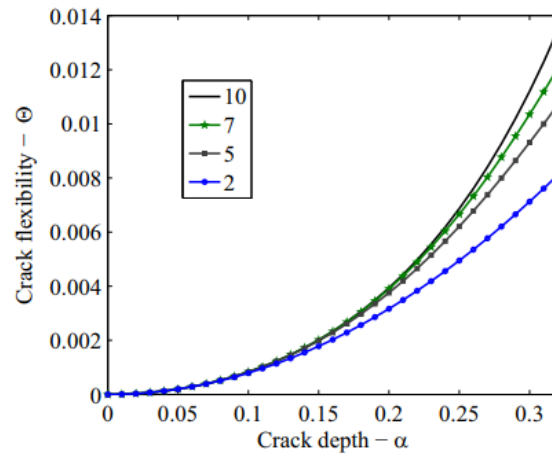


Figure 2.14. Crack depth. Source: [Machado et al. 2017].

Fallahian et al. (2022) also investigated damage through DNNs (deep neural networks), together with CSC (coupled sparse coding), the vibration data (acceleration or displacement) from a three-level frame, as a method of damage detection. This approach was employed to address challenges such as low-level damages, noisy signals (uncertainties), and structures with a large number of degrees of freedom (DOFs). The data was decomposed into Discrete Wavelet Transform (DWT) coefficients, which were then utilized to train four distinct damage models based on either Deep Neural Network (DNN) or CSC.

To simulate damage and noise, the authors (Fallahian et al., 2022) reduced the stiffness of one or a group of elements by percentages ranging from 6% to 40%. Additionally, Gaussian noise was added to the signal, constituting 20% of the noise signal ratio. In their final remarks, the authors concluded that by applying wavelet analysis, prior to training the ensemble system with vibration data, it was possible to detect even very low-level damage accurately, even in the presence of noise. Furthermore, this approach enabled accurate localization and quantification of the damage.

2.4 Wavelets and SHM

The Structural Health Monitoring is a system aimed to assure safe conditions to a certain structure. It consists into three steps: data acquisition, data treatment and analysis through a damage index, see Figure 2.1.

Some data treatment methods were presented in previous sections. The Wavelets Transform (WT) is the method of choice for this numerical campaign.

Due to its attributes, it works well alongside SHM. In comparison to other methods, it has a special advantage to monitor most of the modal aspects. This gives the approach the possibility to work with not only a part of the structure, but the structure in its entirety (Wang et al., 2019).

Comparing with the Fast Fourier Transform (FFT) and the Short Time Fourier Transform for an example, the WT stands out for being able to work on both time and frequency domains while the FFT only deals with the frequency domain, not being able to work with nonstationary signals (Sifuzzaman et al., 2009). The STFT in its turn can work on the same domains as the WT but has resolution issues with time and frequency (Amezquita-Sanchez et al., 2013).

Kankanamge et al. (2020) investigated a bridge based on acceleration data acquired with sensors along the 13.7 meters of the beam length. The author compared the WT and the FFT potential to detect damage, see Figure 2.15. The FFT was not able to define precisely the damaged region based on the frequency parameter.

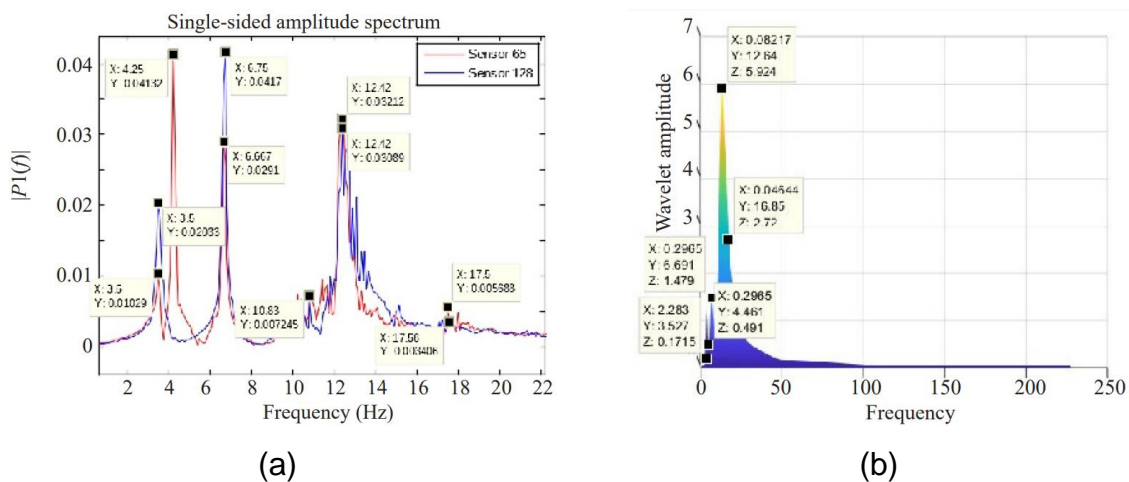


Figure 2.15. Damage detection comparison when utilizing (a) FFT and (b) CWT.

Source: [Kankanamge et al., 2020].

Kankanamge et al. (2020) published a review on the peculiarities that makes the WT so efficient to work with SHM. The author described the advantages and disadvantages of WT usage. As the positive aspects the author lists: excellent ability to work in both time and frequency domains, elimination of aliasing problems and reduced computational resources requirements. Meanwhile as a downside, it cites the mother wavelet selection and the possible spectral leakage.

Saranya et al. (2022) proposed a methodology based on WT. Data was acquired with non-destructive methods with sensors installed along the structure to monitor vibration and acoustic emission signals. The authors were able to detect damage, see Figure 2.16, but they did not develop a damage index for analysis. The damage is observed due to the wavelet coefficients value, when superior to 1 it indicates damage existence.

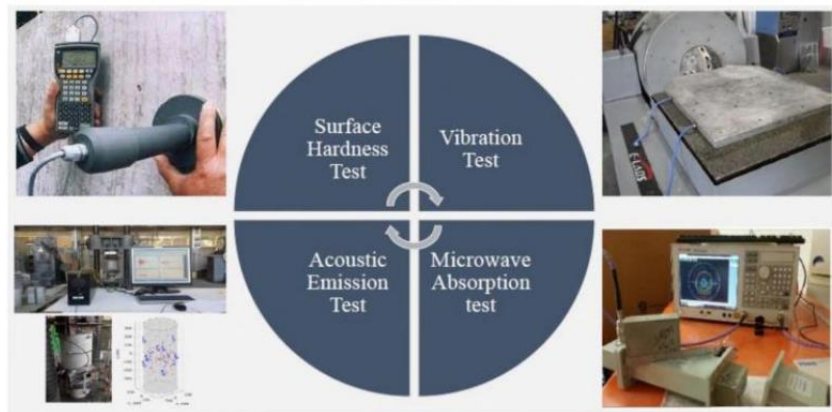


Figure 2.16. Non-destructive monitoring techniques. Source: [Saranya et al. 2020].

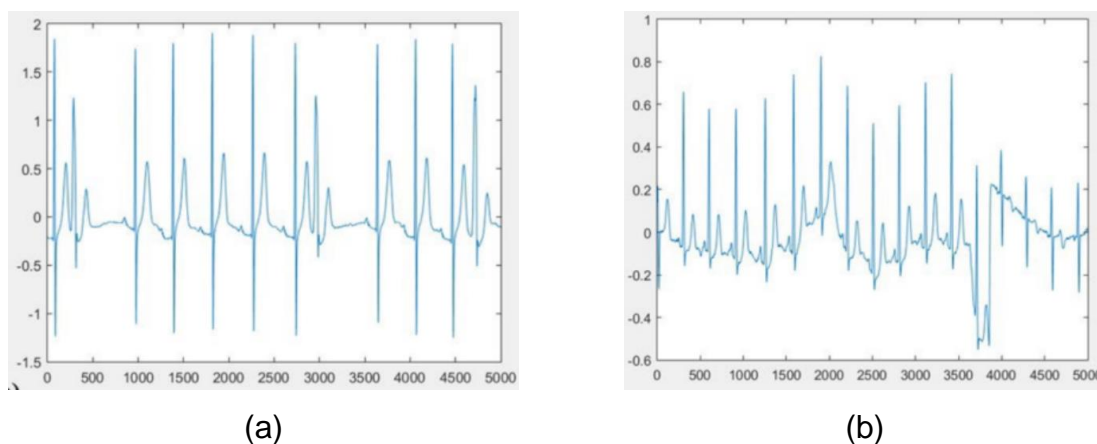


Figure 2.17. Wavelet coefficients of a (a) damaged, and a (b) undamaged beam. Source: [Saranya et al. 2020].

Santos et al. (2022) studied damage detection with discrete wavelet transform (DWT) based on mass discontinuity. A Timoshenko beam was considered. The authors used a roving mass to measure the frequency-shift curve. The method was able to determine damage along the beam span for different levels of damage and element positions.

Saadatmorad et al. (2022) investigated damage on steel beams using DWT. The wavelet analysis is based in mode shapes data. The approach involves damaged and undamaged results so a comparison may highlight the damage existence and location, Figure 2.18. The authors brought a new aspect to the field which is the suggestion to use a regression index, to be used as the original signal. It was observed that this regression index is positive specially for low severity damages, enabling great sensitivity to the approach.

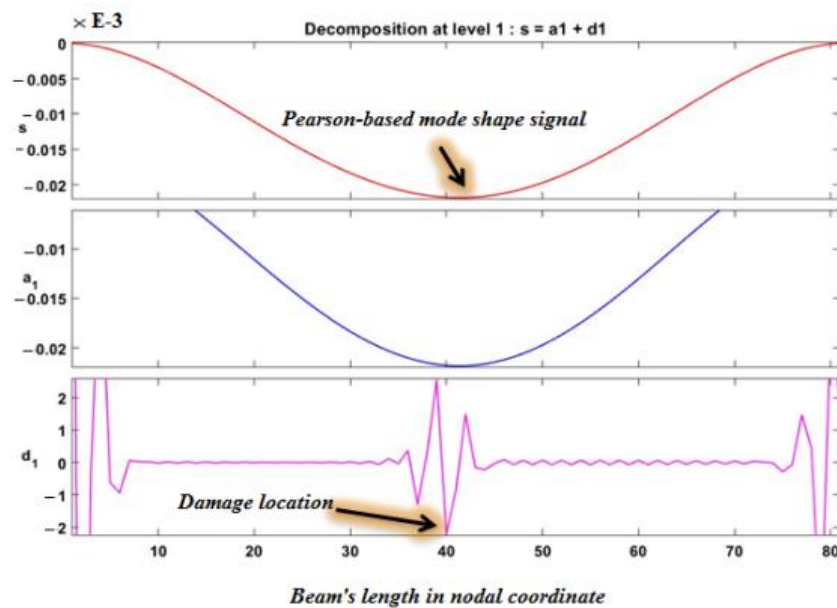


Figure 2.18. Damage detection based on pearson-based mode shape signal.

Source: [Saadatmorad et al. 2022].

3 THEORETICAL BACKGROUND

This chapter presents the theory for the methodology to be developed in Chapter 4. The approach investigates the first three levels of structural health monitoring, regarding detection, localization and quantification.

As presented in previous sections, this process starts from data acquisition, then signal processing and finally the damage index analysis.

For the numerical campaign, data for analysis were obtained through a Matlab toolbox, detailed at Chapter 4. This toolbox is able to model the beam-like structures with finite elements and calculate both displacement and mode shapes.

This data was then treated with the discrete wavelets transform (WT) and presented with a boxplot statistical tool.

3.1 Signal Processing for Damage Detection

Signal processing techniques are classified as an analysis in the time domain, frequency domain and time-frequency domain (Silva, 2015). Time-frequency domain analysis represents the signal at a certain interval of time, while simple frequency domain analysis decomposes the signal into a set of sines and cosines, in the case of Fast Fourier Transform (FFT).

To investigate these domains, the Fourier transform is commonly used to reconstruct the signal, enabling the analysis at a certain band of frequency. For damage detection the Wavelet Transform deserves a highlight due to its ability to aim a certain portion of the signal and investigate it statistically while working for both the time and frequency domain. This double localization property brings an equilibrium to the calculations on each of the domains.

3.1.1 Signal Analysis on the Frequency Domain

The wavelet transform is a robust method of signal analysis, enabling the view of both time and frequency domains, differently from the Fourier Transform for example. Fourier itself shows what frequency components appear in the function or signal. The construction of a time-frequency analysis starts from splitting the signal into windows

and then transforming it into the frequency domain through a convolution of the signal within the window.

3.1.1.1 Fourier Transform

The Fourier Transform (FT) is a useful tool that makes it possible to determine the contribution that each sine and cosine function, present in a time series (periodic). It decomposes the signal into these two functions and then the signal is reconstructed through Fourier Coefficients, which can be analyzed in a specific band of frequency.

The FT is defined by Eq. (3.1):

$$x(f) = \frac{1}{2\pi} \int_{-\infty}^{\infty} x(t)e^{-ift} dt \quad (3.1)$$

where $x(f)$ are the Fourier coefficients and the basic functions e^{ift} are pure frequency waves f , in other words, these are periodic functions with a 2π period.

Equation (3.1) has a problem regarding the decomposition of the frequencies of a signal with respect to its location in time. Gabor (1946) noticed its deficiency in non-stationary time series, which in fact is the most common case in real world. Therefore, he improved the FT to represent this type of series. His solution was to split the time series into equal intervals and then apply the FT to each of these. This method is known as the Window Fourier Transform (WFT), detailed on the next section.

For signals represented in a discrete form, the Discrete Fourier Transform (DFT) is used. Equation 3.2 presents its coefficients.

$$x(f) = \frac{1}{N} \sum_{n=0}^{N-1} x(t_n) e^{-i\frac{1}{N}f2\pi n} \quad , n \in Z \quad (3.2)$$

The probability density function FT is named characteristic function:

$$\Phi(f) = \int_{-\infty}^{\infty} p(x)e^{ifx} dx \quad (3.3)$$

The Fourier Transform of the autocorrelation function is called energy spectrum or power and relates with the second momentum (variance) on each frequency:

$$P_{xx}(f) = \int_{-\infty}^{\infty} R_{xx}(\tau) e^{-2\pi f t} dt = \lim_{\Delta f \rightarrow 0} \frac{\sigma_x^2(f, \Delta f)}{\Delta f} \quad (3.4)$$

The energy spectrum is defined by Eq. (3.5):

$$P_{xx}(f) = |x(f)|^2 \quad (3.5)$$

A usual method for calculation of the power spectrum of a discrete function consists in splitting the series into small segments and then applying the FT to each one of these segments and finally calculating the mean between the parts for each frequency. This process reduces random error on the spectrum determination (Bendat and Piersol, 1971).

3.1.1.2 Signal Analysis on the Time-Frequency Domain

Time-frequency domain approach is guided by the WFT. The difference between the FT and the WFT is that the signal is divided into small segments, while being assumed as stationary. For this purpose, a “W” window function is chosen. The width of this window shall be equal to the part of the signal where stationarity is valid (Polikar, 1994). Through WFT the presence of intermittences and transitory phenomena may be observed (or not), whereas will be totally dissimulated on the Fourier space, since $\hat{x}(f)$ coefficients refer to all the time-series domain. Fourier components have finite support, localized in frequency, but extends through the time-series domain. Thus, $\hat{x}(f)$ represent a mean value for the domain for f frequency.

The WFT is an attempt to enable a temporal analysis, using FT. Windows are applied to the signal, as given by Eq. (3.6). Thus, the WFT is basically the product of the FT and a window function. For each t and ω value, a new WFT coefficient is calculated by:

$$x(t_0, f) = \int_{-\infty}^{\infty} x(t)g(t-t_0)e^{-i2\pi ft} dt \quad (3.6)$$

where t_0 is the instant when a transform is calculated and g the window function.

Despite its large usefulness, WFT is also affected by the Heisenberg uncertainty principle (KAISER, 1994). The principle states that the exact time-frequency of a signal cannot be determined, so one cannot know which spectral components belong to a certain time interval. Polikar (1994) said that what can be determined are the time intervals in which a certain frequency band exists.

In addition, WFT has another problem: its window has a finite length. Hence, it can only analyze a portion of data, not being possible to determine the exact frequency component, but the existing frequency band. On the other hand, for a window of infinite length, the FT gives perfect frequency resolution but no time information.

3.2 Wavelet Transform

This section presents the definition, some aspects and details of the Wavelet Transform, as well as the Wavelet Mother Types. The mathematical formulation is also described, for both Continuous and Discrete Transforms.

3.2.1 Introduction to Wavelets

The Wavelet transform is a mathematical microscope. It consists of the idea that any signal can be split into a series of basic functions called “waves”. This approach allows the the compressing and dilating a window, maintaining the same functions, therefore allowing a better temporal localization on both high and low frequencies, Figure 3.1.



Figure 3.1. Wavelet Transform. Source: [Misiti and Poggi, 2001].

The basis of the Wavelets Transform (WT) are both the time and frequency domain. This double localization property brings an equilibrium to the calculations in each of the domains.

Daubechies (1992) stated that the temporal resolution gain is compensated with a loss of frequential resolution. The opposite is also valid. This relation between domains is explained by the Heisenberg uncertainty principle which determines that for any given function the exact location on time and frequency is mutually exclusive.

From another point of view, Kaiser (1994) stated that the measurements of time and frequency are incompatible once both cannot be measured simultaneously. Moreover, Vallens (1999) said that due to this acquisition problem a signal cannot be shown through a point in the space of time-frequency.

Thus, signal characteristics are properly given through coefficients associated to infinite area rectangles resulted from the product of the time considered by the scale, or frequency, being necessary a greater acquisition time to observe lower frequencies, again the inverse is also true.

As wavelets are not exact periodic functions, an alternative way to calculate scale correspondent frequencies is a periodic approximation with the Fourier Transform (FT). The frequency of the maximum approximation module of the FT is considered as a pseudo-frequency F_{ψ} of the wavelet, while the correspondent frequency to each scale is given by Eq. (3.7).

$$f_a = F_{\psi} \frac{f_s}{a} \quad (3.7)$$

The above equation is useful when the function does not have an analytical expression and then F_{ψ} cannot be determined.

A $\psi(t)$ function with an R domain is satisfied with two basic properties:

$$\int_{-\infty}^{\infty} \psi^2(t) dt = 1 \quad (3.8)$$

$$\int_{-\infty}^{\infty} \psi(t) dt = 0 \quad (3.9)$$

where Eq. (3.9) indicates that the $\psi(t)$ function has an effective support limited to a finite interval $[-T, T]$, tending towards zero outside this interval. Beyond, it has values different of zero. From Eq. (3.9), positive values are cancelled by the negatives, as in a wave. This property is known as the admissibility and is due by Eq. (3.10):

$$C_{\psi} = 2\pi \int_0^{\infty} \left| \frac{\psi(f)}{f} \right|^2 df < \infty \quad (3.10)$$

Other important wavelet properties are: orthogonality, regularity, null moments, temporal localization and frequential localization.

Orthogonality ensures fast calculation of wavelet coefficients. Two wavelet functions $u(x)$ and $g(x)$ are orthogonal if their inner product is zero:

$$\begin{aligned} \langle u(x), g(x) \rangle &= \int_a^b u(x) g^*(x) dx \\ &= 0 \quad ; \quad g^* : \text{conjugate complex of } g(x) \end{aligned} \quad (3.11)$$

Regularity is given by the number of times this function is continuously variable.

The number of null moments, M , is related with the regularity and is calculated by Eq. (3.12):

$$\int_{-\infty}^{\infty} t^m \psi(t) dt = 0 \quad m = 0, 1, \dots, M-1 \quad (3.12)$$

A wavelet with M null moments is orthogonal to $M-1$ degree polynomials (Mallat, 1998). Thus, the analysis conducted on a wavelet with M null moments ignores the regular part (polynomial) of the analyzed function to $M-1$ degree. It determines the degree of the polynomial that can be approximated. This property is used to select the most suitable mother wavelet for damage detection.

The temporal and frequential localization of a wavelet is related with its support width respectively in the time and frequency domains and indicates the ability to

localize singularities in the respective domains. In general, smooth wavelets are better to be localized on the temporal domain. Haar function for example, which is very well localized on the temporal domain, is a discontinuous function and its frequential localization is poorly defined.

The wavelets basis is generated through dilatations and translations of a single wavelet:

$$\Psi_{a,b}(t) = \frac{1}{\sqrt{a}} \Psi\left(\frac{t-b}{a}\right), \quad a, b \in \mathbb{R}, \quad a > 0 \quad (3.13)$$

where a is the scale and b is the position of the wavelet. Following, associated to each wavelet there is a scale function, $\phi(t)$, which satisfies the basic property:

$$\int_{-\infty}^{\infty} \phi(t) dt = 1 \quad (3.14)$$

the scale function also generates a basis through dilatations and translations:

$$\phi_{a,b}(t) = \frac{1}{\sqrt{a}} \phi\left(\frac{t-b}{a}\right), \quad a, b \in \mathbb{R}, \quad a > 0 \quad (3.15)$$

The objective of this scale function is to obtain coefficients which represent the weighted average of the signal for the considered scales. Meanwhile, the wavelet function obtains oscillations around this weighted average, based on the same scales.

The wavelet transform associates a signal to wavelet coefficients, as follows:

$$X(a, b) = \int_{-\infty}^{\infty} x(t) \Psi_{a,b}(t) dt \quad (3.16)$$

the inverse transform is calculated by Eq. (3.17).

$$x(t) = \frac{1}{C_{\Psi}} \int_0^{\infty} \int_{-\infty}^{\infty} \Psi x(t) X(a, b) \frac{da db}{a^2} \quad (3.17)$$

where C_{Ψ} is defined by Eq. (3.10). Following, the WT conserves the energy of the signal with Eq. (3.18).

$$\int_{-\infty}^{\infty} |x(t)|^2 dx = \frac{1}{C_{\psi}} \int_0^{\infty} \int_{-\infty}^{\infty} |X(a,b)|^2 \frac{da db}{a^2} \quad (3.18)$$

Energy conservation is calculated for a scale with Eq. (3.19). The energy of the signal is represented on the time or frequency-scale originates the wavelets spectrum.

$$\varepsilon(a) = \frac{1}{C_{\psi}} \int_{-\infty}^{\infty} |X(b,a)|^2 \frac{db}{a^2} \quad (3.19)$$

Furthermore, the generated basis with Equations (3.13) and (3.14) are continuous, with coefficients a and b varying continuously. Meaning that even if a discrete signal is being analyzed, the study is done for each possible scale and each point on the domain. These bases are not orthogonal since the information is seen in more than one coefficient and therefore generate a great amount of redundant data.

From another point of view, this redundant representation uses a much greater number of values of scale and position than the orthogonal representation. Thus, it has a greater number of coefficients. The relation of redundancy is given by the division between number of coefficients of the transform and the number of space dimensions of the transform. For a time-series the number of dimensions is the number of points of the series. Thus, an orthogonal transform must have the same number of coefficients than the original.

Finally, according to Ovanesova (2000) the main advantages of using wavelets for damage identification are:

1. Ability to perform local analysis of a signal in the domain of space or time. Thus, wavelets can reveal aspects that other signal analysis techniques cannot detect.
2. Ability to analyze the signal in any space or time interval where the function changes are fast, which causes problems for the fast Fourier transform. Fourier analysis spreads a rapid change over a small-time interval across the frequency spectrum. The WT, however, produces not only frequency information, but also time information.

3. Elimination of aliasing problems (noise), displayed by Fast Fourier Transform (FFT).

4. Offer a potential reduction in computational resources needed to process a signal transformation

3.2.2 Wavelet Mother Types

Mother wavelets are transformation functions responsible for forming the basis for the diverse transformations processes that the wavelets impose on data. A complete review on all wavelet mother types is presented by Misiti and Poggi (2001).

There are some mother types that may be best suited for a certain application. Each is characterized by its properties such as symmetry, orthogonality and compact support. In other words, mother waves are such as a toolbox of wavelet types which deals with data processing in its own manner, being handful aspect of wavelets.

The first and simplest of the wavelets is the Haar wavelet. The Haar wavelet resembles a step function. It represents the Daubechies db1 wavelet even.

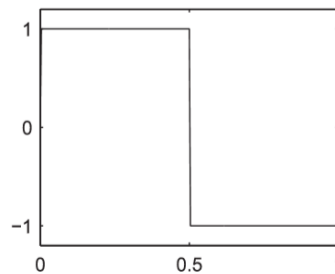


Figure 3.2. Haar wavelet function. Source: [Misiti and Poggi 2001].

Originally, Haar function is given by:

$$\psi^{Haar}(t) = \begin{cases} 1 & 0 \leq t \leq 1/2 \\ -1 & 1/2 \leq t \leq 1 \\ 0 & \text{opposite case} \end{cases} \quad (3.20)$$

It is the only wavelet mother orthogonal and with compact support which is symmetric. However, different from the others, it is not continuous. Only the first moment is null. The scale function associated to the Haar wavelet is defined by:

$$\phi^{Haar}(t) = \begin{cases} 1 & 0 \leq t < 1 \\ 0 & \text{opposite case} \end{cases} \quad (3.21)$$

Ingrid, Daubechies (1992), invented the orthonormal wavelets. This mother wavelet is divided into ten families “dbN”, where N goes from level 1 up to 10. Db1 is the same as the Haar mother wavelet.

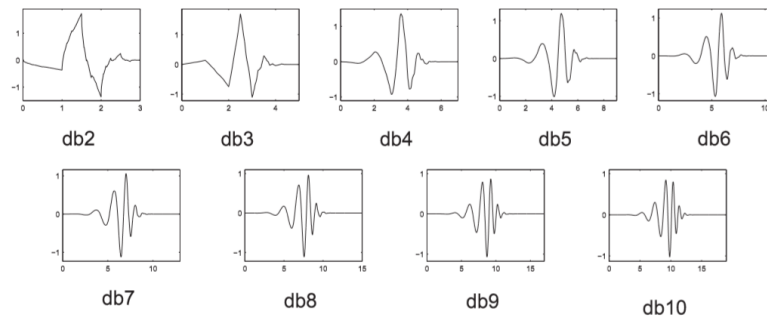


Figure 3.3. Wavelet-Daubechies functions. Source: [Misiti and Poggi 2001].

The Daubechies wavelets have a problem in the frequency domain where they have a high degree of superposition between their levels. Their main advantage is that they are orthogonal, which means that an error in the input signal does not increase with the transformation, and computational numerical stability is ensured.

Symlets have also been created by Ingrid Daubechies, but with the intention of being the most symmetrical possible. It is orthogonal and has compact support.

Symlet wavelets are nearly symmetrical and are proposed by Daubechies as modifications to the db family. The properties of the two families (dbN and Sym) are similar, but the symlet functions tend to be symmetrical. Here are the main wavelet functions.

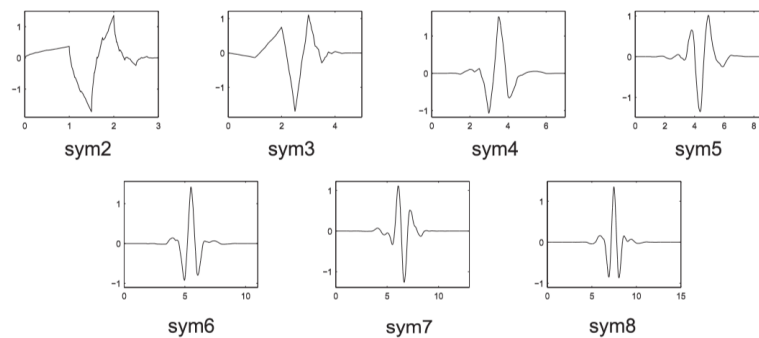


Figure 3.4. Symlet wavelet function. Source: [Misiti and Poggi 2001].

Developed by Daubechies, on a demand from R. Coifman, the wave function has 2^n moments equal to 0, and the scale function has 2^{n-1} moments equal to 0. Figure 3.5 presents the Coiflets wave function. The functions have a support length of 6^{n-1} .

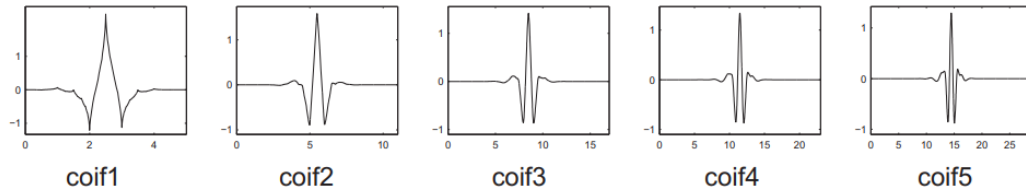


Figure 3.5. Coiflets wavelet function. Source: [Misiti and Poggi 2001].

3.2.3 CWT – Continuous Wavelet Transform

The Continuous Wavelet Transform (CWT) is defined as the sum over all time (or space) of the temporal signal multiplied by the scale. It can be described as an analytic $\psi^{a,b}$ function, which depends on the parameter a (scale), and the parameter b (translation) that changes continuously over all \mathbb{R} , excluding $a \neq 0$. The continuous transform of wavelet is represented by the linear convolution exposed by Eq. (3.22). The wavelet spectrum, or spectrogram, is defined by Eq. (3.23).

$$X_{(a,b)} = \int_{-\infty}^{\infty} x(t)\psi_{a,b}(t)dt \quad (3.22)$$

$$P_{xx(a,b)} = |X_{(a,b)}|^2 \quad (3.23)$$

where $\psi^{a,b}$ is associated with the scale (a) and translation parameters (b). It oscillates at a frequency a^{-1} and is positioned in time (or space) “ b ”.

The scale parameter works similarly to a map: higher scales present lesser detailing. Following this idea, high frequencies present a detailed part of a signal while a low frequency a larger portion, hence with lesser detailing.

The Scalogram process is summarized by the following steps:

- 1) The wavelet is located through a translation of b_0 , at a a_0 scale, at the beginning of the signal $f(t)$ to be studied.
- 2) The wavelet is then compared with a portion of the signal contained in its beginning, through the inner product given by Eq. (3.22), generating a coefficient $X_{(a,b)}$, for b_0 and a_0 given initially. This coefficient represents the correlation of the transform with the fraction of the analyzed signal.
- 3) The wavelet is moved to a second location b_1 and steps 1) and 2) above are started again with b_1 in place of b_0 . This process is repeated until the entire signal is covered by the a_0 -scale wavelet.
- 4) The wavelet scale is changed from a_0 to a_1 and the process from 1) to 3) is repeated.
- 5) The processes 1) to 4) are repeated for the entire signal and for all scales.

One of the disadvantages of CWT is that a very large number of wavelet coefficients are generated during the analysis. Furthermore, few wavelets have an explicit expression, and many are defined with recursive equations. CWT is redundant in this sense, and it is necessary to use the entire domain to reconstruct the signal $f(t)$.

Therefore, instead of using continuous dilation and translation, discrete values of these parameters are used to perform the Discrete Wavelet Transform (DWT) (Ovanesova and Suárez, 2004).

3.2.4 DWT – Discrete Wavelet Transform

Discrete basis can be obtained through the choice of discrete values to scales and positions. This usual choice is the dyadic discretization, in powers of two. By replacing, in Eq. (3.22) and Eq. (3.23), a with 2^j and b with $k2^j$, $(j,k) \in \mathbb{Z}^2$, Eq. (3.24) and Eq. (3.25) are created:

$$\Psi_{j,k}(t) = 2^{-\frac{j}{2}} \psi(2^{-j}t - k) \quad (3.24)$$

$$\Phi_{j,k}(t) = 2^{-\frac{j}{2}} \phi(2^{-j}t - k) \quad (3.25)$$

where j and k are the dilatation and translation coefficients. In this work, the adopted discretization is made with $j \geq 0$ and $k > 0$.

Percival and Walden (2000) defined the DWT as a well-structured sub-sampling of the CWT but in dyadic scales. The discrete wavelets spectrum is given by Eq. (3.26).

$$D_{j,k}(t) = \sum_t x(t) \psi_{j,k}(t) \quad (3.26)$$

$$P_{xx}(j,k) = |D_{j,k}|^2 \quad (3.27)$$

The time-series number of points limits the number of possible transformation levels. Differently from Fourier, the wavelet coefficients are related to lower frequencies. Hence, the DWT of a 2^N series is calculated until a certain $J < N$. The mean values information is given by Eq. (3.28):

$$C_j(t) = \sum_{k \in Z} C_{j,k} \phi_{j,k}(t) \quad (3.28)$$

where the $C_j(t)$ tends to the μ_x mean for a J sufficiently large. For small values of J , the approximation is the mean added to the higher scale fluctuations. The calculation of the vector coefficients $d_j = \{d_{j,k}, 1 \leq k \leq 2^{N-j}\}$ and $c_j = \{c_{j,k}, 1 \leq k \leq 2^{N-j}\}$ for each DWT j level is done through a pyramidal algorithm, developed by Mallat (1989). This algorithm enables the calculation of the coefficients by a number of multiplications of 2^N order, this being the length of the sample.

Thus, if the functions of the wavelets base have compact support on the frequency domain, they will act as filters on the real space, maintaining only the signal fraction that corresponds to its frequency interval.

The first stage of this pyramidal algorithm for the DWT calculus consists in transforming the $x(t)$ time-series with a 2^N and $2^{N/2}$ wavelet coefficients and $2^{N/2}$ scale coefficients of first level (d_1 and c_1 vectors). There are $(N - 1)$ subsequent stages of the algorithm. The generic j stage transforms the c_{j-1} of $2^N/2^{j-1}$ length is considered the same way as $x(t)$ on the first stage: its elements are filtered separately by the scale and wavelet filters. Figure 3.6 shows the behavior of the WT through of a binary tree.

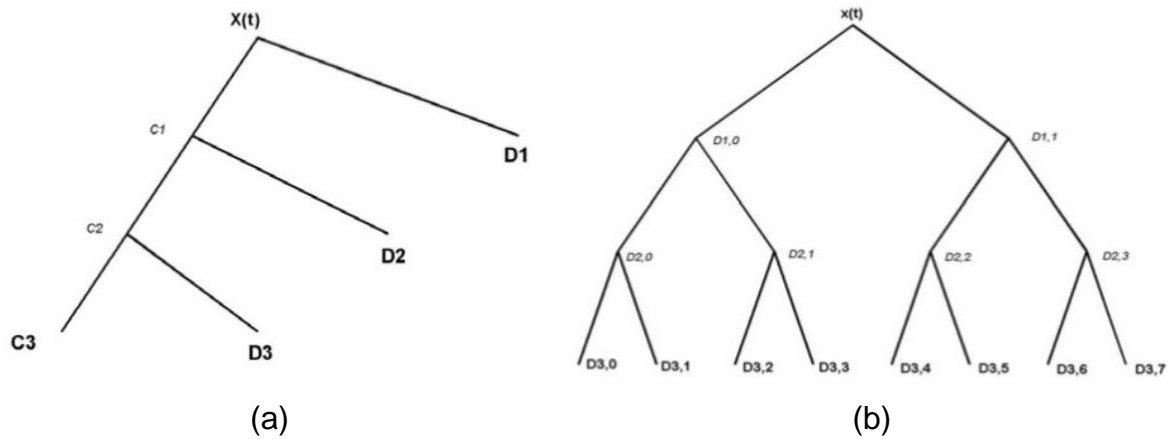


Figure 3.6. Wavelets tree for a $j = 3$ level of decomposition for (a) wavelets and (b) wavelets package. Source: [Indrusiak and Moller, 2004].

The original function may be reconstructed through the sum of the latter approximation and all details, which contain the lost information between two successive approximations:

$$x(t) = C_3 + D_3 + D_2 + D_1 \quad (3.29)$$

where C_3 , D_3 , D_2 and D_1 , are the wavelet coefficients.

An important characteristic of the DWT, with its dyadic scales, is that the wavelets coefficients of a j level may be associated to frequencies at the interval $[1/2^{j+1}, 1/2^j]$ while the scale coefficients at the same level are associated to the frequencies $[0, 1/2^{j+1}]$. These levels of resolution or scales are however dyadic, the following scale is always the double of the previous. Thus, the frequency intervals are also dyadic, and the following interval is always half of the previous size. To analyze intervals of frequency of equal size, the DWT is used.

Furthermore, DWT enables us to compute a set of coefficients connected to either lower or higher frequencies from an original signal " S ". The frequencies (or scales) associated to the coefficients are computed by passing the original signal through a low-pass filter, h , and high-pass filter, g , (LPF and HPF). The LPF (h) gives a set of coefficients called approximation, " A ", while the details, set of coefficients which contains the higher frequencies of the signal, are so-called details, " d " and give rise from the HPF (g). The process of filtering downsamples the original signal " S "

whenever a new filtering step is performed in the approximation coefficients. The process can be repeated by providing different levels of decomposition, “ J ”. For each J level of decomposition, $J+1$ subbands of frequencies will be provided. For instance, for $J = 3$, the signal “ S ” will be split into A_3 , D_3 , D_2 , and D_1 levels for frequency. A sketch of the DWT decomposition, at $J=3$, is shown in Figure 3.7.

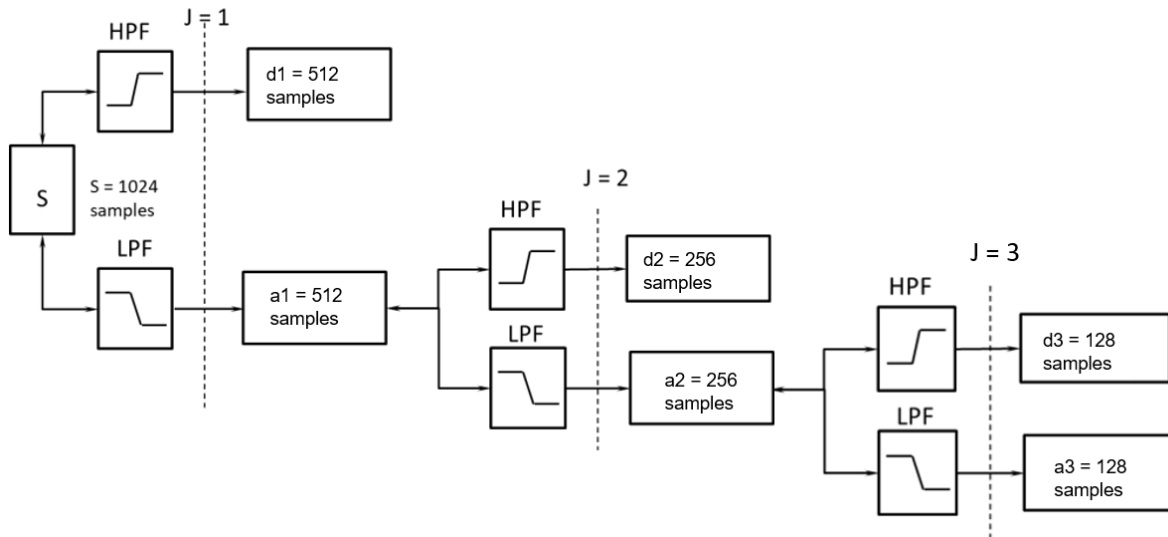


Figure 3.7. Sketch of DWT transform.

Filters h and g , come from the wavelet mother, whose functions are carefully chosen, taking into account some necessary features such as compactness and orthogonality. Each wavelet mother possesses its very own low and high decomposition filters coefficients, h and g , respectively, and the approximation, “ A ” and the details, “ D ”, coefficients arise from the convolution of the signal “ S ” and the filters, as follow in Eq. (3.30) and Eq. (3.31). Thus, approximation (A) and details (D) are products of the discretization of the DWT.

$$A_r[n] = \sum_{k=0}^k S_r[n] \cdot h_r[k-n] \quad (3.30)$$

$$d_r[n] = \sum_{k=0}^k S_r[n] \cdot g_r[k-n] \quad (3.31)$$

It is important to note that this research deals only with the details, d .

3.3 Static Analysis

This section presents the necessary concepts and equations for the obtention of the displacement data necessary for the damage detection methodology further developed in chapter 4.

Hence, it covers the theory of deflection, how a beam behaves when submitted to transversal static loads, the diagrams of bending and shear stress, the elastic line equation and finally the maximum deflection.

3.3.1 Deflection

A beam is a projected to support some structural phenomena, such as pure bending, bending moment, shear stress, tensions, and the beam's deflection.

All these factors, have a maximum admissible value. The beam deflection is illustrated in Figure 3.8, where P is the concentrated load, xy is the symmetry plane, v is the deflection, and the deformations only obey the pure flexion.

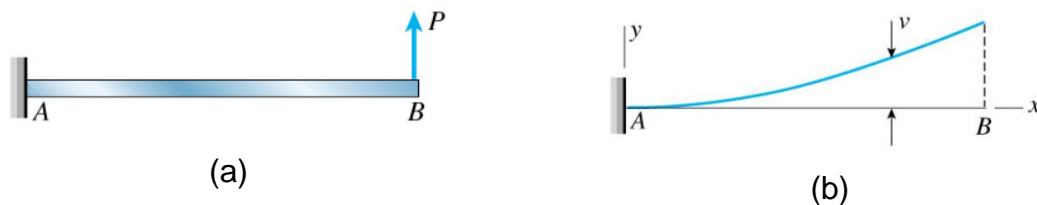


Figure 3.8. Deflection curve of a cantilever beam (a) beam under a punctual load; (b) deflection curve diagram. Source: [Gere, 2009].

A beam, only submitted to pure bending while at an elastic regime, is deflected in a circumference arch which can be expressed as Eq. 3.32, where M is the bending moment, E is the elasticity module, I is the moment of inertia, and ρ is the curvature radius.

$$\frac{1}{\rho} = \frac{M}{EI} \quad (3.32)$$

The same beam, but now with a transversal static load, as illustrated in Fig. 3.8, has a different bending moment and curvature radius for each section. While the principle of Saint-Venant is respected, Eq. 3.32 may be rewritten into:

$$\frac{1}{\rho} = \frac{Px}{EI} \quad (3.33)$$

while x being the distance of the section from the left end of the beam. P is the concentrated load at the beam's free end, at Fig. 3.8 (a).

In this sense, the comprehension of how this deflection develops is necessary. The elastic line equations define this behavior.

3.3.2 Diagram of Bending Moment and Shear Stress

Before the elastic line, the concept of bending moment (M) and shear stress (V) is extremely important to understand deflection.

These diagrams, Figure 3.9, are elaborated from the analysis of moments and forces on the beam. Initially a cut is made in the beam in regards to external and internal forces. The shear stress is positive when the forces external factors acting on it tend to break it. Meanwhile, the bending moment is positive when external forces tend to flex it. Figure 3.9 illustrates the step-by-step elaboration of the bending moment and shear stress diagrams for a simply supported beam.

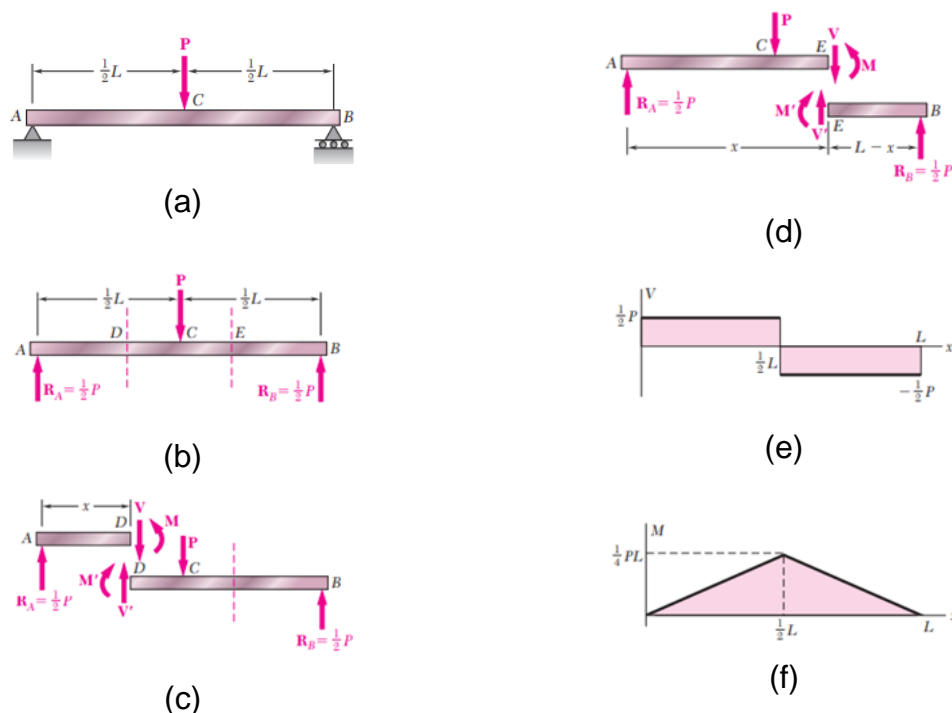


Figure 3.9. Bending moment and shear stress of a simply supported beam. (a-d) diagram development; (e) shear stress; (f) bending moment. Source: [Beer, 2011].

Initially the reactions, $P/2$, are determinate with a free body diagram, Fig. 3.9 (b), due to a $L/2$ distance from the supports. Then, cuts are made on sections AD and AB. Free body diagrams writes that the sum of the vertical components and the sum of the moments with respect to the forces acting on the free body are equal to zero.

Thus, $V = -P/2$ and $M = P(L-x)/2$, therefore, the shear force is negative and the bending moment is positive. To complete the diagram, the shear force has a constant value $V = -P/2$ between C and B, while the bending moment decreases linearly from $M = PL/4$ in $x = L/2$ up to $M = 0$ at $x = L$.

3.3.3 Equation of the Elastic Line

The elastic line, by definition is the deflection diagram of the longitudinal axis that passes through the centroid of each beam cross-sectional area. The understanding of the elastic line is easier when started with the bending moment diagram, see Fig. 3.10.

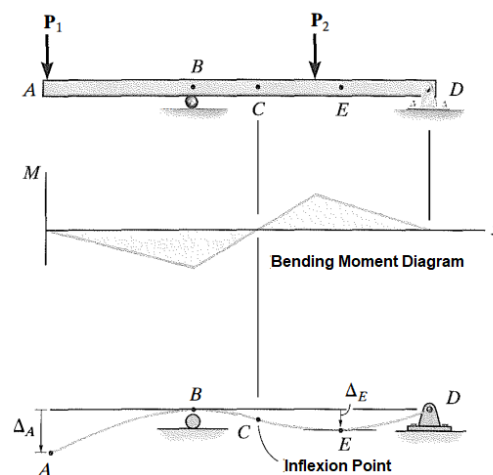


Figure 3.10. Elastic Line. Source: [Hibbeler, 2010].

On point E, the slope of the elastic curve is zero and therefore the deflection of the beam is maximum.

Equation 3.32 represents the curve of the elastic line in terms of the curvature radius, ρ , the deflection, y , and the location along the beam, x . Considering a beam under pure flexion its elastic solution may be simplified as:

$$\frac{d^2 y}{dx^2} = \frac{M}{EI} \quad (3.34)$$

Equation 3.34 is then differentiated two times in terms of x , substituting ($V = dM/dx$) and ($-w = dV/dx$), to obtain the Equation of the beam, Eq. 3.35.

$$EI \frac{d^4 y}{dx^4} = -w(x) \quad (3.35)$$

Then, it is successively integrated to obtain the shear stress, the bending moment, the rotation and finally the elastic line equation, respectively.

$$EI \frac{d^3 y}{dx^3} = V(x) \quad (3.36)$$

$$EI \frac{d^2 y}{dx^2} = M(x) \quad (3.37)$$

$$EI \frac{dy}{dx} = \theta(x) \quad (3.38)$$

$$EI y = f(x) \quad (3.39)$$

where EI is the flexural stiffness of the beam, w is the load/weight, V is the shear stress, M is the bending moment, θ is the rotation and y is the deflection. To obtain the elastic line equation, the four integration steps yield four integration constants:

$$\begin{aligned}
 EI \frac{d^4 y}{dx^4} &= -w(x) \\
 EI \frac{d^3 y}{dx^3} &= V(x) = -\int w(x) dx + C_1 \\
 EI \frac{d^2 y}{dx^2} &= M(x) = -\int dx \int w(x) dx + C_1 x + C_2 \\
 EI \frac{dy}{dx} &= \theta(x) = -\int dx \int dx \int w(x) dx + \frac{1}{2} C_1 x^2 + C_2 x + C_3 \\
 EI y &= f(x) = -\int dx \int dx \int dx \int w(x) dx + \frac{1}{6} C_1 x^3 + \frac{1}{2} C_2 x^2 + C_3 x + C_4
 \end{aligned} \quad (3.40)$$

The integration constants of Figure 3.40 are determined by the boundary conditions applied to each support type, as presented by Figure 3.11. The illustration exhibits these conditions for a double-clamped, a simply supported and a cantilever beam, respectively.

For the double-clamped, rotation and deflection are null at both supports. For the cantilever, these are null at the fixed end and at the free-end, the shear stress and the bending moment are null instead. For the simply supported, deflection and the bending moment are the null conditions at both supports.

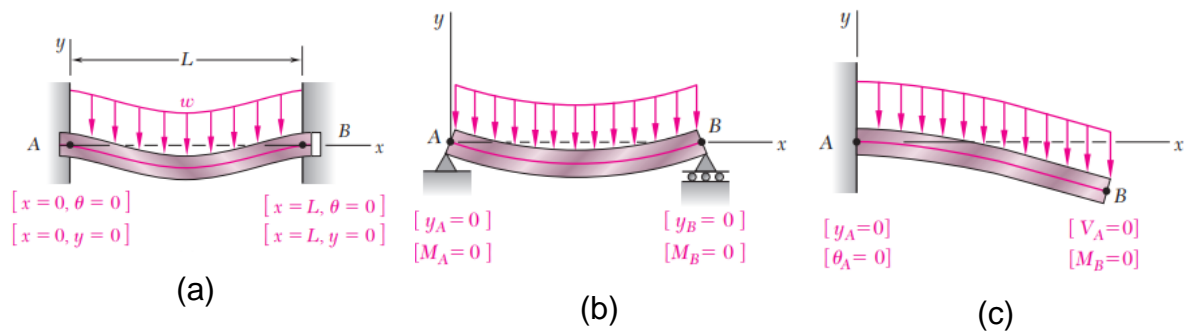


Figure 3.11. Boundary conditions for a (a) double-clamped; (b) simply supported; (c) cantilever beam. Adapted from: [Beer, 2011].

The presented formulation yields the following elastic line equation for the double-clamped, Eq. 3.41, the simply supported, Eq. 3.42, and the cantilever Eq. 3.43.

$$y = \frac{w}{24EI} (-x^4 + 2Lx^3 - L^2x^2) \quad (3.41)$$

$$y = \frac{w}{24EI} (-x^4 + 2Lx^3 - L^3x) \quad (3.42)$$

$$y = \frac{w}{24EI} (-x^4 + 4Lx^3 - 6L^2x^2) \quad (3.43)$$

Another particularization that needs to be made is regarding the type of load. The above approach is adequate for beams submitted to continuous distributed loads. In the case of punctual loads, the reactions on the supports cause discontinuity on the shear force. Thus, the boundary conditions now need to be analyzed through a free

body diagram, regarding the loads, reactions and moments on each support and load locations.

These boundary conditions can now be used in the bending moment, Eq. 3.37, to define the integration constants. The following mathematical steps are the same as for the distributed loads.

Hence, the elastic line equations for the analyzed beams for a punctual load, are given by equations 3.44 to 3.46 for the double-clamped, the simply supported and the cantilever, respectively.

$$y = \frac{P}{48EI} (3Lx^2 - 4x^3) \quad (3.44)$$

$$y = \frac{P}{48EI} (4x^3 - 3L^2x) \quad (3.45)$$

$$y = \frac{P}{6EI} (-3Lx^2 + x^3) \quad (3.46)$$

Furthermore, to define the value of the maximum deflection, the x correspondent to the position of maximum deflection determined by the elastic line must be substituted into the elastic line equation.

The equations for the maximum deflection for each beam and load type is disposed in Appendix A.

3.4 Modal Analysis

This investigation deals with discrete structures, hence involving a geometry defined by differential equations only at the temporal variable. This type of structure requires a dynamic analysis via FEM – Finite elements method.

The equations of movement of these models are amplifications of the static equilibrium equations, through the inclusion of inertia and damping forces, in addition to consideration of external actions as functions of time. Thus, the structural dynamics analysis methods are independent of the form in which the equations of motion are obtained. This section describes the necessary theory for understanding and obtaining the mode shapes for the investigated beams.

3.4.1 Equation of Motion in Free Vibration

This section defines through an analytical model, the equation of motion and its solution for a free-vibration at a continuous analysis system.

The Euler-Bernoulli theory, states that when a beam flexes, the cross-section of the beam remains in a plane shape. Figure 3.12 illustrates a simply supported beam and its free body diagram for a dx discrete element, with notation to the loads, bending moment, shear stress, and the moment of inertia.

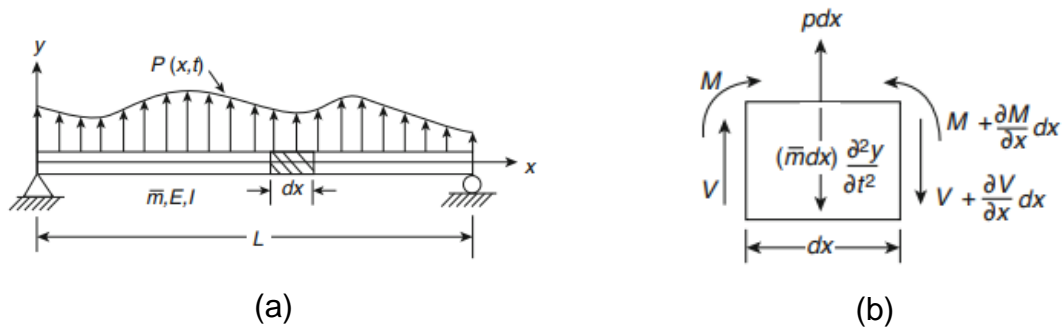


Figure 3.12. (a) simply supported beam and its (b) elements free body diagram.

Source: [Paz and Kim, 2019].

The theory states, as described in section 3.3, that if the deflection is small enough when compared to the beam's length, the inclination of the element from the unloaded position is also small. By this condition, the equation of motion is given:

$$\frac{\partial V}{\partial x} + \bar{m} \frac{\partial^2 y}{\partial t^2} = p(x,t) \quad (3.47)$$

where \bar{m} is the mass per unit length. As described in section 3.3, the bending moment and the shear stress are given by Equations 3.48 and 3.49:

$$M = EI \frac{\partial^2 y}{\partial x^2} \quad (3.48)$$

$$V = \frac{\partial M}{\partial x} \quad (3.49)$$

Then, Eq. 3.50 is combined with Equations 3.47, 3.48 and 3.49. It is a fourth order differential equation. As an approximate equation, it considers only the flexural

deflections. This equation when considered the shear deformation and moment of inertia is named as Timoshenko equation.

$$EI \frac{\partial^4 y}{\partial x^4} + \bar{m} \frac{\partial^2 y}{\partial t^2} = p(x,t) \quad (3.50)$$

Ahead, considering a free-vibration [$p(x,t)=0$], Eq. 3.50 is reduced to:

$$EI \frac{\partial^4 y}{\partial x^4} + \bar{m} \frac{\partial^2 y}{\partial t^2} = 0 \quad (3.51)$$

This equation solution is then found by the separation variables method, when it is expressed as a product of position $\Phi(x)$ and time $f(t)$. Then, it is solved as:

$$\Phi(x) = A \sin ax + B \cos ax + C \sinh ax + D \cosh ax \quad (3.52)$$

where A, B, C and D are integration constants. These constants determine the shape and amplitude of the free-vibration beam.

3.4.1.1 Simply Supported Mode Shape

The integrations of Eq. 3.51 leads to four constants that need definition. The same approach as used to determine the equation of the elastic line is given. Also, the same boundary conditions presented in Figure 3.11 are valid.

For a simply supported beam, the boundary conditions determine that at both supports the displacement and the bending moment are null:

$$\begin{aligned} y(0,t) &= 0, & M(0,t) &= 0 \\ y(L,t) &= 0, & M(L,t) &= 0 \end{aligned}$$

These conditions yield Equations 3.54 and 3.55.

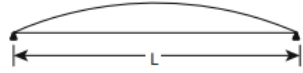
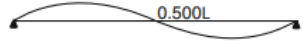
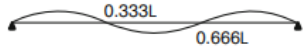
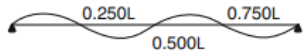

$$\Phi(0) = 0, \Phi''(0) = 0 \quad \text{for } x = 0 \quad (3.54)$$

$$\Phi(L) = 0, \Phi''(L) = 0 \quad \text{for } x = L \quad (3.55)$$

The first five natural frequencies and mode shapes for a simply supported beam are disposed in Table 3.1.

Table 3.1. Simply supported beam natural frequencies and mode shapes.

Source: [Paz and Kim, 2019].

Natural frequencies $\omega_n = C_n \sqrt{\frac{EI}{mL^4}}$		Normal modes $\Phi_n = \sin \frac{n\pi x}{L}$	
n	C_n	I_n^a	Shape
1	π^2	$4/\pi$	
2	$4\pi^2$	0	
3	$9\pi^2$	$4/3\pi$	
4	$16\pi^2$	0	
5	$25\pi^2$	$4/5\pi$	

$$^a I_n = \int_0^L \Phi_n(x) dx / \int_0^L \Phi_n^2(x) dx$$

3.4.1.1 Double-Clamped Mode Shape

Now for a double-clamped beam, with initial boundary conditions being:

$$y(0,t) = 0, \quad y'(0,t) = 0$$

$$y(L,t) = 0, \quad y'(L,t) = 0$$

The substituting these into the Frequency equation is given:

$$\cos a_n L \cosh a_n L - 1 = 0 \tag{3.56}$$

Further, through Eq. 3.56 the mode shapes are obtained with the following equations:

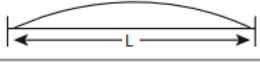
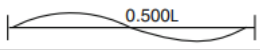

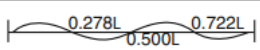
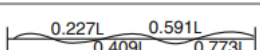
$$\Phi_n(x) = \cosh a_n x - \cos a_n x - \sigma_n (\sinh a_n x - \sin a_n x) \tag{3.57}$$

$$\sigma_n = \frac{\cos a_n L - \cosh a_n L}{\sin a_n L - \sinh a_n L} \tag{3.58}$$

The first five natural frequencies and mode shapes for a double-clamped beam are disposed in Table 3.2.

Table 3.2. Double-clamped beam natural frequencies and mode shapes.

Source: [Paz and Kim, 2019].

Natural frequencies		Normal modes		
$\Phi_n(x) = \cosh a_n x - \cos a_n x - \sigma_n(\sinh a_n x - \sin a_n x)$				
$\omega_n = C_n \sqrt{\frac{EI}{mL^4}}$		$\sigma_n = \frac{\cos a_n L - \cosh a_n L}{\sin a_n L - \sinh a_n L}$		
n	$C_n = (a_n L)^2$	σ_n	I_n^a	Shape
1	22.3733	0.982502	0.8308	
2	61.6728	1.000777	0	
3	120.9034	0.999967	0.3640	
4	199.8594	1.000001	0	
5	298.5555	1.00000	0.2323	

$$^a I_n = \int_0^L \Phi_n(x) dx / \int_0^L \Phi_n^2(x) dx$$

3.4.1.1 Cantilever Mode Shape

At last, for a cantilever beam, with the boundary conditions:

$$y(0, t) = 0, \quad y'(0, t) = 0$$

$$M(L, t) = 0, \quad V(L, t) = 0$$

Leads to the Frequency equation:

$$\cos a_n L \cdot \cosh a_n L + 1 = 0 \tag{3.59}$$

And the mode shape by Equations 3.60 and 3.61.

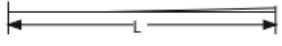

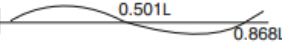
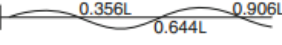

$$\Phi_n(x) = (\cosh a_n x - \cos a_n x) - \sigma_n(\sinh a_n x - \sin a_n x) \tag{3.60}$$

$$\sigma_n = \frac{\cos a_n L + \cosh a_n L}{\sin a_n L + \sinh a_n L} \tag{3.61}$$

The first five natural frequencies and mode shapes for a cantilever beam are disposed in Table 3.3.

Table 3.3. Cantilever beam natural frequencies and mode shapes.

Source: [Paz and Kim, 2019].

Natural frequencies		Normal modes		
$\Phi_n = (\cosh a_n x - \cos a_n x) - \sigma_n (\sinh a_n x - \sin a_n x)$				
$\omega_n = C_n \sqrt{\frac{EI}{mL^4}} \quad \sigma = \frac{\cos a_n L + \cosh a_n L}{\sin a_n L + \sinh a_n L}$				
n	$C_n = (a_n L)^2$	σ_n	I_n^a	Shape
1	3.5160	0.734096	0.7830	
2	22.0345	1.018466	0.4340	
3	61.6972	0.999225	0.2589	
4	120.0902	1.000033	0.0017	
5	199.8600	1.000000	0.0707	

$$^a I_n = \int_0^L \Phi_n(x) dx / \int_0^L \Phi_n^2(x) dx$$

3.4.2 Numerical Model for Natural Frequencies and Mode Shapes

Natural frequency and mode shapes have great importance in the dynamic analysis. This section defines the equations for a discrete numerical analysis, to be conducted on a FEM – finite elements method, regarding these two parameters.

The FEM is summarized in five major steps:

1. Definition of the problem – this includes the material properties, the beam type, loads and the boundary conditions;
2. Discretization – in this phase the analyzed body is defined through elements connected via nodes; here the elements types are determined;
3. Definition of the stiffness and mass matrices – this step consists into defining the matrices for all the finite elements of the body, individually;

4. Assemble the global stiffness and mass matrices – this matrix defines how the body responds to forces, stresses and strains;
5. Solve – as the name, it solves the eigenvalue problem to obtain natural frequencies and mode shapes.
6. Post processing – this phase deals with the analysis of the results calculated with FEM;

The discretization defines the type and number of elements, its arrangement and the mesh geometry. For each element there is a $\{u\}$ vector that contains all the possible displacements for the nodes, including rotations.

In a 2D analysis, each node has 3 degrees of freedom (DOF). The nodes can move along the x and y-axis and rotate on z-axis.

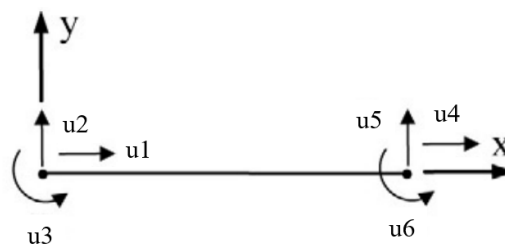


Figure 3.13. 2D beam nodes degrees of freedom for x, y and z-axis.

Figure 3.13 illustrates a single LINE element with 3 DOF in each node, hence 6 total DOF at the observed single element beam. The degrees of freedom presented may vary regarding the boundary conditions of each structure. The conditions for this research are presented in previous sections 3.3 and 3.4.1.

The described model is governed by Equation 3.62, where $\{F\}$ is the vector for the nodal forces and moments, $\{u\}$ is the vector of nodal displacements and $[k]$ is the stiffness matrix of the element.

$$\{F\} = [k]\{u\} \tag{3.62}$$

The element stiffness matrix determines how much each node in a certain element will displace under specific conditions.

For a 2D structure beam with 6 DOF, undergoing bending and extension, illustrated in Figure 3.13, the stiffness matrix has the format:

$$[k] = \begin{bmatrix} \frac{AE}{L} & 0 & 0 & -\frac{AE}{L} & 0 & 0 \\ 0 & \frac{12EI}{L^3} & \frac{6EI}{L^2} & 0 & -\frac{12EI}{L^3} & \frac{6EI}{L^2} \\ 0 & \frac{6EI}{L^2} & \frac{4EI}{L} & 0 & -\frac{6EI}{L^2} & \frac{2EI}{L} \\ -\frac{AE}{L} & 0 & 0 & \frac{AE}{L} & 0 & 0 \\ 0 & -\frac{12EI}{L^3} & -\frac{6EI}{L^2} & 0 & \frac{12EI}{L^3} & -\frac{6EI}{L^2} \\ 0 & \frac{6EI}{L^2} & \frac{2EI}{L} & 0 & -\frac{6EI}{L^2} & \frac{4EI}{L} \end{bmatrix} \quad (3.63)$$

With $[K]$, a system of linear equations can be solved with Eq. 3.62. As described, each element has its own stiffness matrix. Then, each of these matrices are combined to form the global matrix.

A statical problem is solved with the global matrix. Meanwhile a modal problem, the solution of the eigenvalues and eigenvectors with mass and stiffness matrices, both global.

The mass matrix might be defined by two methods, the lumped-mass and the consistent mass. Equation 3.64 gives the consistent mass matrix, for a prismatic beam, and with 6 DOF, illustrated in Figure 3.13, the relation between modal axial forces and accelerations:

$$[m] = \frac{\rho L}{420} \begin{bmatrix} 140 & 0 & 0 & 70 & 0 & 0 \\ 0 & 156 & -22L & 0 & 54 & 13L \\ 0 & -22L & 4L^2 & 0 & -13L & -3L^2 \\ 70 & 0 & 0 & 140 & 0 & 0 \\ 0 & 54 & -13L & 0 & 156 & -22L \\ 0 & 13L & -3L^2 & 0 & 22L & 4L^2 \end{bmatrix} \quad (3.64)$$

where ρ is the mass per unit length. The calculation of the consistent mass matrix needs to first, establish the displacement functions regarding an axial unit displacement at a modal coordinate. Then, the equations are governed as followed by Eq. 3.33.

Furthermore, in the case of an undamped free-vibration, we have Eq. 3.65, while assuming that an initial perturbation is given to the system, the harmonic solution of the nodal displacements is given by Eq. 3.66.

$$M\ddot{d}(t) + Kd(t) = 0 \quad (3.65)$$

$$d(t) = \hat{\phi}_j \cos(\omega_j t - \phi_j) \quad (3.66)$$

In this solution, $\hat{\phi}_j$ is the j -th natural vibration mode, ω_j is the free vibration natural frequency and ϕ_j is the phase angle. Substituting Eq. 3.66 into 3.65, a homogeneous algebraic equations have a non-singular solution given by:

$$K\hat{\phi}_j = \omega_j^2 M\hat{\phi}_j \quad (3.67)$$

where ω_j^2 expresses the eigenvalue and $\hat{\phi}_j$ the eigenvector. With n DOF, an equal number of eigenpairs are numerated in increasing order of frequency magnitude, which are positive if there are sufficient restrictions to prevent rigid body displacements and the formation of mechanisms internal to the structure.

Equation 3.66 expresses that all DOF execute harmonic movement characteristic of a vibration mode at the corresponding natural frequency. Thus, natural frequencies and natural modes of vibration are independent of external forces, as functions only of the mass and stiffness distributions of the model. Further, Eq. 3.68 groups the natural frequencies:

$$\Omega = \begin{bmatrix} \omega_1^2 & 0 & \dots & 0 \\ 0 & \omega_2^2 & \dots & 0 \\ \vdots & \vdots & \ddots & \vdots \\ 0 & 0 & \dots & \omega_n^2 \end{bmatrix} \quad (3.68)$$

Then, the mode shapes may be united in the modal matrix:

$$\hat{\Phi} = [\hat{\phi}_1 \quad \hat{\phi}_2 \quad \cdots \quad \hat{\phi}_n] \quad (3.69)$$

With these matrices, the eigenvalue acquires the Eq. 3.70 form.

$$K\hat{\Phi} = M\hat{\Phi}\Omega \quad (3.70)$$

Equation 3.70 solution is the modal analysis.

4 METHODOLOGY

A method is proposed for the detection, localization and quantification of damage. This chapter sets the boundaries and the parameters for the investigation, such as the model description, the toolboxes utilized for obtaining the displacement and modal data for analysis, and the wavelets transform, finally the damage indexes.

The methodology was validated through the analytical equations presented in section 3.3 for the static analysis and section 3.4 for the modal analysis.

4.1 Model Description

A beam, in structural terms, is a structural element, designed to withstand loads and stresses, while having supports and fixed-edges.

Three beam types were investigated: simply supported, cantilever and double-clamped. Figure 4.1 shows an schematic of each beam, as well as its discretization. The mesh is constituted by 100 elements, and 1 meter long, hence each element having 10 mm. Analysis were made on a 1D dimension enabling 3 DOF for each node (x and y – displacements and z-rotation).

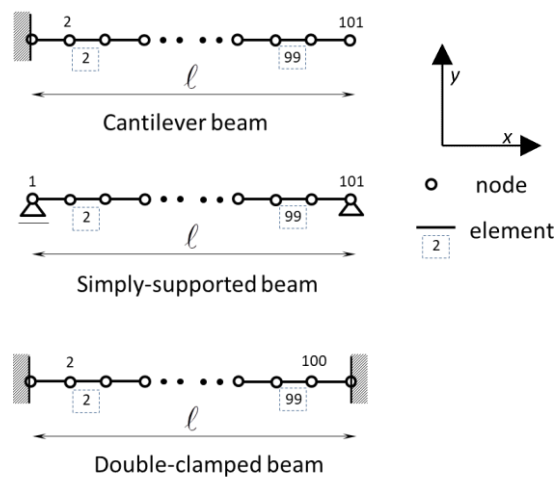


Figure 4.1. Discretized beams models for the finite element method.

The double-clamped beam has two fixed supports with the three DOF restricted. The simply supported has two supports and both have the z-rotation DOF free, having x and y displacement restricted. Finally, the cantilever has only one support and a free-

edge. This beam has a support which restricts the three DOF while the free-edge has the three degrees enabled.

Damage was simulated as an elasticity module (E) percentual reduction in its value. The reduction of E simulates an approximate reduction on the stiffness, provoking a fragility into the beam's elements, which could be caused by diverse natures, such as corrosion, natural wear and tear, cracks, impacts, and others. This approach was also used by several authors, such as: Surace and Ruotolo (1994), Okafor and Dutta (2000), Alvandi and Cremona (2006), and Katunin et al. (2021).

During all procedure, damage severity ranged from 5% to 50%, and was analyzed along the structures.

Damaged elements of choice were 5, 25, 50, 76 and 96, being 5% 25% and 50% distant from the supports. These specific positions were defined so to have an equal analysis on both side of the beam, enabling to understand if locating damage or load near to both of the supports on an equal distance, results into the same readings.

Damage detection was made through a comparison between damaged and intact beams for a baseline value.

Finite elements (FE), methodology was used to numerically model the computational setup for analysis. The FE considered a uniform and isotropic beam.

Beam structural properties are given: ρ is the mass density of 0.783 kg.m^{-1} , A is the cross-section area, $1\text{E-}4 \text{ m}^2$, l is the element length, 10 mm , I is the cross-section moment of inertia, $8.3\text{E-}10 \text{ m}^4$, and E is the elastic (or Young's) module of the material, 200 GPa . These values are due to the material being Steel. The Euler-Bernoulli beam model assumption does not consider the transversal section rotational inertia and shear deformations on the differential equation.

4.1.1 Static Analysis

Two types of loads were investigated: concentrated and distributed load. On both cases, the load was set to a value of 1 Newton. For the distributed one, this magnitude was split along the beam nodes.

Regarding to the punctual load, transverse static loads are applied at different locations on the beam to evaluate possible effects of force location relative to the damaged sites.

Load location points for this study were chosen in nodes 5, 25, 51, 77 and 97, this due to 51 being located on the center of the beam, 5 and 97 at a distance of 5% of the beam length distant from the supports, and 25 and 77 a distance of 25% from the supports. Nodes 5 and 97 are equally distant, 4 nodes, from the beam extremities, while 25 and 77 are equally distant 24 nodes from the edges of the beam.

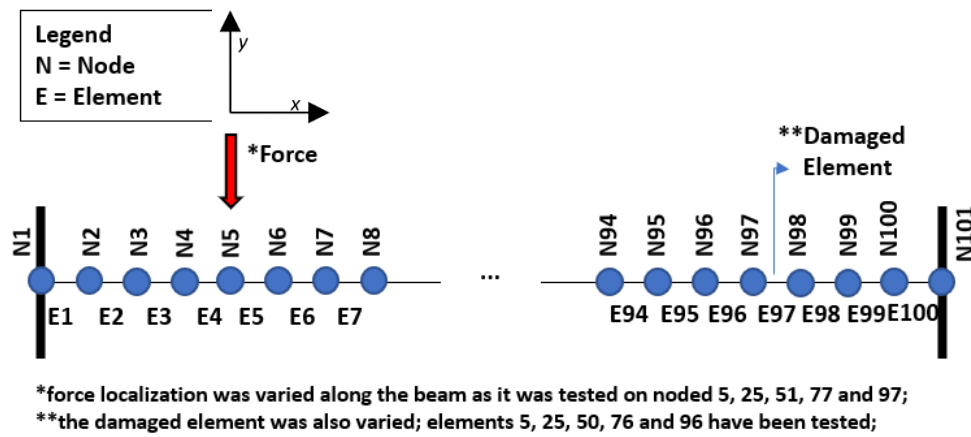


Figure 4.2. Finite element beam discretization.

4.1.2 Modal Analysis

For the modal analysis, the mode shapes are investigated instead of loads on specific nodes. Another difference is that a mode is set on the entire structure of the beam and not just a single node or region. It determines the dynamic characteristics, damping factors and mode shapes, and uses them to determine its dynamic behavior. Section 3.4 deeply details these factors.

For this research, the first five mode shapes were presented, due to the efficacy of the method, while for higher modes no change in results were noticed.

Mode shapes and natural frequencies are obtained from the frequency response function. This function relates excitation and structure vibrational responses.

In this investigation, the Damage Sensitivity Technique (DST), Du et al. (2019), is employed to analyze the disparities between the mode shapes of a structure before

and after it incurs damage. The modal properties are derived through the conventional eigenvalue problem of an undamped MDOF discrete system.

Meanwhile, when simulating damage through stiffness reductions in specific elements of the discretized structure, the matrix is recalculated for each damage scenario, while the mass matrix remains constant and unchanged.

Damage does impact both the natural frequencies and mode shapes, these alterations are typically minimal when the damage levels are small. In the suggested approach, only the Damage Sensitivity Technique (DST) applied to mode shape differences is employed for damage identification and quantification. This preference is due to the fact that modal deflections are better suited for a comprehensive assessment applied across the entire structural span.

4.2 Wavelet Toolbox – MATLAB®

The Wavelet toolbox is a collection of functions built into MATLAB software, technical computing environment. The complete theory behind the method is described in section 3.2. It provides tools for analysis and synthesis of signals and images, and tools for statistical applications, using wavelets and wavelet packages within MATLAB. The toolbox provides two tool categories:

- Command line functions;
- Interactive graphics and tools;

The first category of tools is made up of functions, called directly from the command line or from your own applications. Most of these functions are M – files. A summary of the Wavelet Toolbox functions that are available in MATLAB.

The second category of tools is a set of interface tools graphic that allows access to extensive functionality. Access to these tools is do so by typing “wavemenu”, where a window is appeared, Figure 4.3.

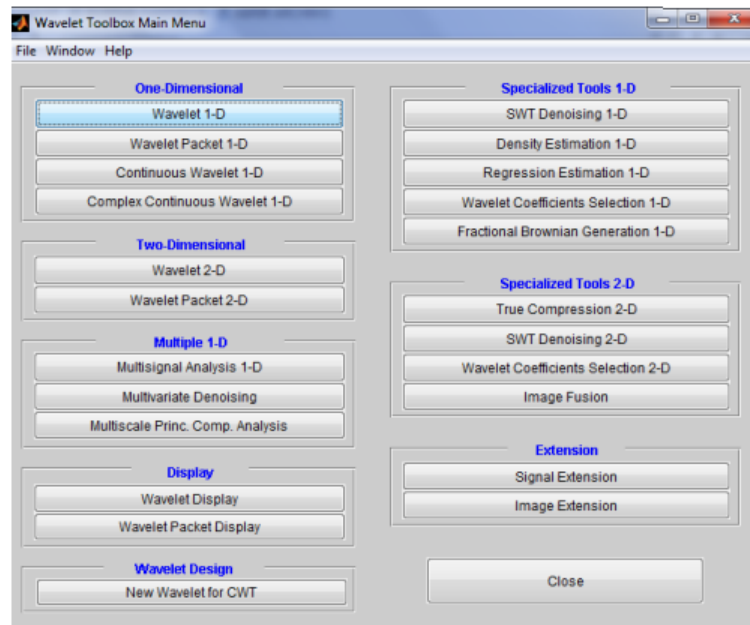


Figure 4.3. “Wavemenu” window - MATLAB.

The different wavelet functions available in the program tools MATLAB are:

- Haar Wavelet – “haar”
- Daubechies Wavelet – “db”
- Symlets Wavelet – “sym”
- Coiflets Wavelet – “coif”
- Biorthogonal Wavelets – “bior”
- Meyer Wavelets – “mey”
- Gaussian Wavelets – “gaus”
- Morlet Wavelets – “mor”
- All wavelet mother types are described in Misiti and Poggi (2001).

4.3 Damage Indicator: d^1 -index and d^2 -index

This work aimed to detect, localize and quantify damage. The approach used was based on the Discrete Wavelet Transform (DWT) to the beam’s deflection function and mode shapes. To achieve such goal different indexes were created. All the wavelet coefficients of DWT were generated at $J=1$ using the wavelet mother Coiflets 2.

According to Katunin (Katunin, 2010 and Katunin, 2011), the analysis based on approximation coefficients was seen to be the most efficient for damage localization, therefore considering the wavelet tree represented on Figure 3.6, a_0 coefficients, approximation, were used in this investigation. To perform such analysis, we first found the approximation vector of DWT coefficients for non-damaged beam, producing a d_0 -vector, at level of decomposition, $J=1$.

In sequence, the same steps were followed for the damaged beam, yielding also a d_d -vector with the same length of d_0 . To perform the final evaluation a damage indicator, d^1 is then created, by subtracting d_d , and d_0 . To eliminate negative values of this vector, the resulting vector was then squared and normalized by its maximum value, as follows in Eq. (4.1):

$$d^1_{index} = \frac{(d_d - d_0)^2}{\max[(d_d - d_0)^2]} \quad (4.1)$$

The vector is then plotted along the beam. The idea behind this is to identify and localize the damaged region of the beam through a normalization by the maximum value of the index, hence being the most probable region of damage.

Further, the d^2 -index was created for damage quantification. An adjustment was made to enable the analysis of a damage severity prediction curve. This adjustment scaled the squared wavelet coefficient variation by using the squared variation of the intact and damaged beam with 25% of damage as the maximum damage severity due to the this being the range where the most precise results were found.

$$d^2_{index} = \frac{(d_d - d_0)^2}{(d_{max} - d_0)^2} \quad (4.2)$$

Figure 4.4 presents the scheme for damage localization (d^1 -index) and for quantification (d^2 -index). The difference between the two indicators is the dividend, where for the d^1 -index, it is the maximum of the squared difference between the damaged and the undamaged DWT coefficients, and for the d^2 -index, it is the square between the maximum DWT coefficient amongst all analyzed cases and the undamaged coefficient.

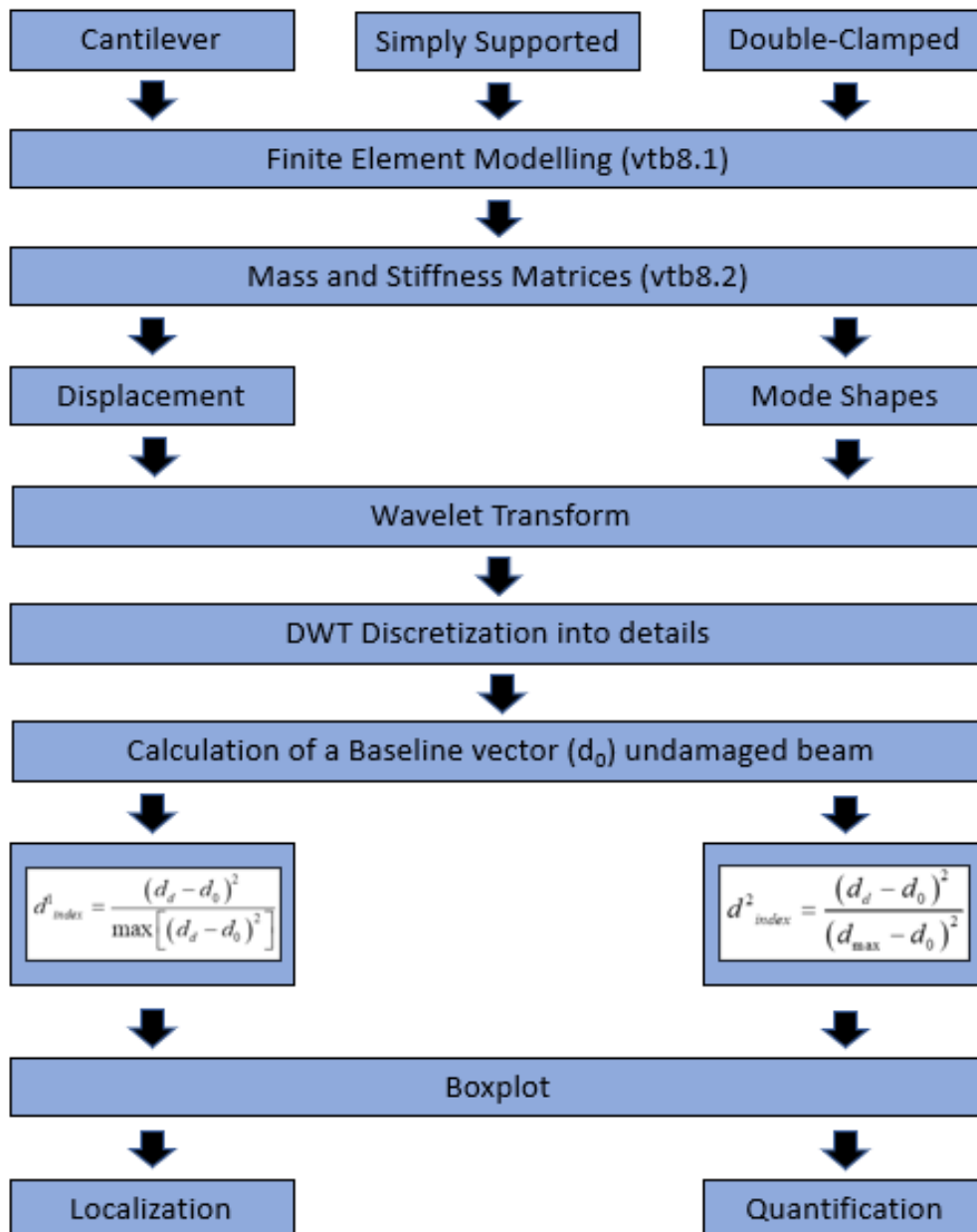


Figure 4.4. d^1 -index and d^2 -index flowchart for damage detection, localization and quantification.

5 RESULTS OF DAMAGE IDENTIFICATION AND LOCALIZATION

Damage detection and localization is aimed to determine most probable regions of having damage. During these processes diverse variables are involved.

In this sense, chapter 5 presents the technique to be used to investigate damage identification and localization through wavelet transform. Also, chapter 5 adds to the study an investigation on the effects of the load location, mother wavelet, decomposition level, beam type supports, and the severity of the damage over the probable damaged region identification and localization.

Throughout this campaign, analysis is done with the use of the two statistical indexes exposed in section 4.3, based on damaged and undamaged beam displacement and vibration mode shapes.

First, section 5.1 validates the model presenting a comparison between the analytical and the numerically obtained results for displacement and natural frequencies.

Section 5.2 investigates damage localization with data simulated through a static analysis. This case analyses displacement data over damaged and non-damaged beams to detect damage.

Section 5.2.1 investigates the three beam support types: simply supported, cantilever and double-clamped beam, respectively. In each of these, the d^1 -index approach is applied. The visualization of the functions is presented with boxplot tools median values. Following, section 5.2.2 presents a study of influence of damage localization parameters regarding damage severity, decomposition level, boundary conditions and wavelet mother type. It is aimed to structure the optimum setup for damage localization based on the proposed d^1 -index parameters.

Section 5.3 investigates damage localization by means of a dynamic analysis based on the vibration mode shapes of the beams. This study aims the first five modes.

5.1 Model Validation

As presented, the approach consists into obtaining the displacement and the mode shapes trough the vtb engineering toolbox. Then, these data are treated with

the wavelets transform, and finally the results are presented through two damage indexes regarding localization (d^1 -index) and quantification (d^2 -index).

Damage is simulated with a module of elasticity percentage reduction on one or more elements. This phase is conducted during the structure's discretization inside the vtb toolbox (vtb8_1). Results presented in section 5.2.1 and 5.2.2.6 shows that the method is able to localize the exact element which was previously set to be damaged, during the discretization phase.

Before the wavelets transform, the presented method simulates the structural behavior of the beams, based on the equations disposed in sections 3.3 and 3.4, and generate the displacement and mode shapes.

These numerical values are validated through a comparison with analytical values from the presented equations.

Table 5.1 presents the analytical results for the maximum deflection on the investigated beams for both concentrated and distributed loads. The results verify the numerical model due to the great accordance observed, where a margin of error under 1% is noted in all cases.

Table 5.1. Maximum deflection for the analyzed beams.

Beam	Concentrated Load			Distributed Load		
	Analytical	Numerical	% error	Analytical	Numerical	% error
Simply Supported	1,25E-4	1,25E-4	0,72%	7,84E-5	7,81E-5	0,38%
Cantilever	2,00E-3	1,98E-3	0,75%	7,53E-4	7,49E-4	0,53%
Double Clamped	3,17E-5	3,14E-5	0,71%	1,57E-5	1,58E-5	0,63%

Mode shapes are also validated through the equations presented in section 3.4. This research considers the first five mode shapes of the beams. Table 5.2 compares the natural frequencies obtained for the analytical and numerical approaches.

Table 5.2. Natural frequency for the analyzed beams.

Mode	Model	Simply Supported		Cantilever		Double-Clamped	
		ω_n [Hz]	% error	ω_n [Hz]	% error	ω_n [Hz]	% error
1 st	Analytical	22,8482	0,101%	8,10354	0,545%	51,8460	0,002%
	Numerical	22,8714		8,14791		51,8469	
2 nd	Analytical	91,3929	0,100%	51,0592	0,004%	142,917	0,001%
	Numerical	91,4857		51,0610		142,918	
3 rd	Analytical	205,634	0,102%	142,972	0,001%	280,176	0,001%
	Numerical	205,842		142,974		280,176	
4 th	Analytical	365,571	0,101%	280,171	0,001%	463,141	0,001%
	Numerical	365,942		280,173		463,146	
5 th	Analytical	571,205	0,103%	463,141	0,001%	691,855	0,001%
	Numerical	571,795		463,146		691,860	

Table 5.2 presents very low difference between the numerically obtained results and the analytical natural frequencies values. Percentage of error was kept under 0,004% in most cases, and 0,101% at the highest variations.

Furthermore, Figure 5.1 compares the fifth mode shape obtained with the method and the theoretical mode shape.

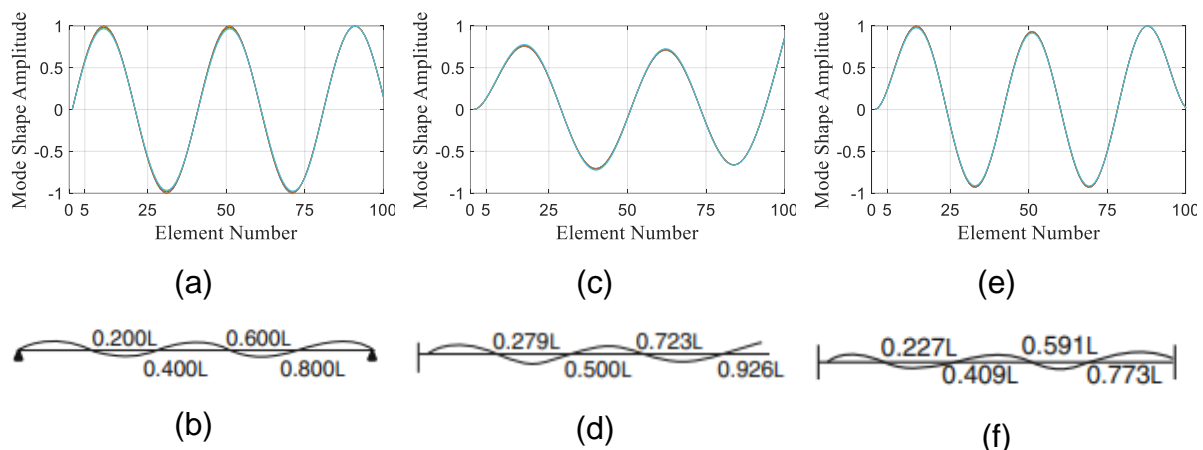


Figure 5.1. Mode shape comparison for a (b,d,f) theoretical behavior and (a,c,e) numerical obtained results for the simply supported, the cantilever and the double-clamped beams respectively.

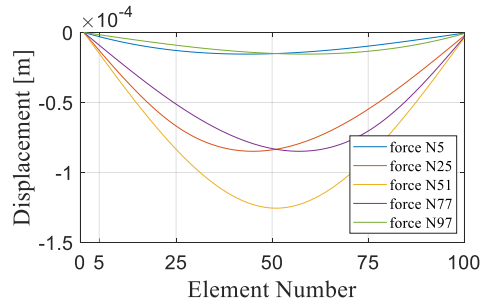
5.2 Static Analysis

5.2.1 d¹-index Damage Detection and Localization

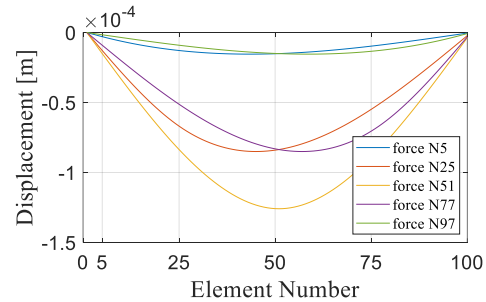
This section presents the results for the first two levels of SHM: detection and localization. Results are presented in terms of the d¹-index for the three studied beam types.

5.2.1.1 Simply Supported Beam

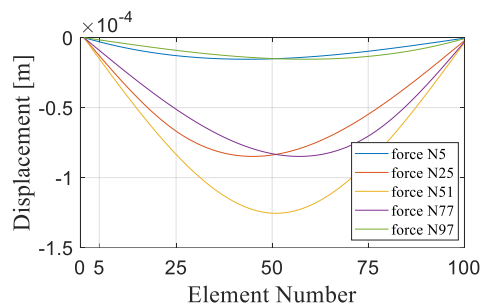
A simply supported beam, see Figure 4.1, has two supports, both enabling rotation in the x-y plane. Figure 5.2 (a) shows the displacement for a non-damaged beam for different positions of load application for a simply supported with 100 elements, each with a length of 10mm. The displacement is observed to be higher when the force is applied on the center of the beam. The same result was compared for different positions of damage, see Figure 5.2 (b-f). Damage was set 50% of the original elasticity module value.



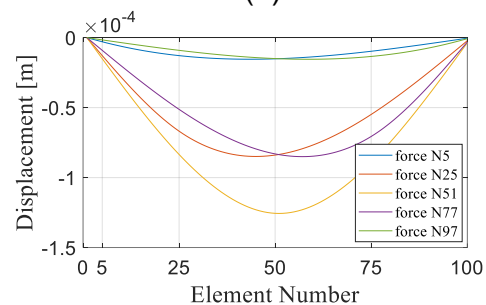
(a)



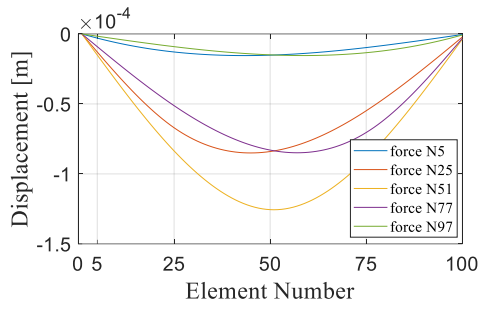
(d)



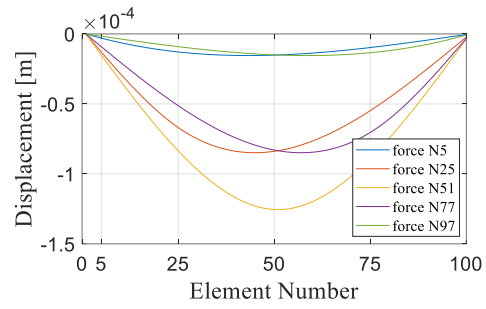
(b)



(e)



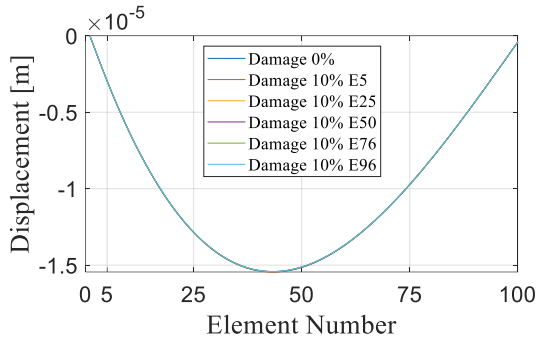
(c)



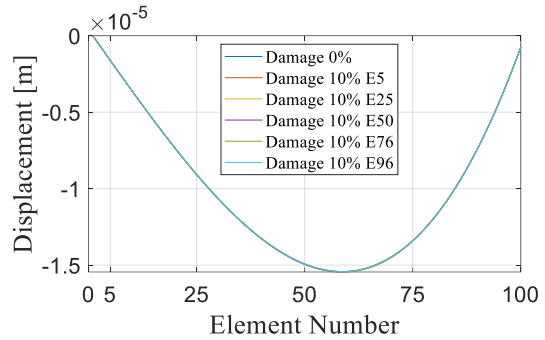
(f)

Figure 5.2. Beam displacement for the same load applied to different nodes with a (a) undamaged and damaged beams on elements (b) 5; (c) 25; (d) 50; (e) 76; (f) 96.

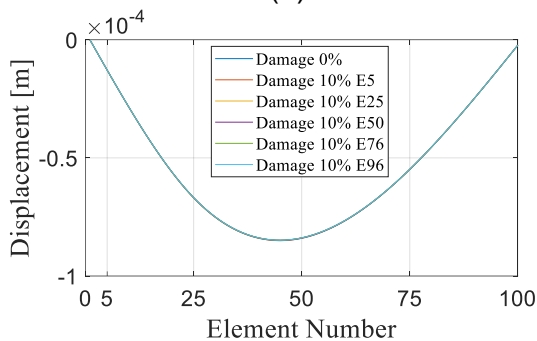
It is noticed from Figure 5.2 that the displacement function varies symmetrically based on the load location, in other words the displacement curve of a load 4 nodes distant from the supports, which is the case of N5 and N97, is mirrored. To enlighten this displacement behavior regarding load location, Figure 5.3 exhibits the displacement along the beam for different damaged elements.



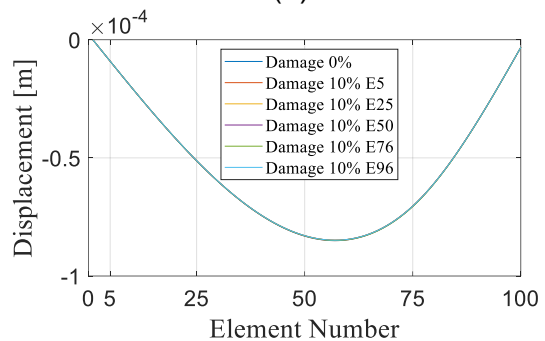
(a)



(b)



(c)



(d)

Figure 5.3. Beam displacement for the same load applied to different damaged elements; load was located on node (a) 5; (b) 97; (c) 25 and (d) 77.

The impact of the location where the load is positioned is observed. Figure 5.3 (a-b) shows displacement for loads on nodes 5 and 97 respectively. In comparison to (c-d), it is observed that in both cases the curve bends to the near-edge part of the beam, although this proximity to the supports is shown in the magnitude of the displacement, five times smaller when near to the supports. The graphics show that the damage location do not affect the displacement curve, only being sensitive to load location.

Ahead, the displacement data is now treated with the DWT – Discrete Wavelet Transform. Coiflets 2 wavelet mother at $J=1$ level of decomposition was adopted. Figure 5.4 shows the DWT coefficients resulted from the displacement data from load on nodes 5, 25, 77 and 97, for different damaged elements. Further, the damage severity was kept constant at 10%. Figure 5.4 shows the difference between a damaged and an undamaged beam $(d_d-d_0)^2$.

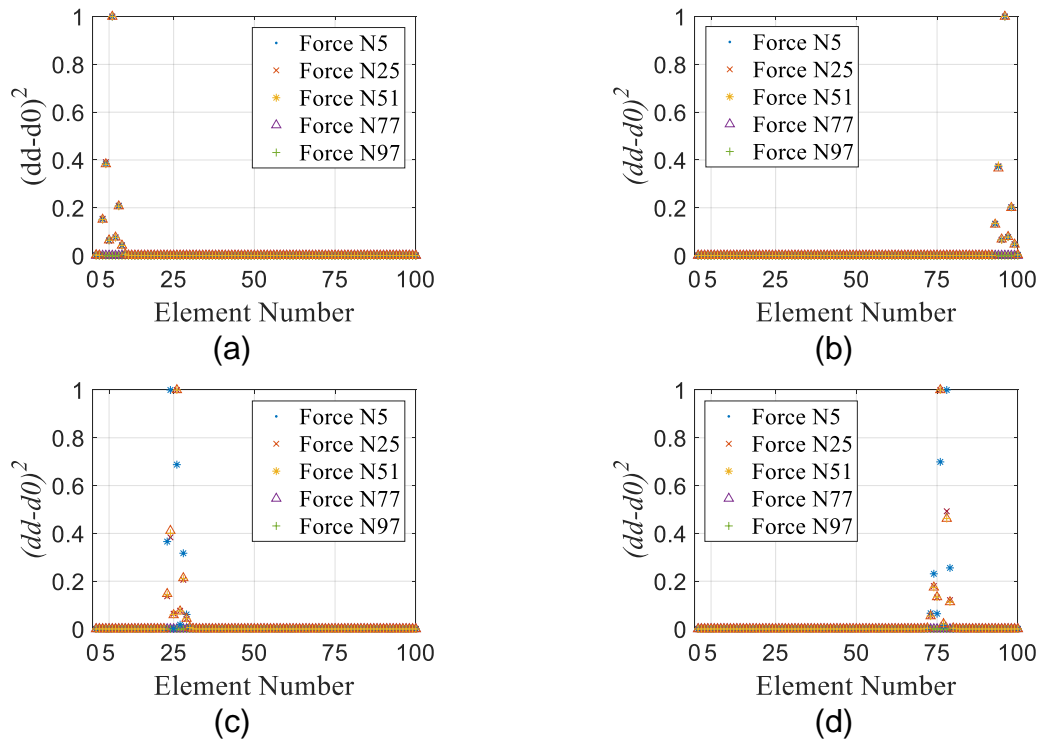


Figure 5.4. Squared difference of $(d_d-d_0)^2$ coefficients of displacement for the same load applied to different damaged elements: (a) 5; (b) 96; (c) 25 and (d) 76.

The analysis from Figure 5.4, shows the most likely damaged region. A cloud of points is clearly manifested along the damaged stretch. As expected, the coefficients are higher on the nodes next to the damaged element. Notice that the parts of the

graph where there is no damage, there are almost zero appearance of points, with non-significant value.

Continuing the investigation, Figure 5.5 shows d^1 -index as a function of the beam length, by using the boxplot tool, instead. Damaged elements were: 25, 50 and 76. Boxplot has many statistical indexes, between them the ones which led to the best results were the median and the box height (3rd quartile). Both indexes are disposed, in each column of Figure 5.5.

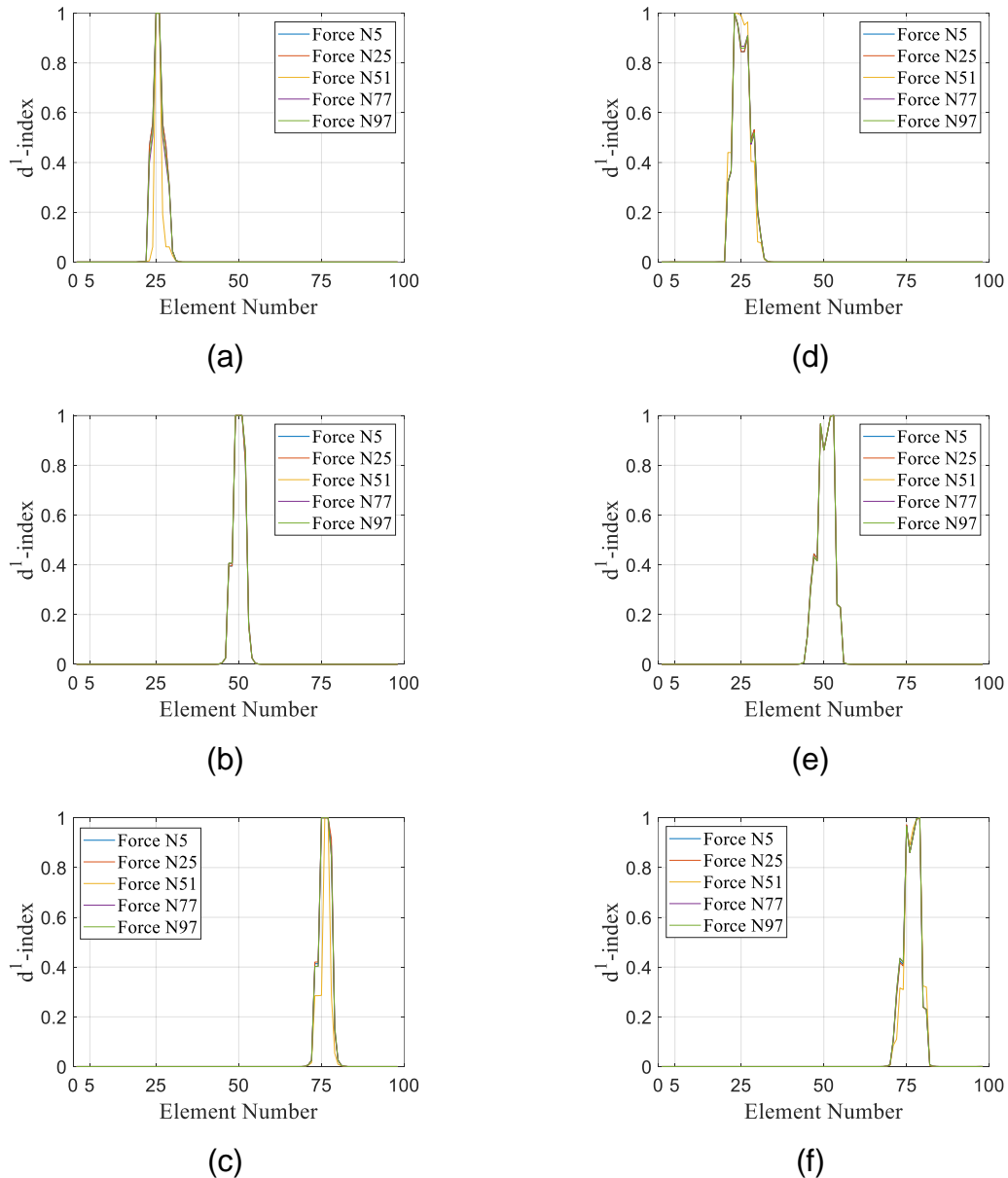


Figure 5.5. d^1 -index for simply supported beam for different load application point using COIF2, considering the: (a-c) median values; (d-f) box height.

Figure 5.5 (a-f) shows that the damage was successfully localized by both d^1 -index, the median and the box height. The point where the concentrated load was applied did not cause any affect in terms of location of the damage.

Moreover, many questions remain, such as the precision of the localization and the sensitivity regarding damage severity. A study regarding what is the wavelet decomposition level which best obtains the clearest results and the most adequate wavelet mother type. Section 5.2.2 presents a study on the influence of these damage localization parameters. Nonetheless, a detailed study on near-supports readings is needed while intense indicators have been noted.

5.2.1.2 Cantilever Beam

In this section and the following, two different cases of degrees of freedom at the support are presented. At first the cantilever beam is studied using the same wavelet mother and level studied before. To promote a thorough understanding of the problem we also applied the same load at different nodes. In Figure 5.6, the deflection of an undamaged cantilever beam is shown. Curves are displayed according to the point where the load is applied. For instance, curve named N25 is addressed to the load applied at node 25. Despite the different points of application, the load was constant at 1 Newton, while damage was applied on element 25 while the severity was set 10%.

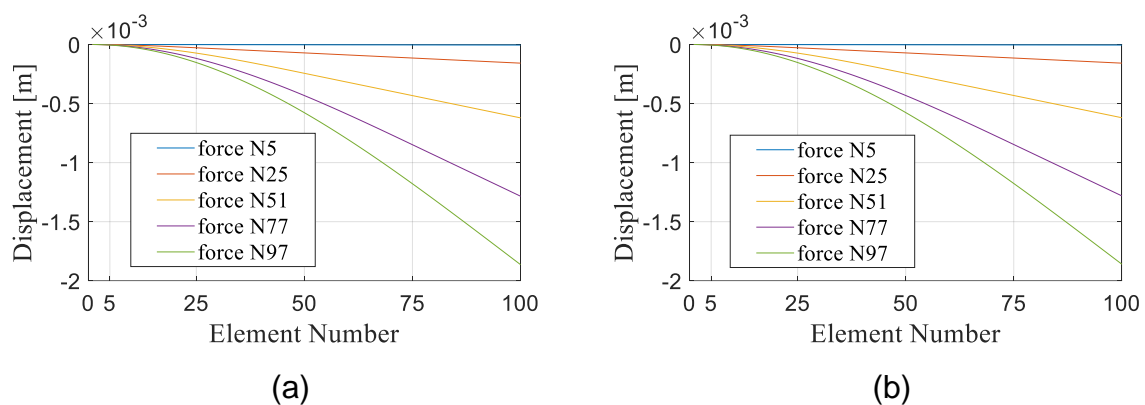


Figure 5.6. Analysis of beam displacement for distinct load application node for a cantilever beam (a) with and (b) without damage.

The deflection of a cantilever beam, Figure 5.6 (a,b), under punctual transverse load show two parts along its length with very distinct characteristics. The stretch from the fixed edge to the load application point deflects in accordance with the resulting bending moment, while the stretch from the load application point to the free edge has zero shear force and bending moment, resulting in an undeformed pattern. Therefore, it is expected that damage in this second stretch would not cause any differences in the total deflection curve of the damaged beam when compared to the undamaged one. Hence, damage can only be detected if applied to an element before the load location. For all cases of load application, simulations considered damage only in the part of the beam subjected to non-zero bending moment and shear force.

Figure 5.7 shows the d^1 -index distribution along the beam damaged in the element 25. Forces were applied at nodes 25 and 77. A case with damage in elements 25 and 76 is presented, for a Coiflets 2 wave at $J=1$, while damage severity remains 10%. Despite the displacement behavior being completely different for each beam, as seen in Figure 5.5, the application of DWT makes it possible to identify possible regions of probable damage.

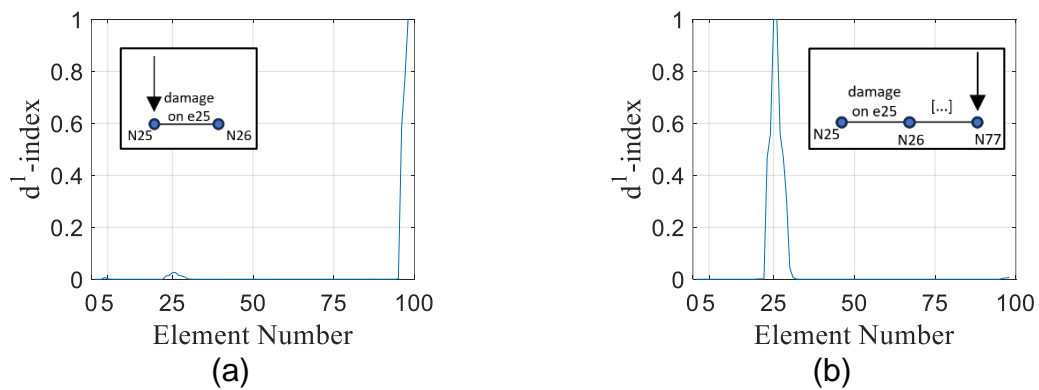


Figure 5.7. Damage localization for DWT coefficients for a cantilever beam with damage on element 25 for load location on node (a) 25 and (b) 77.

Figure 5.7 (a, b) shows two distinct behaviors. In the first case, the load was applied on node 25 and the damaged is on element 25, as well, it means that the node is located before the damaged element (see nodes and elements distribution in Figure 4.2). Such load configuration leads the stretch, where the damaged element is located, to undeformed pattern, due to the zero shear force and bending moment. In the second

case the load application force is the number 77 and the damage was applied on the element 25. To prove this fact, for the first case if to the load is moved one node, now to 26, which is located to the right of the damaged element, damage is identified. The reader must see that this time damaged element belongs to the stretch subject to bending moment and shear force, and therefore, deflects in accordance to these efforts. In short, only in the second case (Figure 5.7 b), the damage could be successfully identified and localized.

Ahead, Figure 5.8 shows another three examples, holding the damaged element location, at number 25, but varying the load positioning 5, 51 and 97, respectively. Again, for the first case, Figure 5.8 (a), the technique could neither identify nor locate the damage, but as the load go farther both identification and localization were successfully achieved.

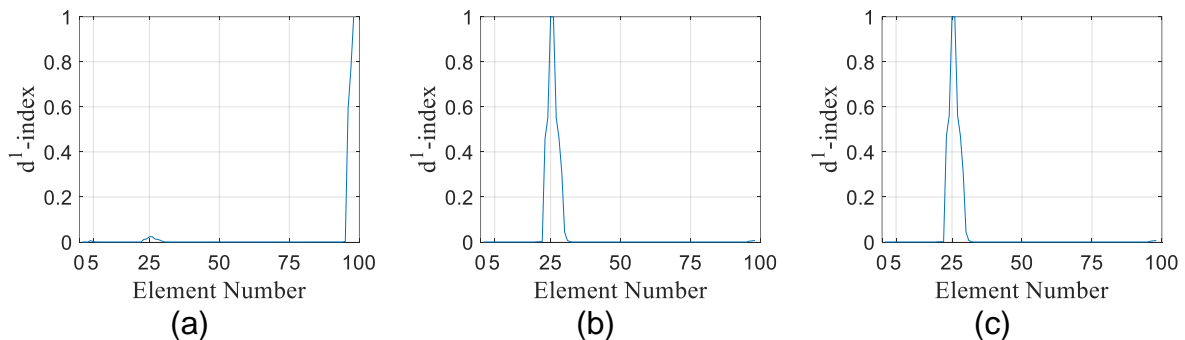


Figure 5.8. Damage localization for DWT coefficients for a cantilever beam with damage on element 25 for load location on nodes (a) 5, (b) 51 and (c) 97.

For the cantilever beam, damage localization was performed using the d^1 -index alongside boxplot tool approach in a damaged and undamaged beam. As for the simply supported beam, Coiflets 2 at $J=1$ level of decomposition produced the clearest readings. Figure 5.9 (a-e) shows the median values of d^1 -index distribution throughout the beam. For these results, the damage severity was kept constant of 10% of elasticity module, at elements $e = 5, 25, 50, 76$ and 96 . For each damage value, the same load was applied at nodes 5, 25, 51, 77 and 97 at once.

Damages at the vicinity of the clamping are very well detected, as in the case of Figure 5.9 (a), whose damaged element was the fifth one. It is verified that damage is well localized independent of the load location.

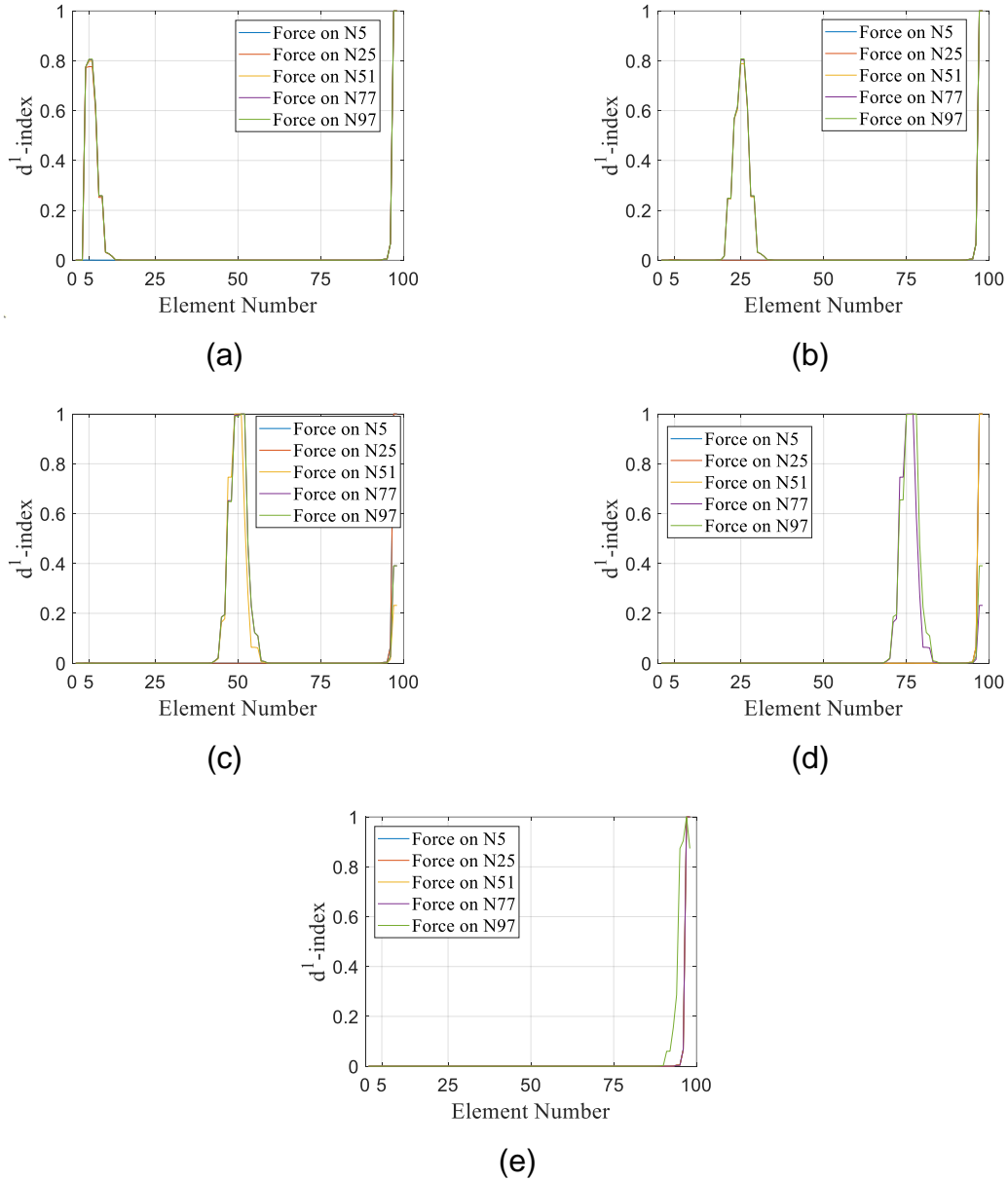


Figure 5.9. median d^1 -index distribution in a cantilever beam for a fixed damage and different nodes load application (a-e) damage at $e=5, 25, 50, 76$ and 96 , respectively.

However, higher coefficients of d^1 -index nearby the free border of the beam are noted on Figure 5.9 (a-e) for the cases of load positioned on the damaged stretch. Again, as observed in Figure 5.7 the part of the where the shear force and the bending moment are null, damage identification and localization is not precise.

5.2.1.3 Double-Clamped Beam

The double-clamped beam has a deflection similar to the simply supported but now with zero rotation at the supports ($\text{rot}_{xy} = 0$ at $x = 0$ and $x = L$). Mathematically, this corresponds to a continuous and smooth function with null first derivatives at the boundary points of its domain. Figure 5.10 illustrates the deflection curves for an (a) undamaged and a (b) damaged double-clamped beam for different load locations. Damage was put on element 25 with severity remaining at 10% and a 1 Newton load.

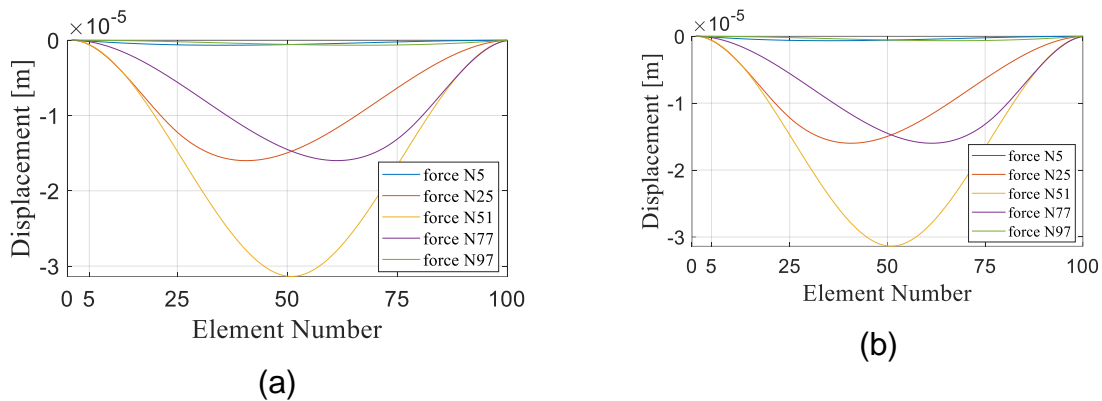
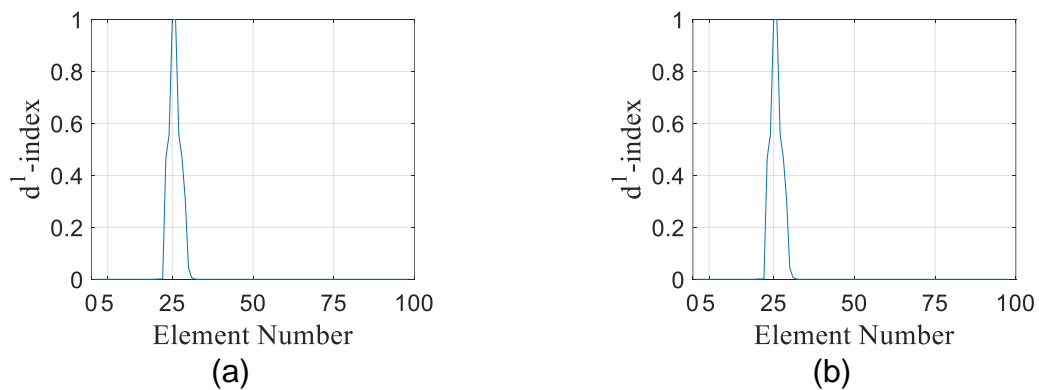


Figure 5.10. Analysis of beam displacement for distinct load application node for a double-clamped beam (a) with and (b) without damage.

Figure 5.11 (a-e) displays the difference between the d^1 -index. Damage was successfully localized on the damaged element 25, with no peaks at the endpoints, as observed for the cantilever. Thus, the damaged region was clearly identified by the method. Results are presented for a Coiflets 2 at $J=1$.



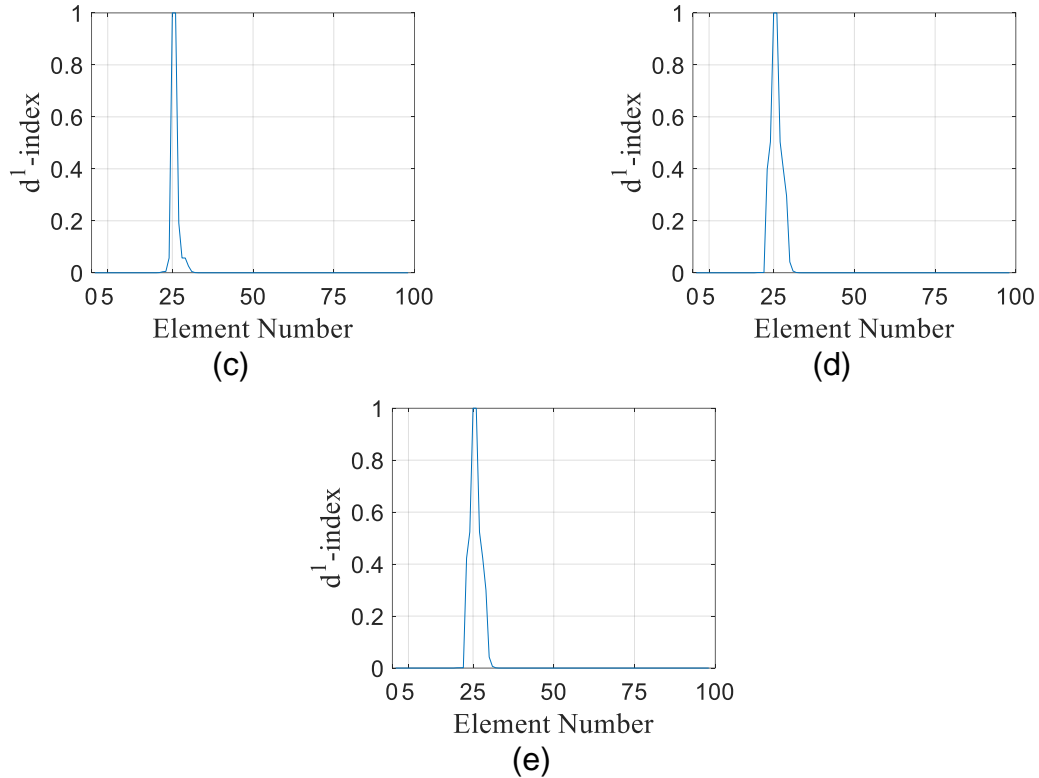
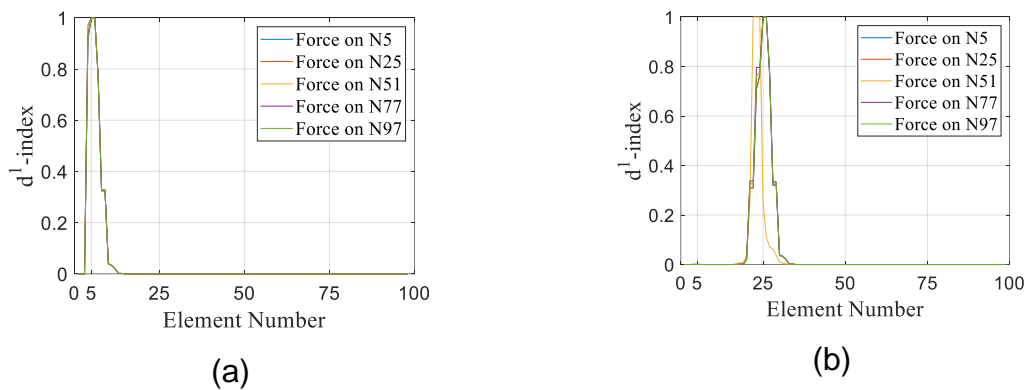


Figure 5.11. d^1 -index distribution of a damaged double-clamped beam at element 25 for load location of nodes (a) 5; (b) 25; (c) 51; (d) 77 and (e) 97.

As for the other beam types discussed, the analysis under the double-clamped shows that the method can detect the probable region of damage, regardless the load location. As in the previous cases, the d^1 -index was used to identify and localize damage on the double-clamped beam. Figure 5.12 (a-e) presents the median of d^1 -index distribution for different points of load application and damaged element. Again, the d^1 -index successfully localized the damaged element, no matter where the load or the damaged element was placed.



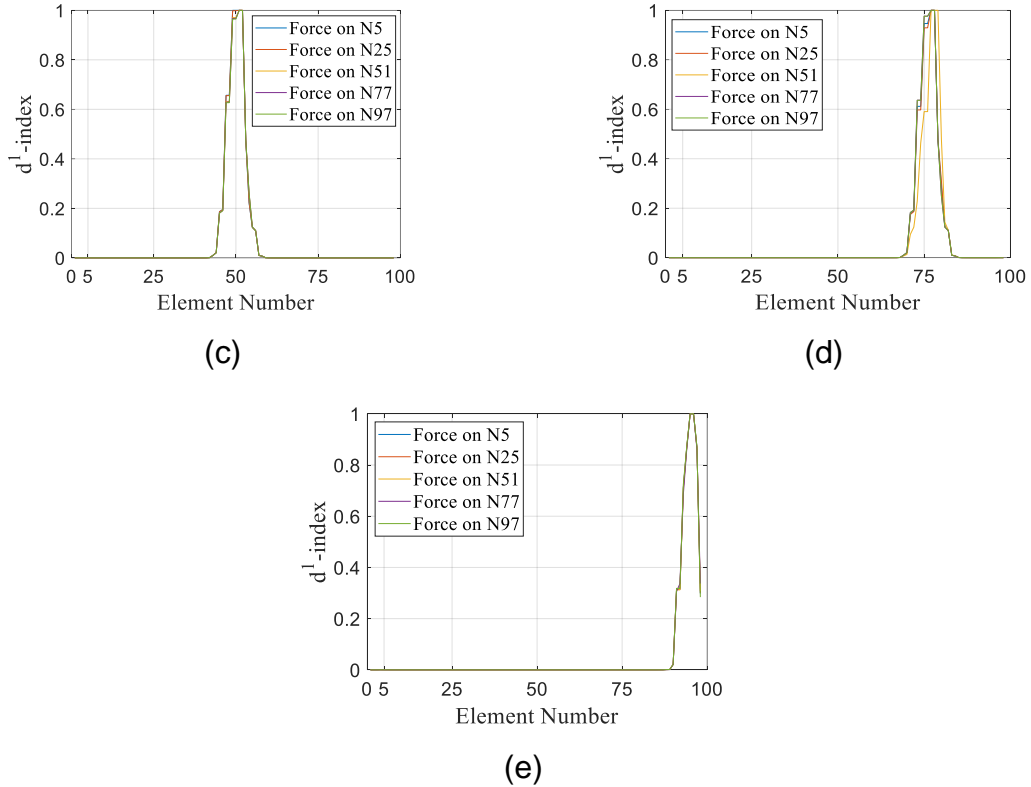


Figure 5.12. d^1 -index distribution in a double-clamped beam for a fixed damage and different nodes load application a-e) damage at $e=5, 25, 50, 76$ and 96 , respectively.

5.2.2 Influence of the Several Parameters of Damage Identification and Localization

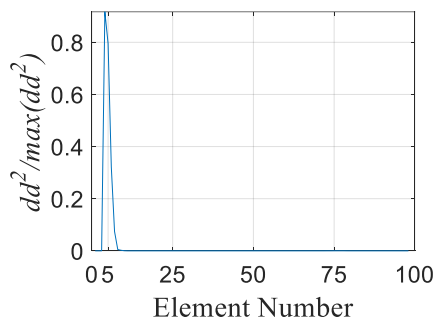
This chapter presents a study of influence of parameters of the wavelet transform with regards the damage identification and localization. Analysis is presented with the d^1 -index through the boxplot. The section investigates parameters such as: the use of a baseline function; damage severity (d_s); wavelet decomposition level; wavelet mother type; boundary conditions (beam support types); multiple damaged elements.

5.2.2.1 Baseline and Baseline-Free

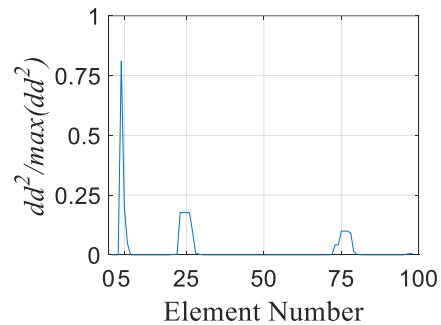
The use of a baseline value, obtained from an intact beam, to identify and localize damage is the matter of this section. As a rule, researchers have been using methods to detect damage which consists in comparing some characteristic of the intact and a damaged structure to identify and localize differences that can be associated to

damages. Solis and his co-authors Solis et al. (2013 and 2018), reported that damage detection can be greatly enhanced by the use of an appropriate baseline. Katunin et al. (2021) conducted comparative studies on the baseline approach. The authors observed that the baseline increases damage identification ability due to a reduction of the measured noise, which is a WT liability.

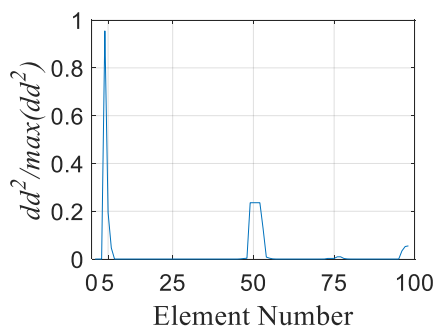
The intact curve is called a baseline function. The original d^1 -index localizes damaged through a difference between damaged and non-damage results ($d_d - d_0$), with this non-damaged being the baseline value. A baseline-free do not considers this d_0 value. Figure 5.13 presents the damage localization for a double-clamped beam with damage on element 76. Hence, results are presented in terms of $dd^2/\max(dd^2)$. Figures 5.13 (a-e) have loads applied on five different points of the beam. Results are presented for a Coiflets 2 with $J=1$. Damage severity was set 10%, while the load magnitude, 1 Newton. Non-baseline damage localization results shows that with the absence of the baseline it is not able to localize damage.



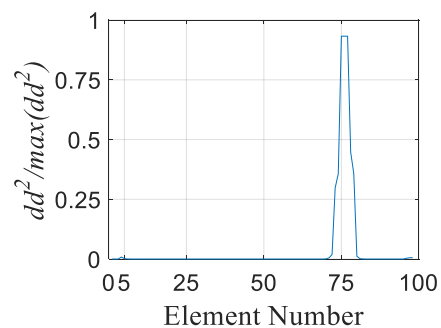
(a)



(b)



(c)



(d)

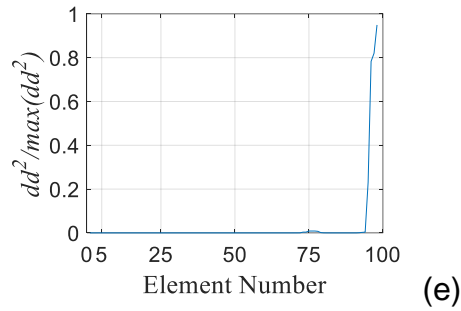


Figure 5.13. Double-clamped beam non-baseline ($d_d^2/\max(d_d^2)$) damage localization analysis for damaged elements (a) E5, (b) E25, (c) E50, (d) E76, and (e) E96.

In each of these cases, it is observed the presence of spurious peaks. Peaks seems to be placed around the vicinity of the node where the load was applied, see Figure 5.13 (a-c). The only location and identification that could be worth to notice was the case whose load was applied on the near-edge regions.

Figure 5.14 compares the damage identification and localization for a baseline and non-baseline analysis. The damaged element was the number 76. Both analyses were done by placing the load at different nodes at each test. Non-baseline graphic presents a confuse result, with diverse peaks indicating some possible locations for damage. The highest peaks are shown near supports region and for the specific case where load is applied at the vicinity of the damaged element (Force N 77). Figure 5.14 (a) presents damage localization through $d_d^2/\max(d_d^2)$, since it eliminates the baseline value of the intact beam. On the other hand, Figure 5.14 (b), which uses baseline for describing d^1 -index, exhibits a much clear and well-defined result of the damaged element. All the five curves have collapsed at the damaged region, without any false positive.

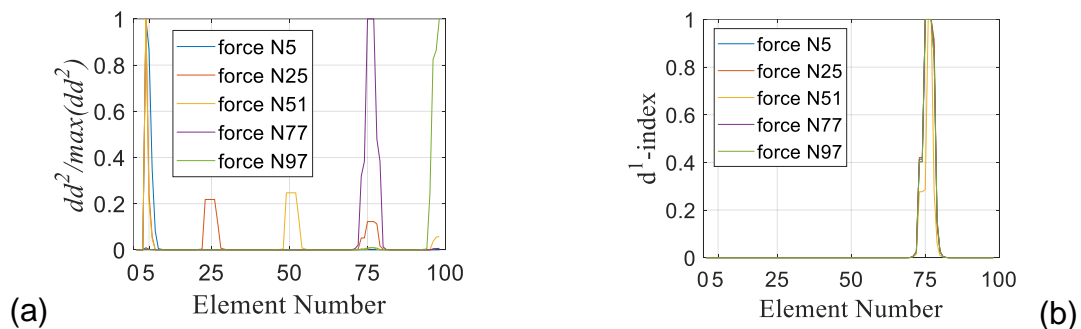


Figure 5.14. Double-clamped beam damage localization for a (a) baseline-free, and a (b) baseline considered simulation.

5.2.2.2 Damage Severity

The damage severity (d_s) influence was also target of this research. In this sense low severity damage was applied to elements. Figure 5.15 displays the d^1 -index using the boxplot for different levels of damage severity. Load location points were positioned at nodes 25 and 77, since these two are equivalent distant from the beam supports. Damage was simulated at element 25, decomposition level at $J=1$, and the wavelet mother type of choice was the Coiflets 2, while the damage severity was ranged from 10% of 50% of the elasticity module. Figure 5.15 presents this analysis for a Simply supported beam.

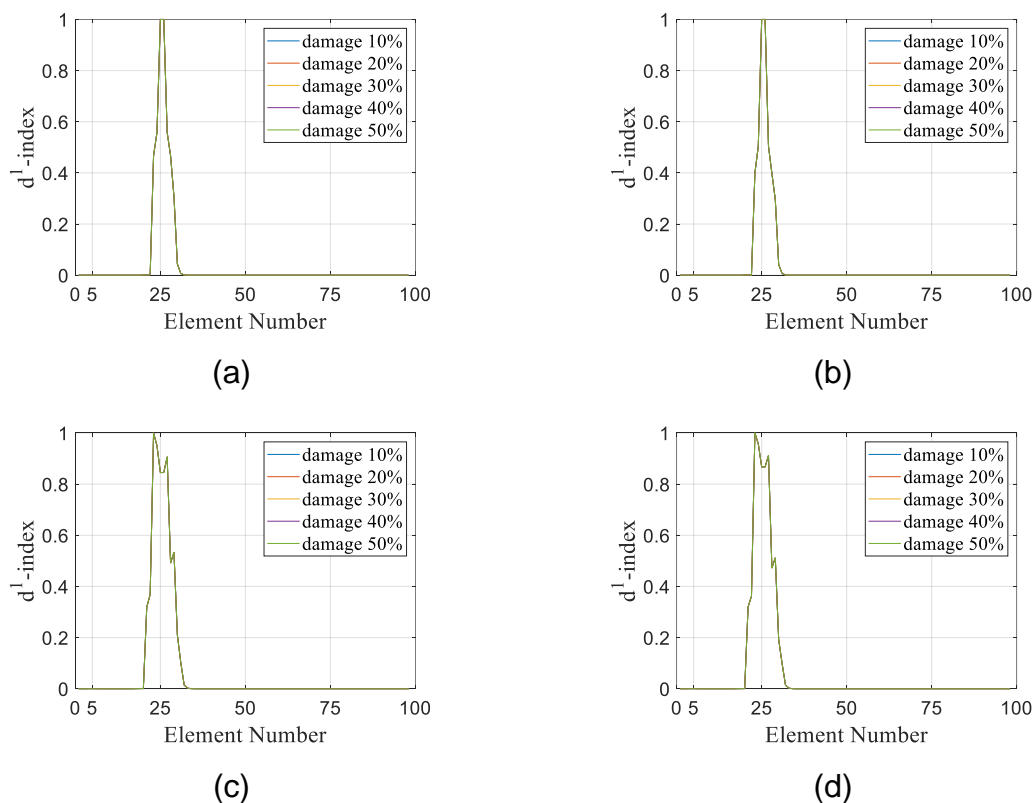


Figure 5.15. d^1 -index for a simply supported beam at different damage severity (10% up to 50%). (a-b) Median values of d^1 -index for load application at nodes 25 and 77. (c-d) Box height values of d^1 -index for load application at nodes 25 and 77.

The reader can see that the d^1 -index was able to localize the damaged element, using either the median of the height of the boxplot (meaning the difference between

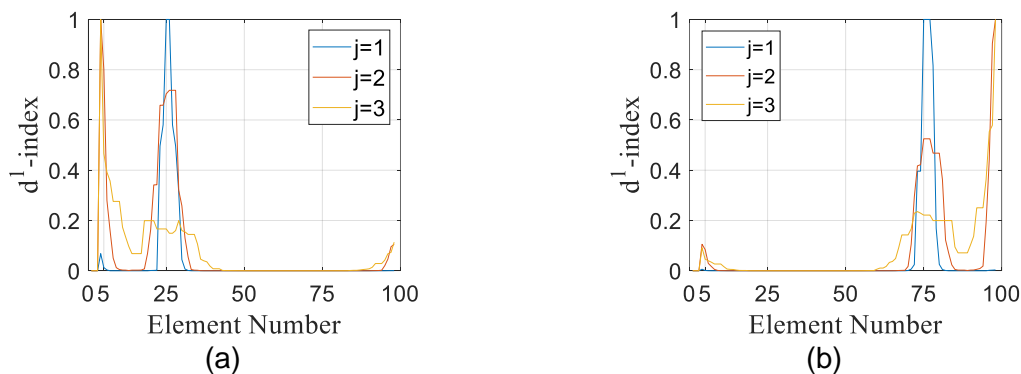
the 25th and 75th percentiles). Peaks of d^1 -index coefficient were seen at element 25, independent to damage severity. Further, it is worth to note that curves of the d^1 -index distribution were completely overlapped, no matter the severity of the damage (10% up to 50% of the elasticity module). However, again, the boundary condition plays important role on the d^1 -index distribution.

As seen for the comparisons between d^1 -index results, the severity of the damage did not show an impact on the detection of the region, so that the curve for the five levels of severity presented the same behavior. Thus, proving the method being able to detect small damage regardless of the severity of the damage on the load location.

5.2.2.3 Decomposition Level

This analysis starts from Figures 3.6 (a-b) where each level of decomposition results into a fraction of an approximation and a detail. This study focuses on the details. Each decomposition level is divided into details and approximations following Equations (3.30) and (3.31), for approximation and for detail, respectively. This fractioning means dividing an initial band of frequency in intervals of time-series so that for each level this frequency decreases, affecting the reading of the signal. This section aims to study the wavelet decomposition level “ J ” which obtains the clearest readings. This research investigates levels of “ J ” from 1 to 3.

Figure 5.16 compares these three levels of decomposition for the three studied beam support types. Damage was simulated on element 25 and element 76 with 10% of elasticity module reduction, while the magnitude of the load was set 1 N. Wavelet mother applied was the Coiflets 2. Load was applied as a punctual force on the center of the beam at node 51. The d^1 -index used was the median value through the boxplot.



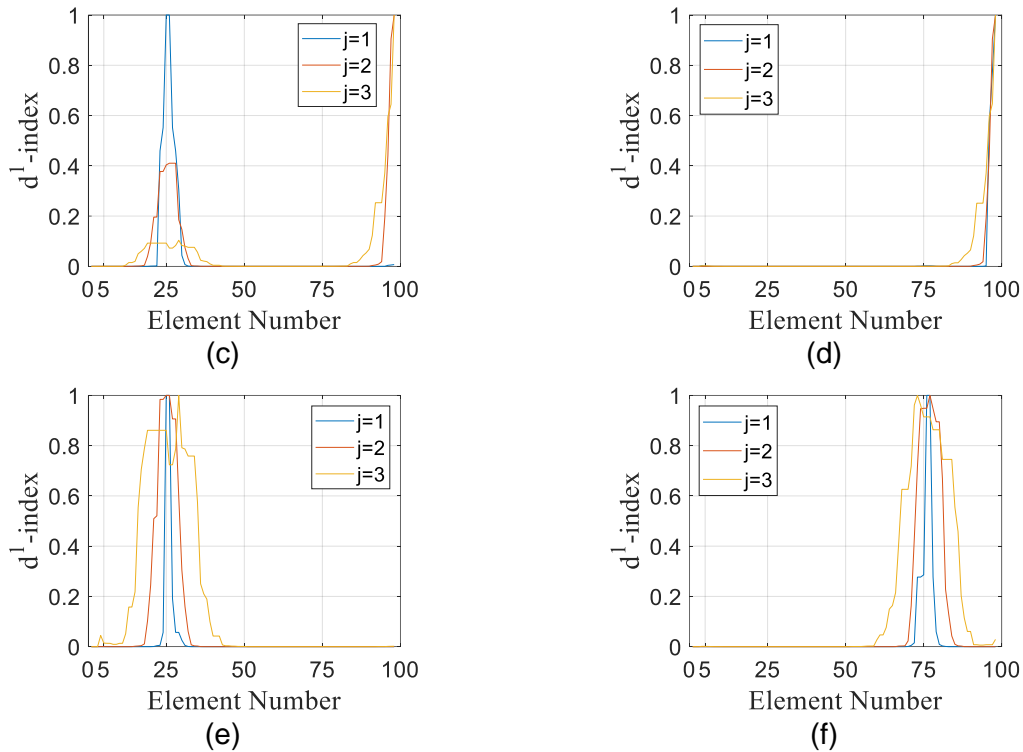


Figure 5.16. Test of influence of wavelet decomposition level “ J ” with damage on elements (a) 25 and (b) 76 for a Simply supported Beam; (c) 25 and (d) 76 for a Cantilever Beam; and (e) 25 and (f) 76 for a Double-Clamped Beam.

From the analysis it is noted that for higher levels of “ J ”, the method loses precision on determining the probable damage region. In Figure 5.16 (a), for a $J=1$ the damage is well seen at element 25 with marginal influence of the function near the support. In the same graphic but for $J=2$, there is an indication at element 25 but the function has higher values of d^1 -index near the support. For $J=3$ the analysis is poorer, where the index determines a probable region of damage between elements 5 and 30. The same is observed for Figures 5.16 (b,c,e,f), with the exception for (d) which is not able to detect damage but due to the bending moment of the beam.

To investigate the effectiveness of the “ J ” level on the near-supports region, Figure 5.17 repeats the same analysis from the previous graphic but for damaged elements being 5 and 96.

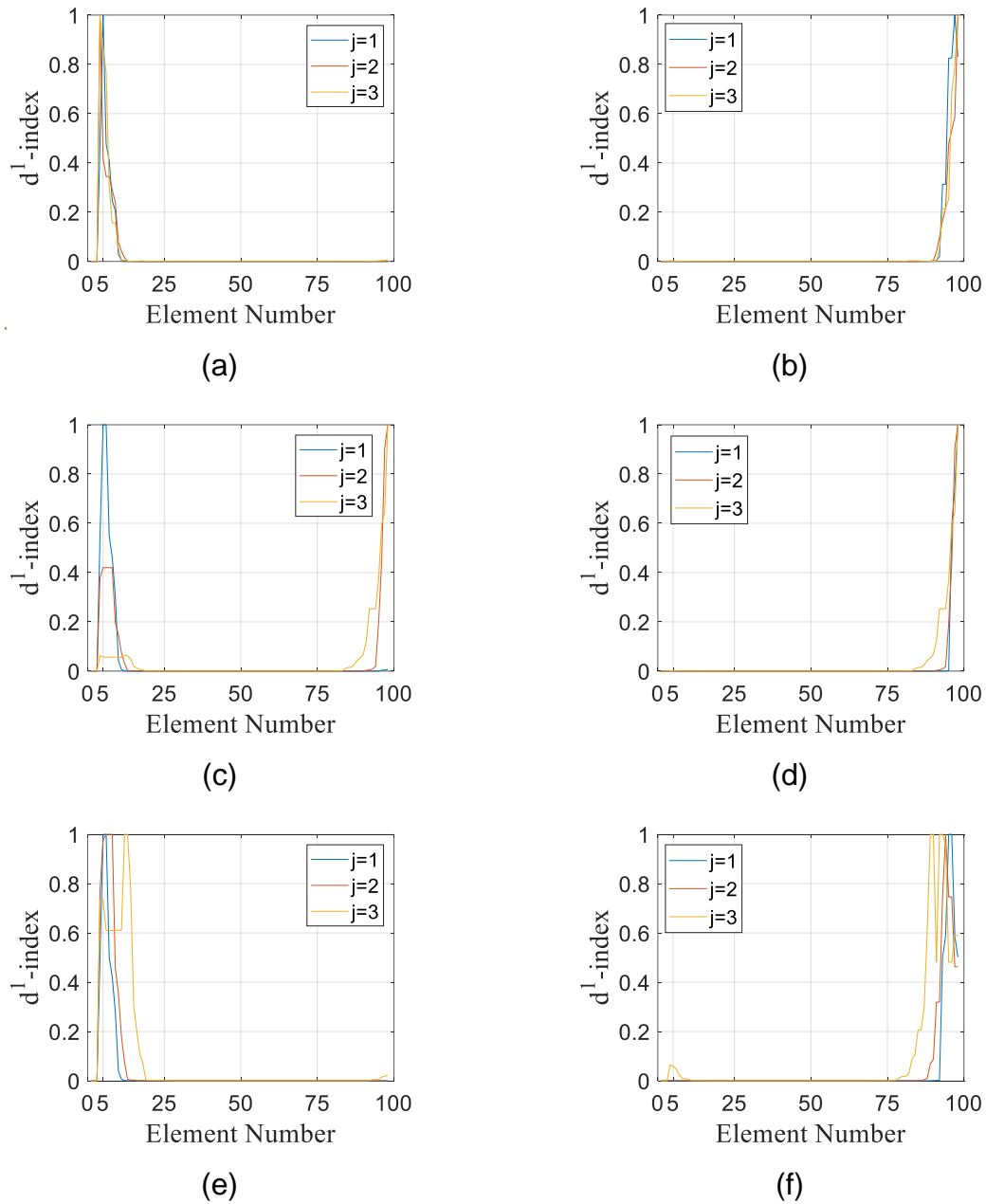


Figure 5.17. Test of influence of wavelet decomposition level “ J ” with damage on elements (a) 5 and (b) 96 for a Simply supported Beam; (c) 5 and (d) 96 for a Cantilever Beam; and (e) 5 and (f) 96 for a Double-Clamped Beam.

It is observed that the d^1 -index gives accurate damage detection readings but with the same comments of Figure 5.16. A new aspect is that for damage near supports, there is some confusion between the damage on the element itself and the appearance of the d^1 -index near the support as observed before.

The comparison between decomposition levels showed that a higher level of J does not localize damage with the precision of lower levels. The analysis shows that the $J=1$ decomposition level presented the best results, since for decomposition levels greater than 1, the d^1 -index distribution becomes scattered.

5.2.2.4 Wavelet Mother Type

In sequence, a study regarding the type of the wavelet mother was conducted. Katunin et al. (2021) states that damage detection regarding sensitivity and accuracy are strongly dependent on the wavelet mother type. As exposed on chapter 2.4, a wavelet is a windowing technique with variable sized regions. There are many types of wavelet mother type, also called families: haar, daubechies, coiflets, symlets and many others. Figure 5.18, 5.19 and 5.20 present a wavelet mother type analysis for a simply supported, a cantilever and a double-clamped beam respectively. Four wavelet mother types are compared, for a beam damaged on element 25. The force is applied at the center of the beam on node 51. Wavelet decomposition level was set $J=1$.

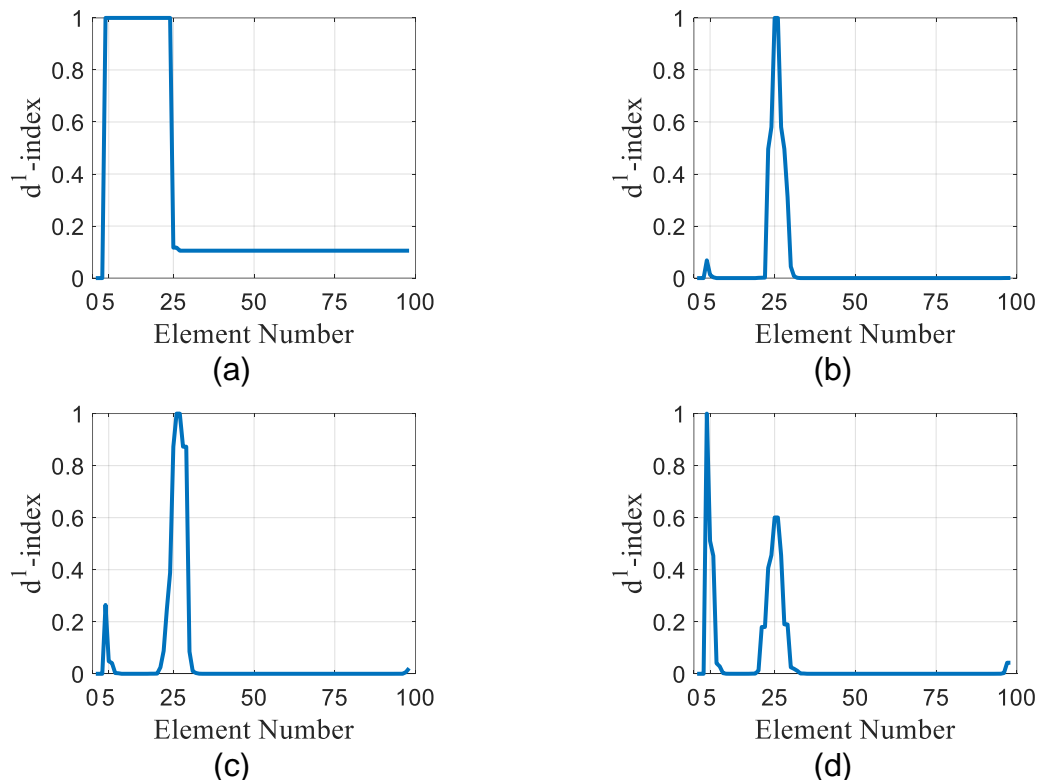


Figure 5.18. Wavelet mother type comparison for a simply supported beam with damage on element 25 for (a) haar, (b) coif2, (c) db5 and (d) sym8.

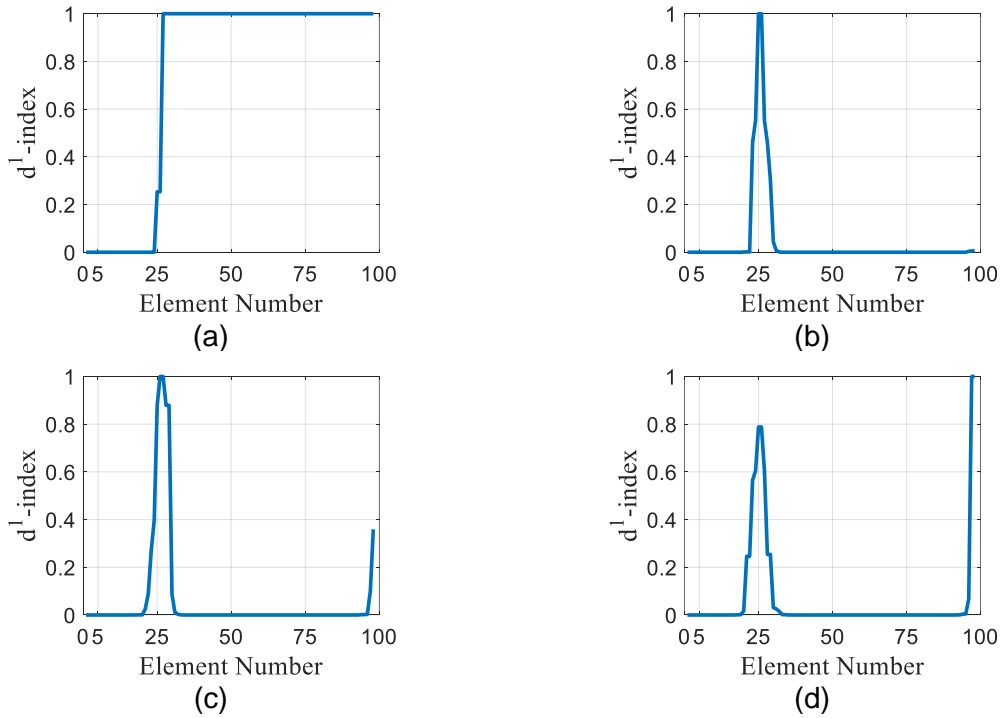


Figure 5.19. Wavelet mother type comparison for a cantilever beam with damage on element 25 for (a) haar, (b) coif2, (c) db5 and (d) sym8.

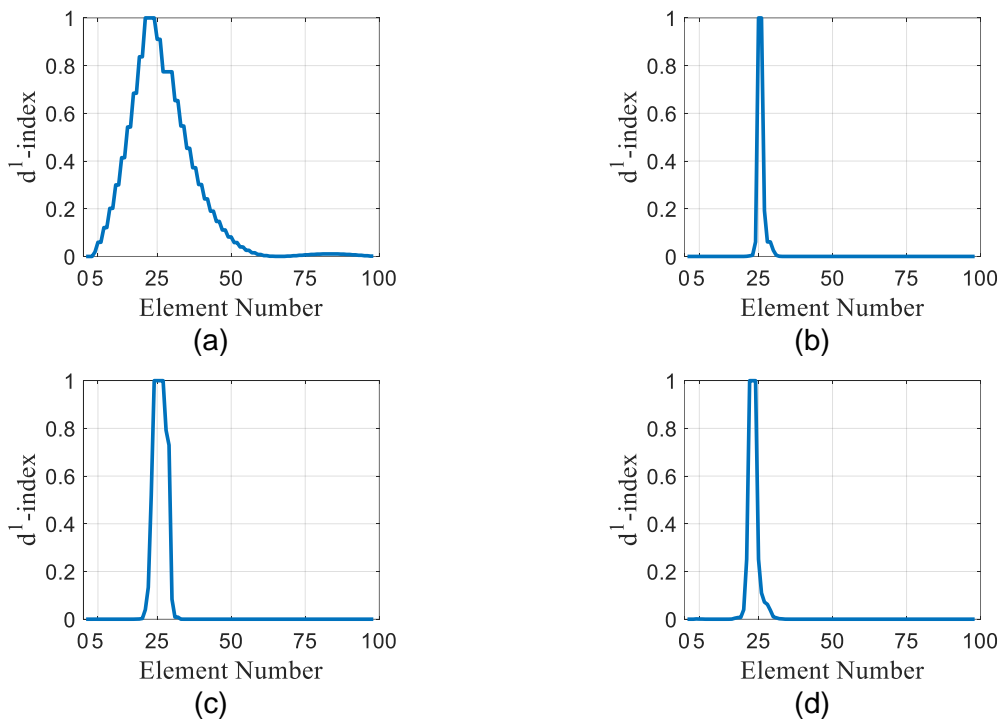


Figure 5.20. Wavelet mother type comparison for a double-clamped beam with damage on element 25 for (a) haar, (b) coif2, (c) db5 and (d) sym8.

Results shows greater precision for the Coiflets 2, regarding damage identification and localization, while for the other mother waves each had its disadvantages. Symlet 8 produced good results but with heavy influence of the supports, having d^1 -index coefficients on the near-edge region higher than at the actual damage location. The Daubechies 5 also presented the near-edge problem, but with lower intensity. While for Haar, localization was imprecise being unsuccessful to determine damage location.

Coiflets 2 was the wavelet mother type which presented the best results, this being the one which developed the clearest readings on the damaged element. At the same time, this wavelet mother presented the results with the lowest coefficients of the d^1 -index values on the near-supports region.

5.2.2.5 Boundary Conditions Influence on the Coefficients Near the Supports

This section presents a study of influence of the support type of the beam. Wavelet decomposition level and wavelet mother type have shown great influence on how the function develops on this region.

Figure 5.21 presents damage identification and detection for near-supports region for the three different types of boundary conditions. The Wavelet mother is Coiflets 2 with DWT decomposition at $J=1$. Load is applied as a punctual force on nodes 5, 25, 51, 77 and 97. Two cases of damage are investigated, on element 5 and 25. As one can see, Figure 5.21 shows damaged element is quite well identified and localized, regardless the kind of support. A very small coefficient peak appears at the wrong localization for a simply supported case, Figure 5.21 (b), but the damage localization is clear. For a double-clamped case (Figure 5.21 e and f), the identification and localization are even better, no spurious peak is seen. In the case of the cantilever beam, Figure 5.21 (c and d), the spurious peaks are in those cases whose load is out of the damaged stretch, as said in the previous section.

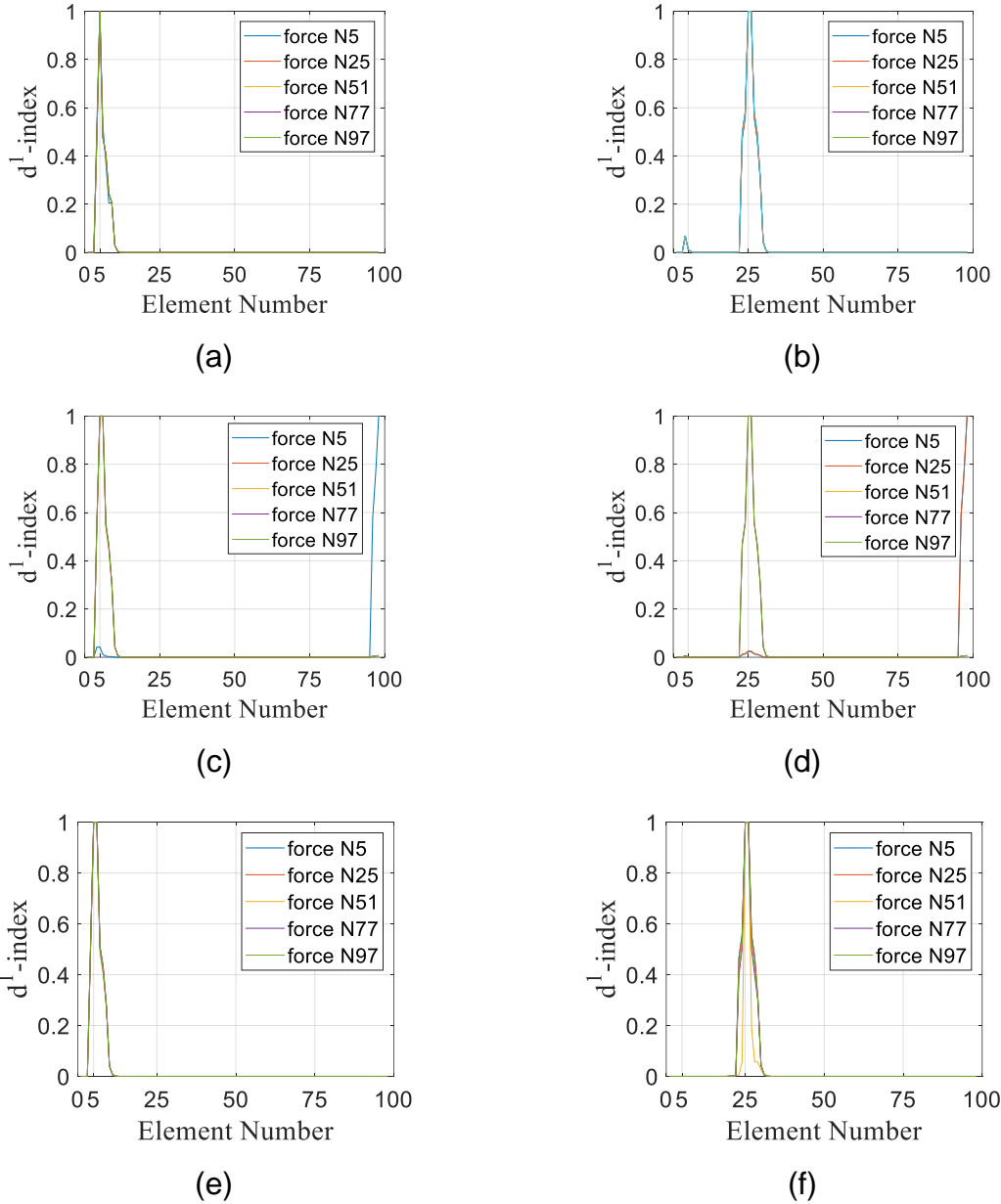


Figure 5.21. Comparison of boundary conditions influence on the d^1 -index coefficients with damage on elements (a) 5 and (b) 25 for a Simply supported; (c) 5 and (d) 25 for a Cantilever; and (e) 5 and (f) 25 for a Double-Clamped Beam.

5.2.2.6 Multiple Damaged Elements

This section analyzes the cases involving two simultaneous damaged elements. Figures 5.22 exhibits the damage identification and localization for a double-clamped beam damaged at different elements at once. The degree of the severity of the damage is also different. Five different beams set are studied: (a) case 1: 15% damage

on element 25 and 35% on element 76; (b) case 2: 35% damage on element 25 and 15% on element 76; (c) case 3: 10% damage on element 25 and 10% on element 76; (d) case 4: 10% damage on element 25 and 15% on element 76; (e) case 5: 10% damage on element 50 and 40% on element 96.

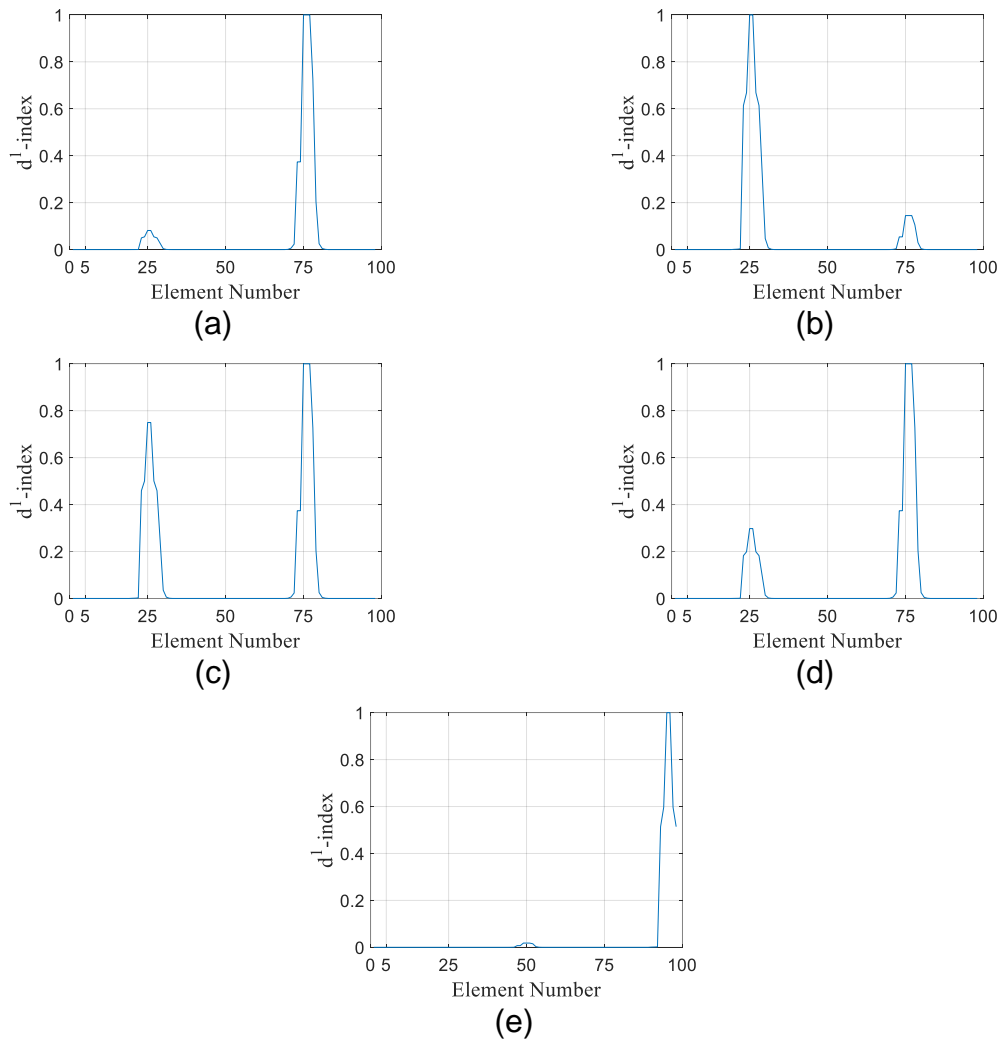


Figure 5.22. Damage localization for double-clamped beam with multiple damaged elements. (a) case 1; (b) case 2; (c) case 3; (d) case 4; (e) case 5.

From the observations a pattern is not distinguished, despite the fact that the damaged element is successfully identified and localized in most cases, except for the result presented by Figure 5.22 (e) where the peaks are not seen proportional to the damage imposed to the element. For instance, the damage of 10% imposed to element 50 barely appears. For this research, further investigations consider a single damaged element at a time.

5.2.2.7 Distributed Loads

The same analysis conducted on section 5.2.1 is now presented for Distributed loads, for the three analyzed beams. The load, 1 Newton per meter, was distributed along the 100 elements. Damage was defined on element 76 with a severity of 10%. Figure 5.23 presents damage localization on both elements 25 and 76 for a simply supported, a cantilever and a double-clamped beam. The results show great precision on damage localization, as found during concentrated load investigations.

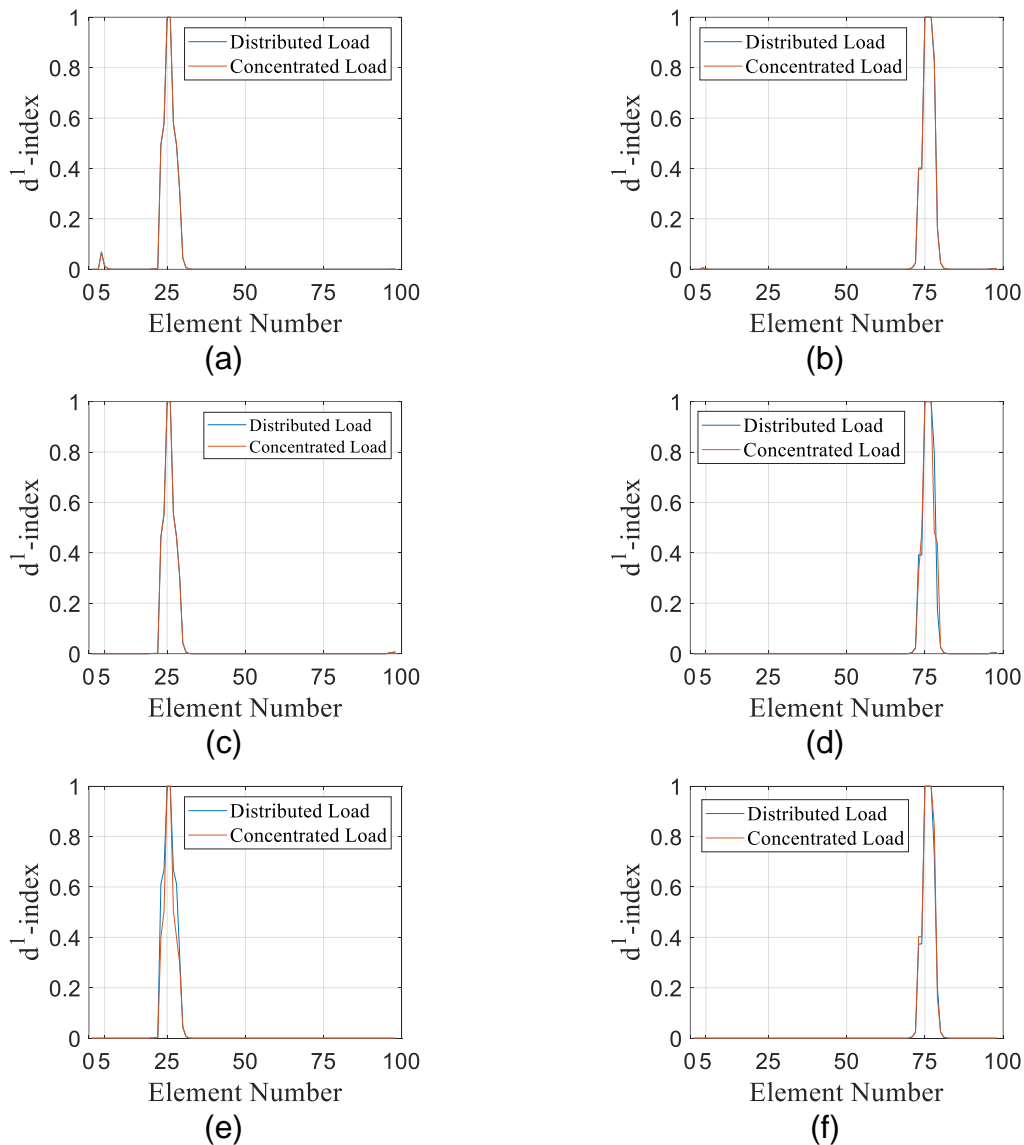


Figure 5.23. d^1 -index damage localization for distributed loads for a simply supported beam with damage on elements (a) 25 and (b) 76; and for a cantilever at elements (c) 25 and (d) 76; and for a double-clamped beam at (e) 25 and (f) 76.

5.3 Modal Analysis

This section presents the dynamic part of the investigation, based on the mode shapes of the structure.

The current approach for identifying and locating damage was also used in modal analysis, where the vibration patterns of both damaged and non-damaged beams were utilized to calculate the d^1 -index.

The FEM followed the same discretization of the static analysis is used. On the other hand, no external loads were necessary for the analysis, the distribution of coefficients was presented based on element numbers and mode shapes. The methodology focused on the first five vibration mode shapes, using wavelet mother Coiflets 2, decomposed at level $J = 1$.

5.3.1 Mode Shapes Analysis

The structure of this section disposes three sub-sections for each beam, while containing the results of the follow analysis for identification and localization of the damaged element:

- i. The influence of the support types;
- ii. The influence of the baseline;
- iii. Influence the mode shape
- iv. Elements 5, 25, 50, 76 and 96 were the damaged element considered for the analyses;

5.3.1.1 Simply Supported Beam

Figure 5.24 presents the first five mode shapes for the simply supported beam. It presents the results for the complete range of damage severity of this research. Damaged element simulated was the 76. It is noted that the curves had no impact in their shapes, regardless how much the damage severity is.

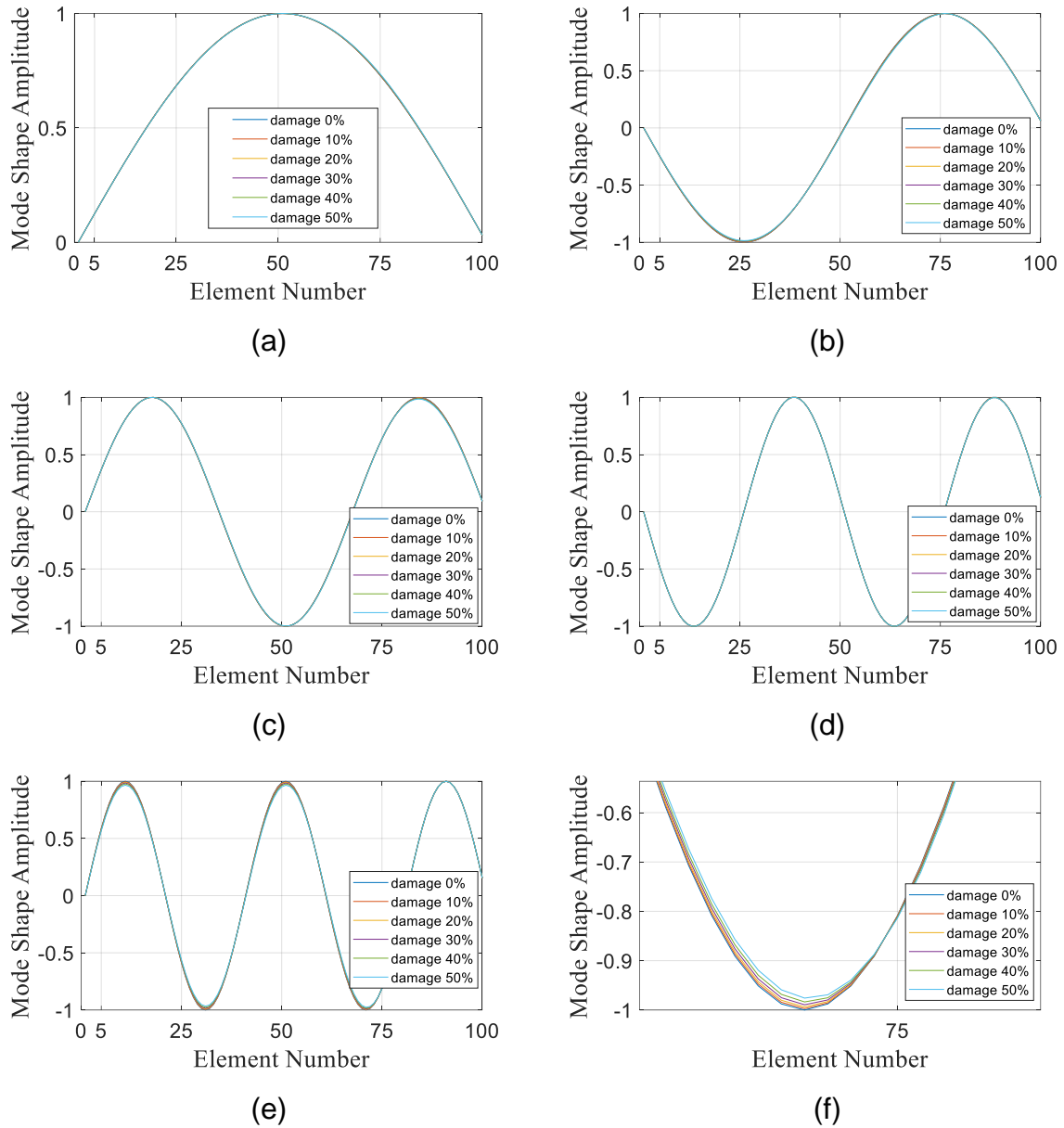


Figure 5.24. Simply supported beam (a) 1st, (b) 2nd, (c) 3rd, (d) 4th, (e) 5th, mode shapes for a damage severity range from 0% to 50%; (f) 5th mode shape approximated peak.

Figure 5.25 presents the first five modes but varying the damaged element. Damage was kept at 10% severity. It is observed through the results that the location of the damage is also unimportant for the mode shapes.

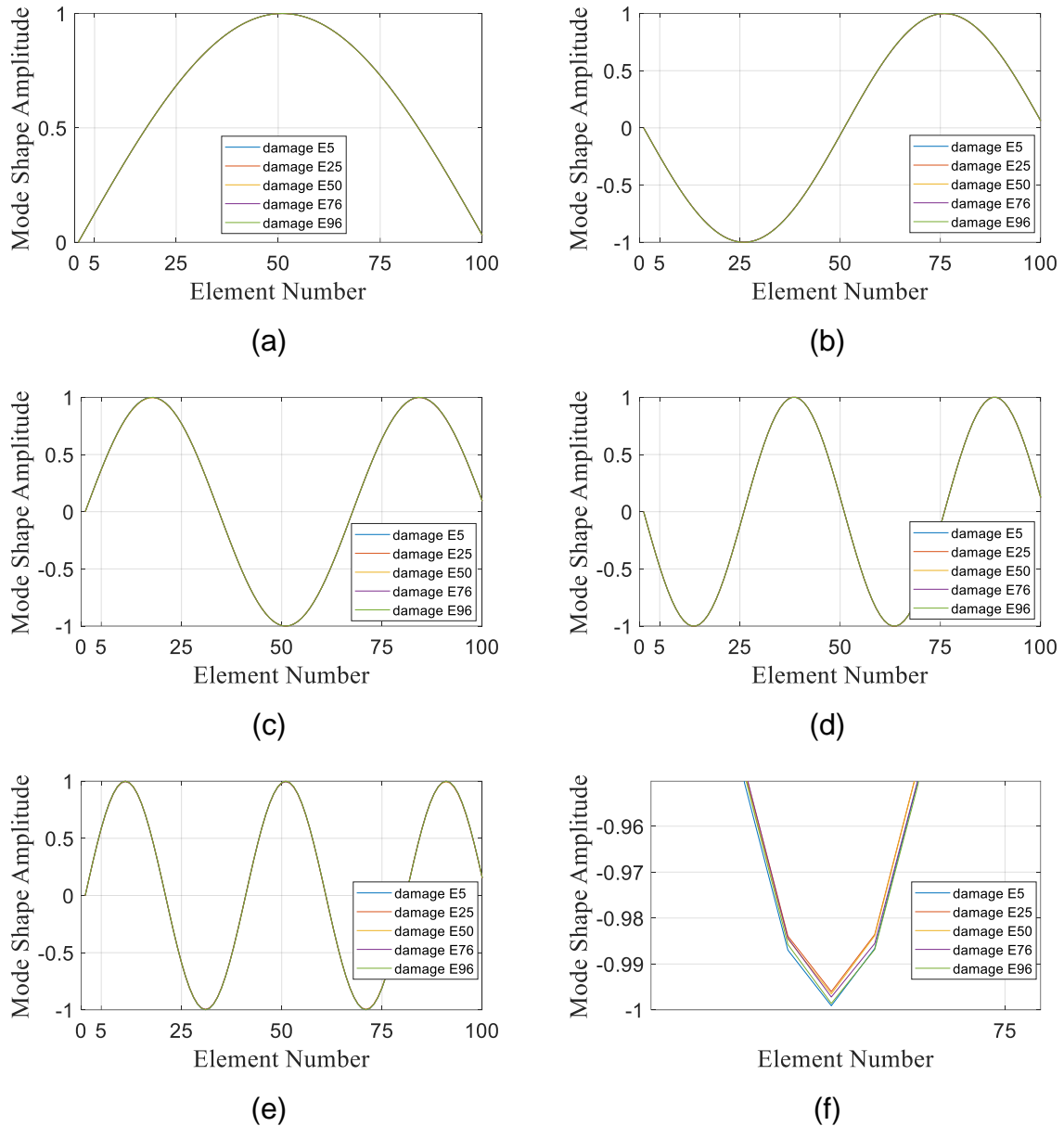


Figure 5.25. Simply supported beam (a) 1st, (b) 2nd, (c) 3rd, (d) 4th, (e) 5th, mode shapes for five different damaged element locations; (f) 5th mode shape approximated peak.

Damage localization is presented in Figure 5.26. Damage severity was kept 10%. It shows that, as well as for the static analysis, this method is capable to identify and locate damage with great precision independent of the analyzed mode shapes and damage location. All mode shapes were able to locate the correct position of damage.

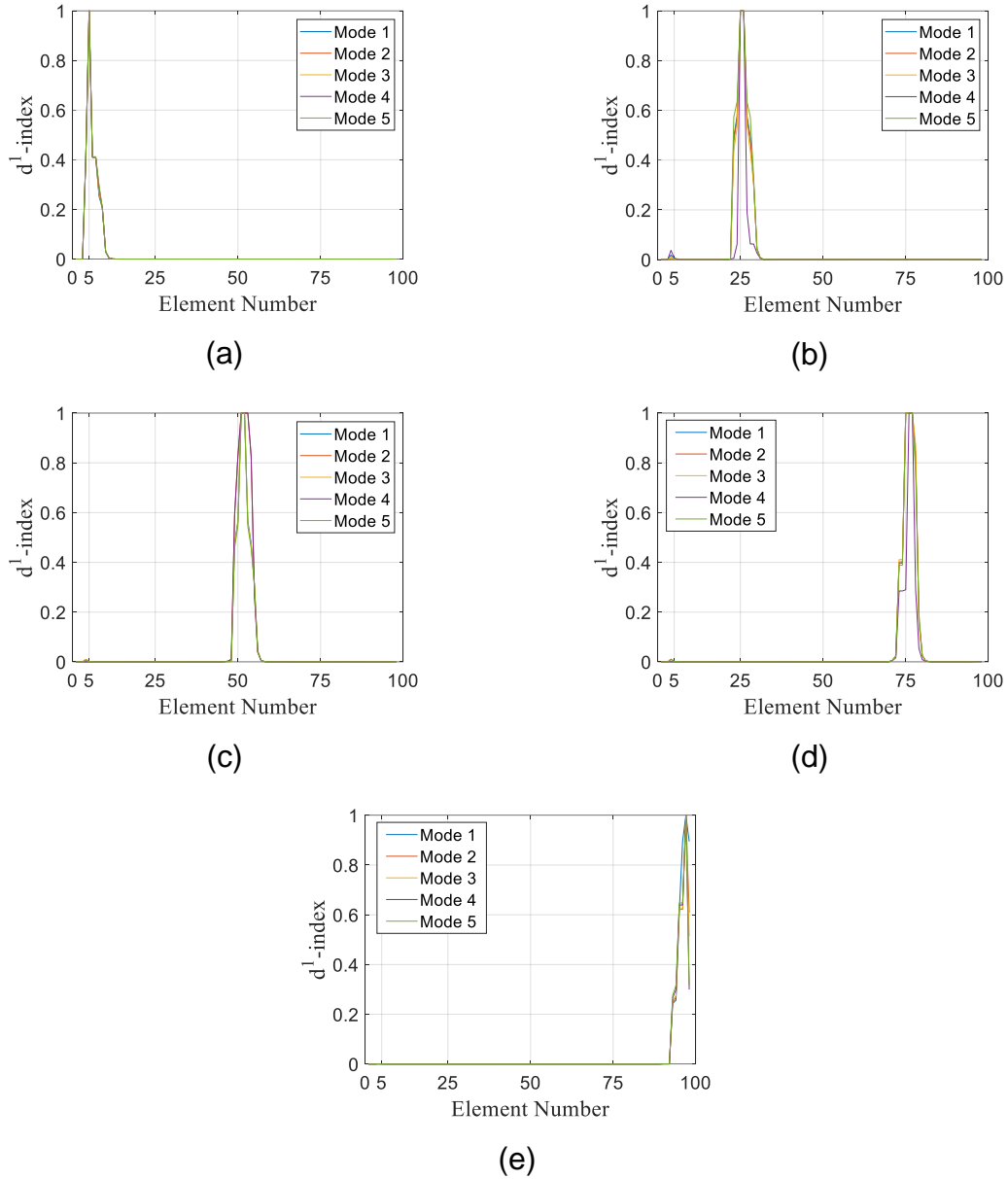


Figure 5.26. Damage localization for the Simply supported beam for damaged elements (a) E5, (b) E25, (c) E50, (d) E76, (e) E96.

The investigation of the effectiveness of the baseline on the damage identification and localization was also made for the modal analysis. Figure 5.27 presents damage localization without the baseline.

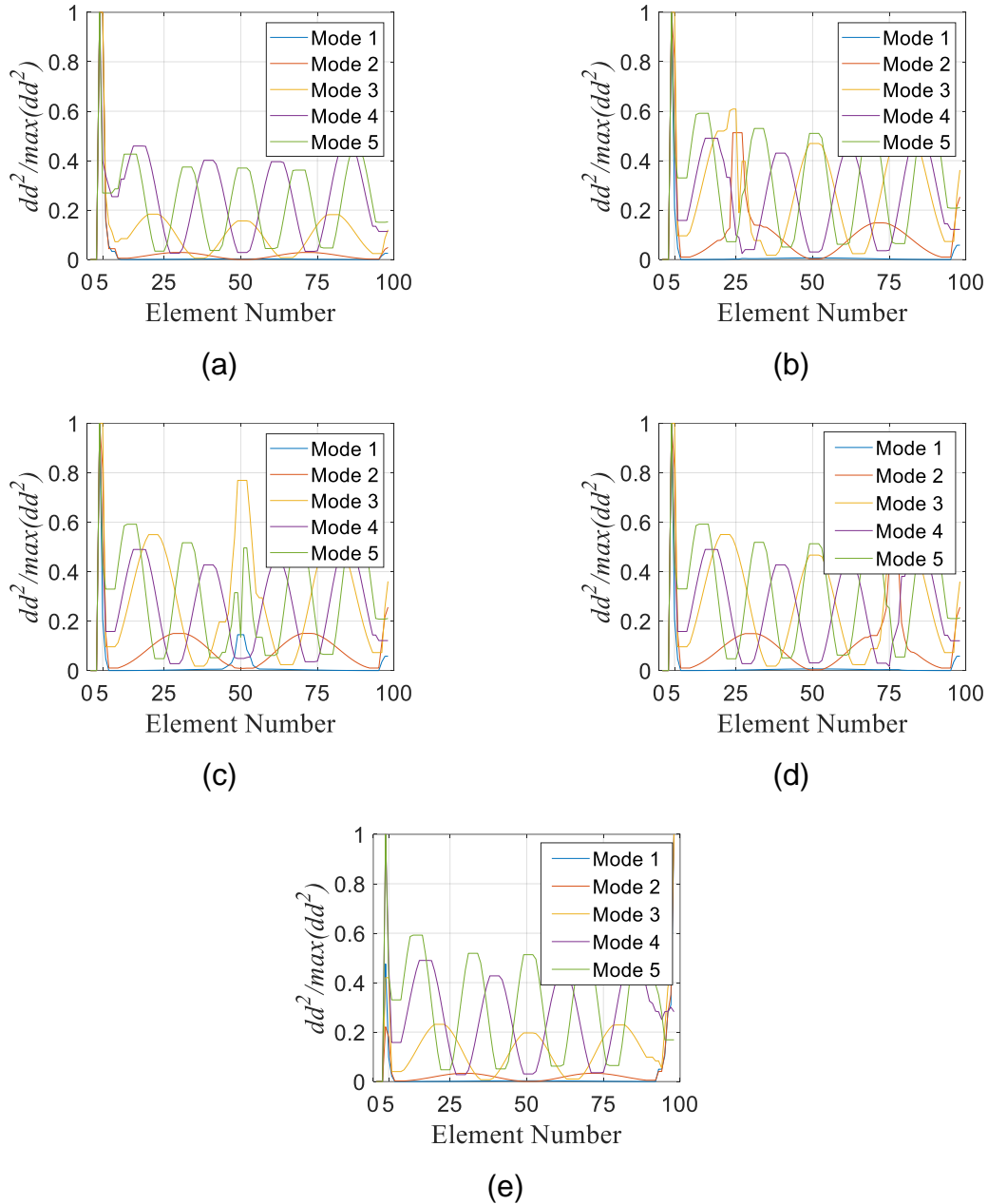


Figure 5.27. Non-baseline damage localization for the Simply supported beam for damaged elements (a) E5, (b) E25, (c) E50, (d) E76, (e) E96.

The results for the simply supported beam show that the absence of a baseline do not result into a conclusive analysis, as seen on Figure 5.27. On the other hand, the method is very effective when using a baseline, as presented on Figure 5.26. So, the use of a baseline enabled the identification and localization of damage for all the mode shapes analyzed.

5.3.1.2 Cantilever and Double-Clamped Beams

This section presents damage identification and localization for a simply supported based on mode shapes. Figure 5.28 (a,c) dispose the first mode shapes for the cantilever, while Figure 5.28 (b,d) for the double-clamped beam. From the analysis, one observes that damage severity does not affect the results, as well as damaged element location.

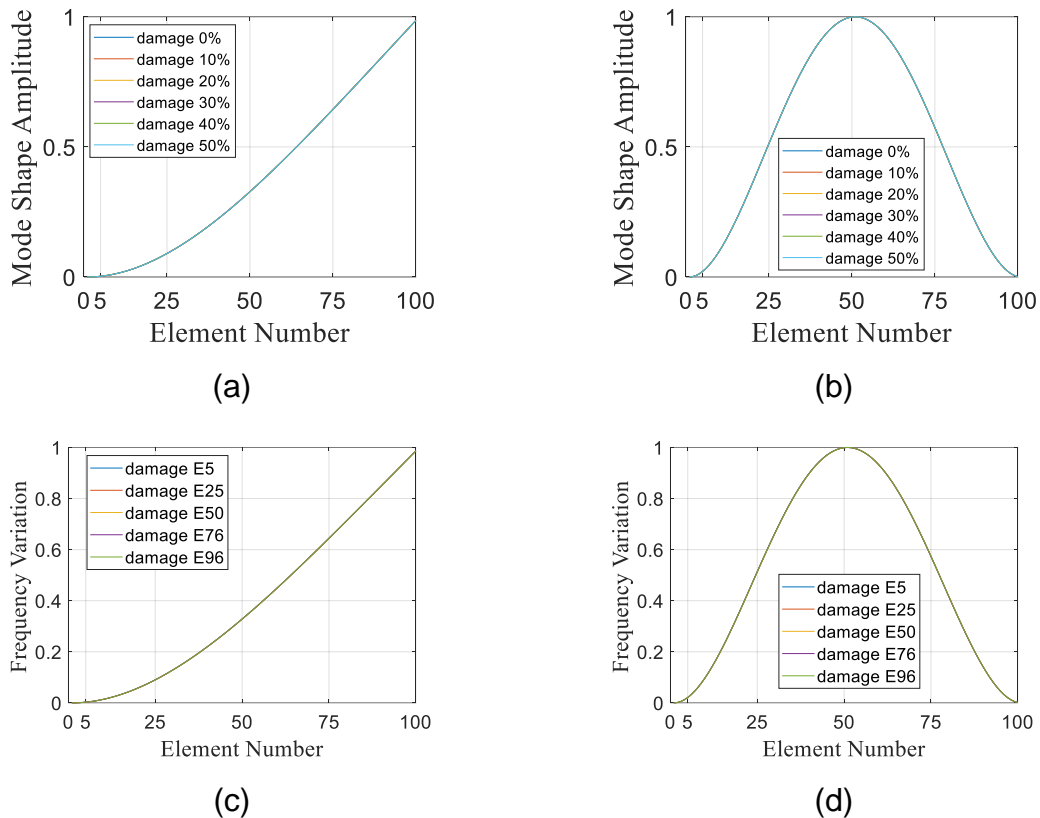


Figure 5.28. Vibration mode shapes (a and c) 1st mode for the cantilever beam. (b and d) 1nd mode for the double-clamped beam.

Moving on, Figure 5.29 disposes the damage localization with a damage severity of 10%. As for the simply supported, it shows that the method is capable to locate damage with good precision independent of the mode shapes analyzed and damage location. For all vibration mode shapes, d^1 -index was able to locate the correct position of damage with precise peaks and did not present the edge-effect near the supports. An advantage that must be noted is, since no loads are required to produce modal

analysis the d^1 -index distribution did not show any spurious peak due to the load positioning, as found in the static case for punctual loads.

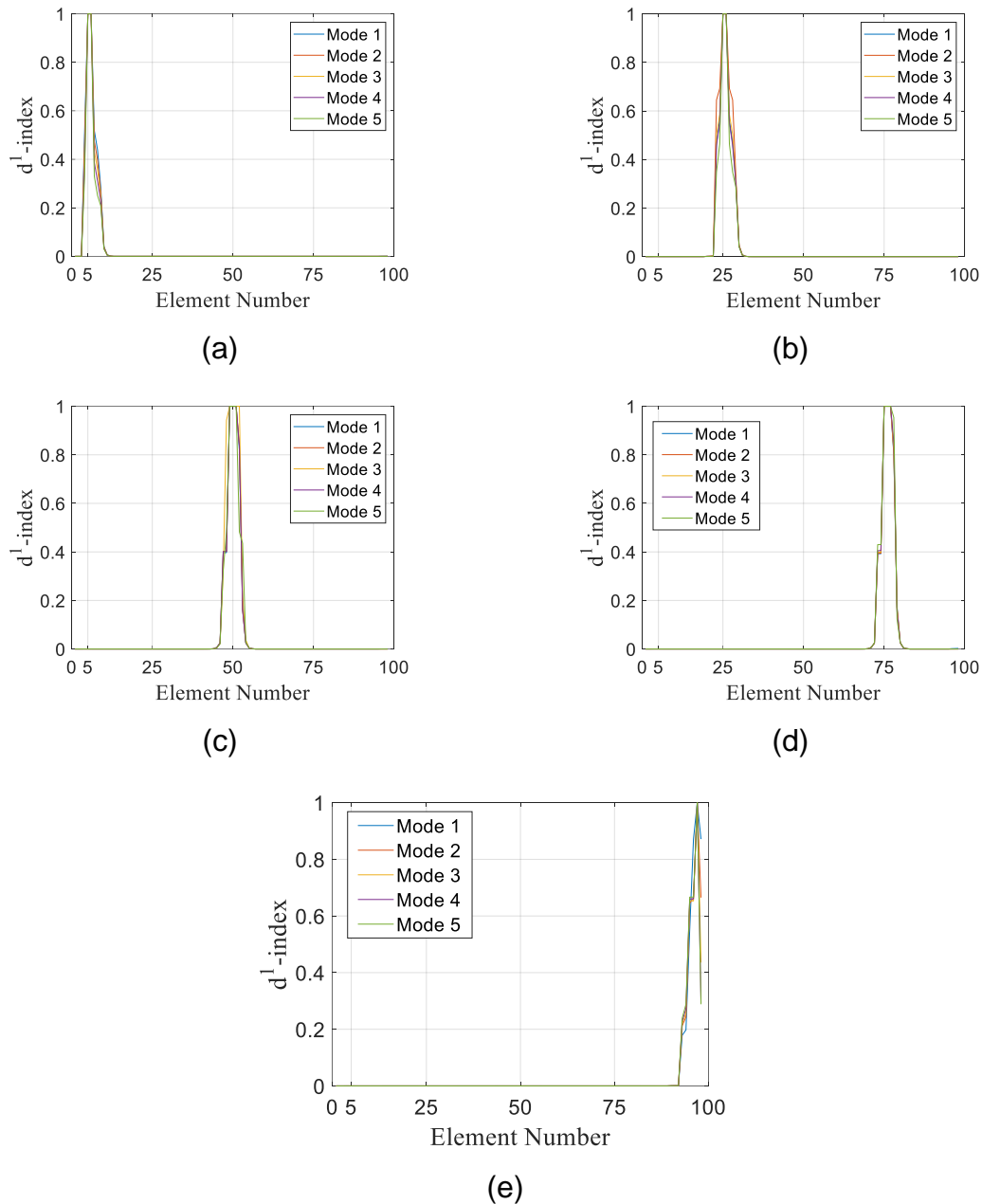


Figure 5.29. Damage localization for the Cantilever beam for damaged elements (a) E5, (b) E25, (c) E50, (d) E76, (e) E96.

Finally, Figure 5.30 presents the damage localization results for the Double-clamped beam. As before mentioned for the cantilever beam type, it has great precision independent of the analyzed mode shapes and damage location.

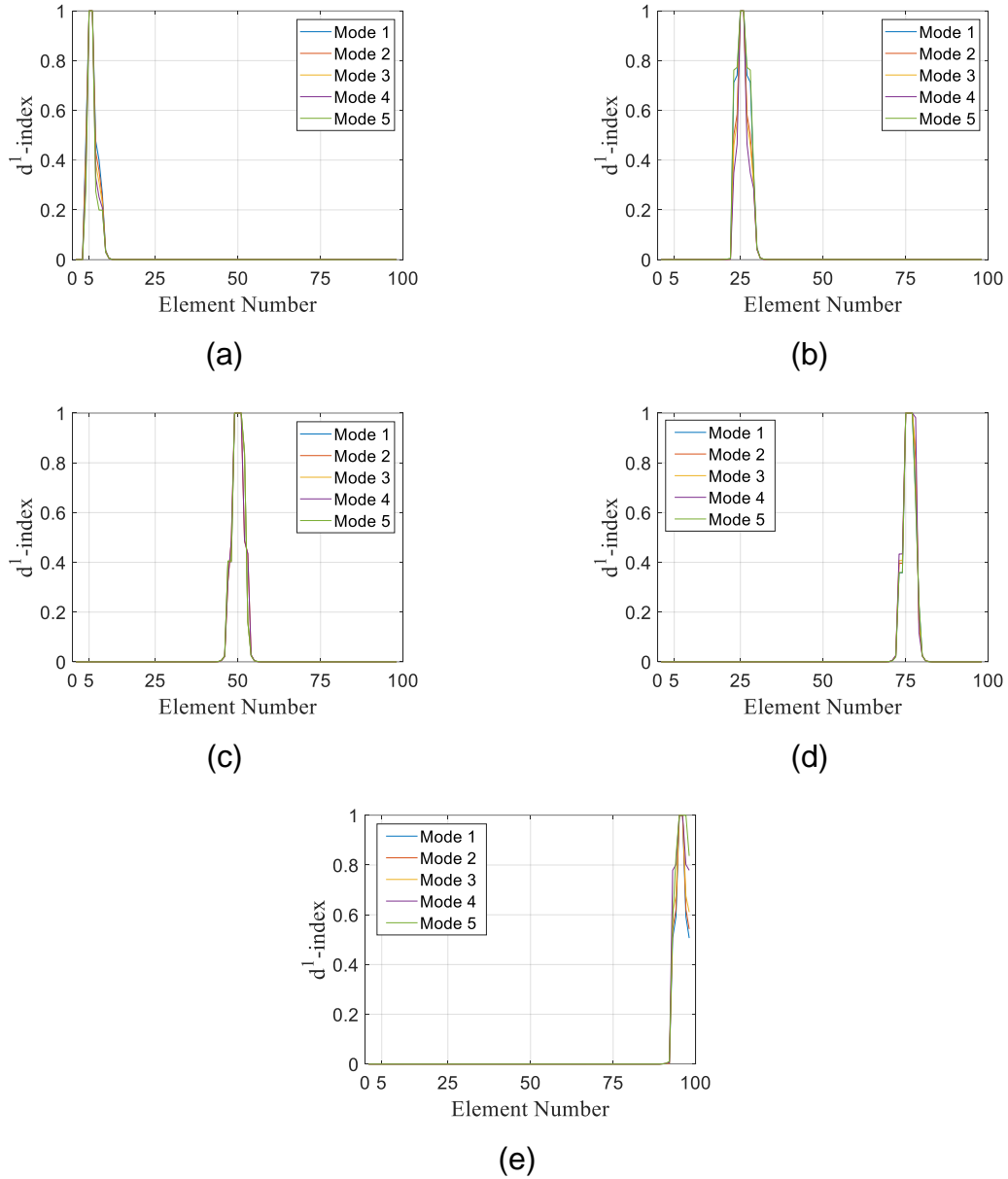


Figure 5.30. Damage localization for the Double-Clamped beam for damaged elements (a) E5, (b) E25, (c) E50, (d) E76, (e) E96.

Results obtained with the mode shapes analysis on the double-clamped beam follow the same aspects of the ones of the simply supported and the cantilever. Damage localization with great precision and independent of the variables involved.

6 RESULTS OF DAMAGE QUANTIFICATION

This section presents a study on the damage severity and its relationship with proposed index d^2 -index. To achieve our results a new index, called d^2 -index, was figured out, ranging the damage severity from 5% up to 50% for each kind of the support beams.

6.1 d^2 -index Damage Quantification

6.1.1 Concentrated Loads

This section presents damage quantification to the beams subjected to static concentrated loads.

Tables 6.1-6.3, present the d^2 -index, see Equation (4.2), for a cantilever beam. The d^2 -index is constructed as a ratio between $(d_d - d_0)^2$ and $(d_{max} - d_0)^2$, where d_d is the DWT coefficient of the damaged beam, d_0 is the same but for an intact beam, and d_{max} is the same but for the maximum severity of 25%. As previous analysis, damage is set for elements 5, 25, 50, 76 and 96. Concentrated loads were applied on nodes 6, 26, 51, 77 and 97. The aim of this study is to investigate the correlation between the d^2 -index coefficients, the damaged element and the load location so to create a correlation with the d^2 -index and the damage severity (d_s).

Tables 6.1-6.3 exhibit these coefficients for a damage severity of 5%. Meanwhile, damage quantification considers a damage interval of 5% to 25% to build the function.

Table 6.1. Squared wavelet coefficients variation $(d_d - d_0)^2$ for a cantilever beam with 5% damage.

Element n#	Load location (Node)				
	6	26	51	77	97
E5	2.8369E-23	6.6207E-20	3.3191E-19	8.2021E-19	1.3436E-18
E25	6.9994E-39	2.8369E-23	1.0254E-19	4.1905E-19	8.0815E-19
E50	5.4069E-37	2.7181E-34	9.6394E-23	1.3402E-19	4.0901E-19
E76	4.0182E-40	2.3137E-37	3.1494E-36	9.6394E-23	8.0688E-20
E96	1.7339E-37	9.3529E-35	1.2261E-33	5.2350E-33	8.0795E-22

Table 6.2. Squared maximum wavelet coefficients variation $(d_{\max} - d_0)^2$ for a cantilever beam with 5% damage.

Element n#	Load location (Node)				
	6	26	51	77	97
E5	1.1379E-21	2.6957E-18	1.3313E-17	3.2900E-17	5.3895E-17
E25	2.9273E-38	1.1379E-21	4.1131E-18	1.6809E-17	3.2416E-17
E50	4.7980E-37	2.6063E-34	3.8665E-21	5.3758E-18	1.6406E-17
E76	5.5444E-38	3.0164E-35	4.0004E-34	3.8665E-21	3.2365E-18
E96	3.2930E-39	1.7893E-36	2.3215E-35	9.5634E-35	3.2402E-20

It is noted that coefficients have a small magnitude, varying from E-17 to E-40. The hatched area highlights the cases where the part of the cantilever beam whose shear stress and bending moment do not cause any displacement. It is noted that, the wavelet coefficients are almost zero for the cases with damage applied in element 50 when the loads are out of the stretch (nodes 6 and 26).

Table 6.3 presents the d^2 -index ratio between the values of Tables 6.1 and 6.2. It shows only the values correspondent to the detectable damage zone, where the load is applied after the damaged element. It is noted that constant values are obtained. This behaviour was found to all damage severities from 5% to 50%. Higher values were found proportional to higher severities values. Further, d^2 -index was seen not affected by the damaged element position. It is observed that the index is affected only by the damage severity.

Table 6.3. d^2 -index values $(d_d - d_0)^2 / (d_{\max} - d_0)^2$ for a cantilever beam with 5% damage.

Element n#	Load location (Node)				
	6	26	51	77	97
E5	2.4931E-02	2.4931E-02	2.4931E-02	2.4930E-02	2.4930E-02
E25		2.4931E-02	2.4930E-02	2.4930E-02	2.4931E-02
E50			2.4931E-02	2.4930E-02	2.4931E-02
E76				2.4931E-02	2.4931E-02
E96					2.4931E-02

The same approach was conducted for the other two types of beams: double-clamped and the simply supported. Interestingly, the calculated d^2 -index was almost the same for the three beam types, despite the squared wavelet coefficients $(d_d - d_0)^2$ and $(d_{\max} - d_0)^2$ being different. The d^2 -index values, again, were not influenced by the location of the load application. The double-clamped beam is the only one, whose d^2 -index values, showed marginal differences, but still very slightly. Tables 6.4 and 6.5 present the adapted d^2 -index values for the double-clamped and the simply supported, respectively.

Table 6.4. d^2 -index values $(d_d - d_0)^2 / (d_{\max} - d_0)^2$ for a simply supported beam with 5% damage.

Element n#	Load location (Node)				
	5	25	51	77	97
E5	2.4930E-02	2.4930E-02	2.4930E-02	2.4930E-02	2.4930E-02
E25	2.4931E-02	2.4930E-02	2.4930E-02	2.4930E-02	2.4931E-02
E50	2.4930E-02	2.4930E-02	2.4931E-02	2.4931E-02	2.4931E-02
E76	2.4931E-02	2.4930E-02	2.4930E-02	2.4930E-02	2.4931E-02
E96	2.4931E-02	2.4931E-02	2.4931E-02	2.4931E-02	2.4930E-02

Table 6.5. d^2 -index values $(d_d - d_0)^2 / (d_{\max} - d_0)^2$ for a double-clamped beam with 5% damage.

Element n#	Load location (Node)				
	5	25	51	77	97
E5	2.5421E-02	2.5422E-02	2.5420E-02	2.5421E-02	2.5420E-02
E25	2.5180E-02	2.5180E-02	2.5294E-02	2.5182E-02	2.5181E-02
E50	2.5069E-02	2.5069E-02	2.5073E-02	2.5073E-02	2.5074E-02
E76	2.5189E-02	2.5192E-02	2.5271E-02	2.5181E-02	2.5180E-02
E96	2.5405E-02	2.5404E-02	2.5403E-02	2.5403E-02	2.5405E-02

The analysis of these results need attention. Cantilever damage quantification table, Table 6.3, has a singularity due to bending moment where some damage locations cannot be correctly pointed depending on the load location. Cantilever and simply supported beams have d^2 -index values of almost the same magnitude independent of load location, $\sim 2.49E-2$. The double-clamped beam also has very similar values independent of the load location but have a slightly variation on its coefficients, and has a different value of $\sim 2.52E-2$.

Furthermore, Table 6.5 shows very small difference in the d^2 -index regarding the double-clamped, which leads to the calculation of the maximum (d^2_{max}) and minimum (d^2_{min}) values, as well as the mean average (d^2_{avg}). For the double-clamped, the greatest variation percentage was noticed to be 1.4%, observed for the lowest values of damage severity. For the simply supported and the cantilever beams, only residual values were observed.

Figure 6.1 (a, b and c) presents the damage quantification curve for the cantilever, the simply supported and the double-clamped, respectively. It relates damage severity (d_s) (x-axis) and the damage index (y-axis), for the three beam support types with concentrated loads for an interval of damage severity between 5% to 25%. The function for all beams has an ax^3+bx^2+cx form. It is observed, for the three cases that the function is not affected by the boundary conditions, but only the load magnitude and the displacement value itself.

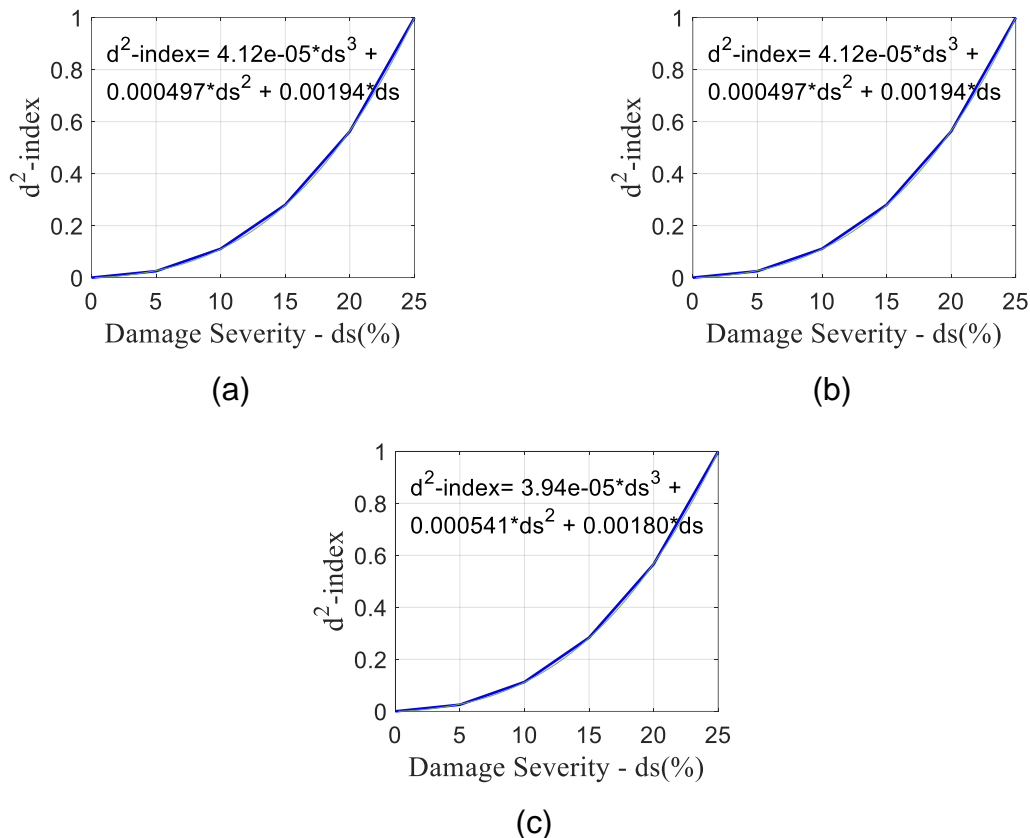


Figure 6.1. Relationship of damage severity and d^2 -index for the (a) cantilever, (b) simply supported, and the (c) double-clamped beam, under concentrated loads.

6.1.2 Distributed Loads

The same analysis of the previous section is carried out, but for distributed loads this time. The load magnitude was 1 Newton per meter. Unlike for the concentrated load analysis, the d^2 -index values were only observed on the damaged element, independent of the beam type. On the other hand, values for intact elements were found null.

Figure 6.2 exhibits the damage quantification curves for the three beam types under distributed loads, where the x-axis represents the damage severity and the y-axis, the d^2 -index.

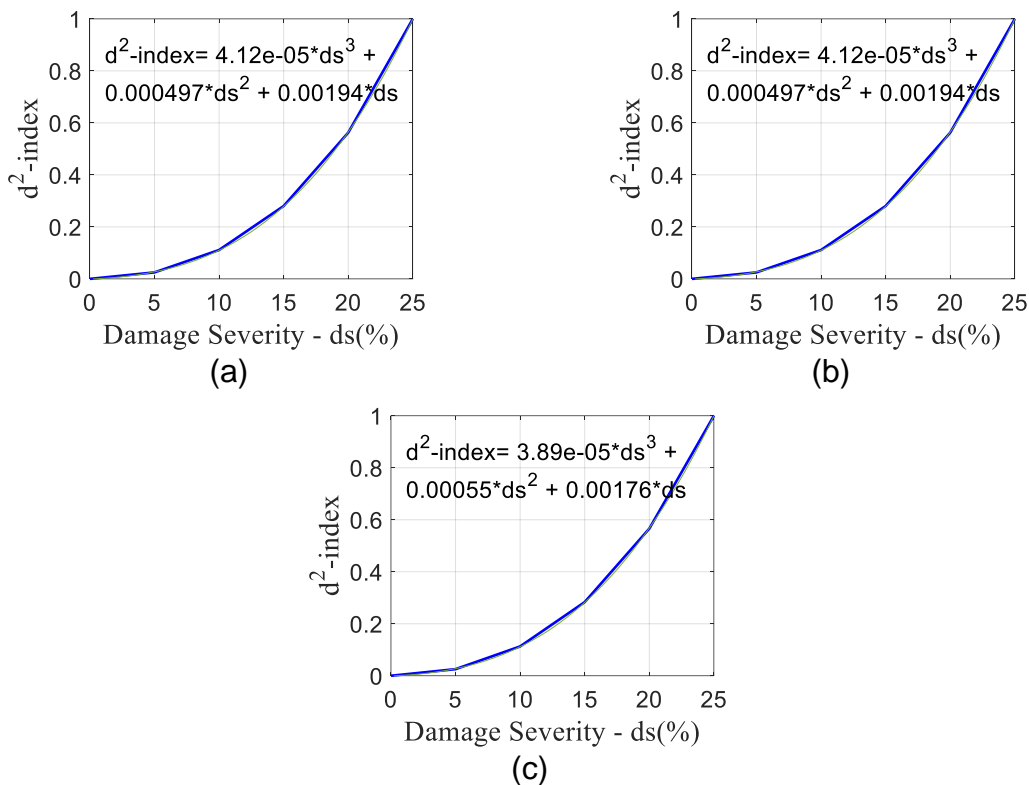


Figure 6.2. Relationship of damage severity and d^2 -index for the (a) cantilever, (b) simply supported, and the (c) double-clamped, under distributed loads.

The same pattern is observed from the concentrated load analysis. The best fit is again a 3th degree polynomial equation, ax^3+bx^2+cx . The same result was observed on the concentrated loads analysis.

6.1.3 Vibration Mode Shapes

The investigation was furthered using the d^2 -index coefficients to obtain the damage severity for modal analysis. The d^2 -index was investigated for the first five mode shapes. Again, the same characteristics of previous sections were observed, however, a slight increase of the d^2 -index values was noted as the mode shapes increases. Moreover, independent of damage severity, the difference ratio between the maximum and minimum d^2 -index values was found to be about 1%. The minimum value was obtained in the 1st mode shapes and the maximum from the 5th mode.

Figure 6.3 exhibits the damage quantification curves for the three beams' support types, based on mode shapes. The x-axis represents the damage severity and the y-axis, the d^2 -index. The third order polynomial precisely fit the quantification curves. Different from the static analysis of both previous sections, d^2 -index functions for the cantilever and the simply supported were not found to be similar.

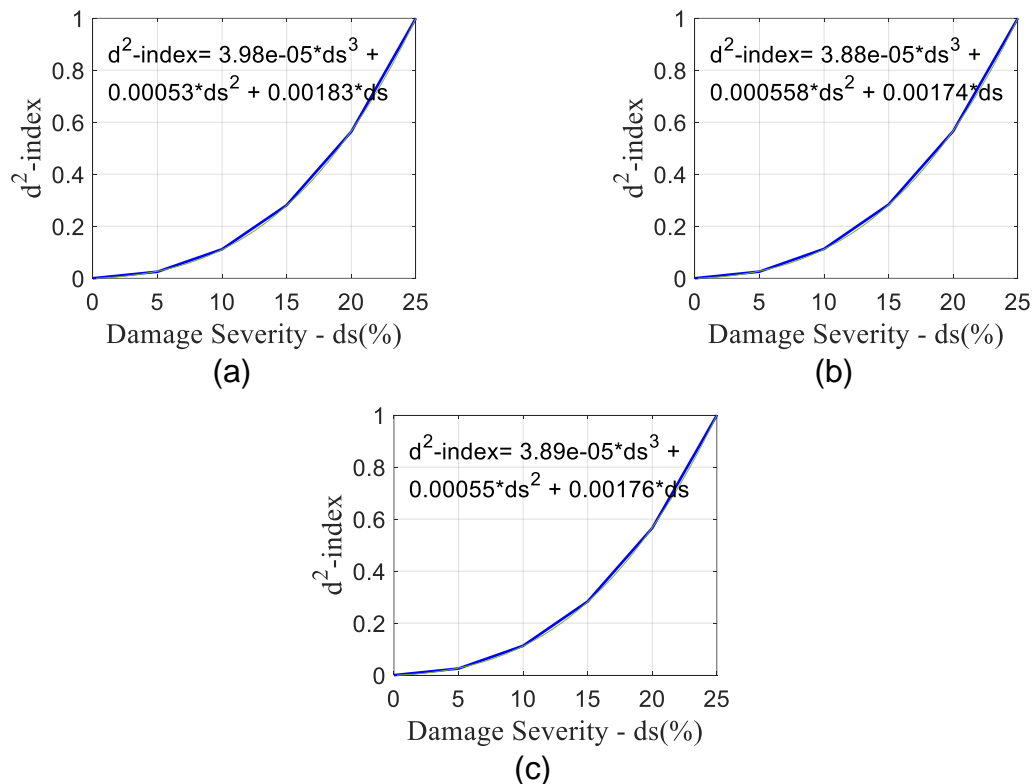


Figure 6.3. Relationship of damage severity and d^2 -index for the (a) cantilever, (b) simply supported, and the (c) double-clamped beam, from mode shapes.

From these observations, damage quantification needs further investigation regarding its calculation and analysis. Results from of damage quantification for a static analysis, for concentrated and distributed loads are presented in Figures 6.1 and 6.2, respectively, while for a modal analysis, in Figure 6.3. Table 6.6 disposes the coefficient values of these polynomials. It shows that the best results were found with a third order degree function. It also compares results obtained for other polynomial formats, from 2nd to 4th orders.

Table 6.6. Polynomial degree influence on damage quantification.

Analysis	Beam	Parameter	Function coefficients ($y=ax^3+bx^2+cx$)			
			a	b	c	R
<i>Punctual Load</i>	<i>Double-Clamped</i>	ax^3+bx^2+cx+d	4.027E-5	5.174E-4	1.869E-3	1
		ax^3+bx^2	3.475E-5	7.281E-4	n/a	0.999
	<i>Simply Supported</i>	ax^3	6.615E-5	n/a	n/a	0.989
		ax^2	1.513E-3	n/a	n/a	0.981
		ax^2+bx	1.962E-3	9.756E-3	n/a	0.977
	<i>Cantilever</i>	ax^3+bx^2+cx	4.123E-5	4.9E-4	1.948E-3	1
	<i>Double-Clamped</i>	ax^3+bx^2+cx	3.943E-5	5.41E-4	1.801E-3	1
<i>Distributed Load</i>	<i>Simply Supported</i>	ax^3+bx^2+cx	4.123E-5	4.9E-4	1.948E-3	1
	<i>Cantilever</i>	ax^3+bx^2+cx	4.123E-5	4.9E-4	1.948E-3	1
	<i>Double-Clamped</i>	ax^3+bx^2+cx	3.899E-5	5.534E-4	1.766E-3	1
<i>Modal</i>	<i>Simply Supported</i>	ax^3+bx^2+cx	3.882E-5	5.583E-4	1.749E-3	1
	<i>Cantilever</i>	ax^3+bx^2+cx	3.982E-5	5.3E-4	1.834E-3	1
	<i>Double-Clamped</i>	ax^3+bx^2+cx	3.899E-5	5.534E-4	1.766E-3	1

It is observed that a third-degree order, $y=ax^3+bx^2+cx$ function is capable of predicting the severity of damage with great precision for the range of damage investigated. Further, no complex functions were needed to fit the relationship between the damage severity and the d^2 -index.

Figure 6.4 presents a comparison on the damage quantification curves obtained on each case of analysis (concentrated and distributed loads, and modal) for the analyzed beams. Note that each modal curve contains all first five vibration mode

shapes for all the damaged cases studied, while the concentrated and the distributed loads, also are constituted of all cases of load position versus damage location.

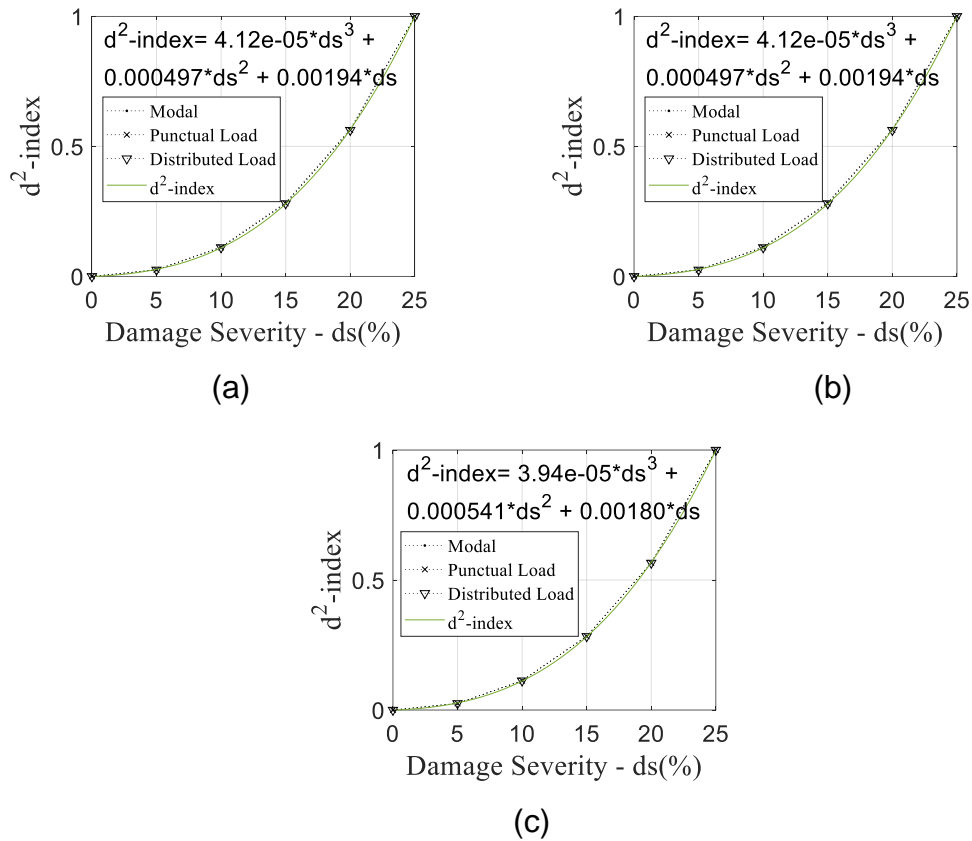


Figure 6.4. Damage quantification analysis over each type of load or mode shapes for the (a) cantilever, (b) simply supported, and the (c) double-clamped beam.

It is observed that the functions for each case (concentrated and distributed loads, and modal) and each beam (cantilever, simply supported and double-clamped) behave pretty much the same with coefficients varying only on the fifth or the sixth order of each, while each coefficient were found with the value: $a=3.92E-5$; $b=5.4E-4$; $c=1.9E-3$; $R=1$.

6.1.4 Influence of the Beam Material (Elasticity Module)

Previous results show a high level of similarity between the damage quantification curves, for all beam types analyzed. Factors such as damage localization, damage severity, wavelet mother type, wavelet decomposition level and even the analysis type

(static and modal) did not influence these quantification functions at all. Thus, a study on the alteration on the beam material is presented.

This section investigates the influence on the d^2 -index for damage quantification regarding the material of the beam. Two types were investigated: steel (200 GPA) and aluminum (70 GPA). Table 6.7 presents the damage quantification curve coefficients for a double-clamped beam with damage on element 76 for a static analysis data. A DWT Coiflets 2 at $j=1$, with baseline was used; $F=1$ Newton.

Table 6.7. Elasticity Module influence on damage quantification.

Analysis	Beam	Parameter	Function coefficients ($y=ax^3+bx^2+cx$)			
			a	b	c	R
Static	Double-Clamped	Steel	4.123E-5	4.9E-4	1.948E-3	1
		Aluminum	4.123E-5	4.9E-4	1.948E-3	1

The analysis presents two exactly the same damage severity prediction functions. The results show that the elasticity module does not influence the d^2 -index damage quantification calculations.

6.1.5 Influence of Other Parameters Investigation

From the observations throughout this chapter, damage quantification needs further investigation regarding its calculation and analysis. Interestingly, for a static analysis the same functions have been found for the cantilever and the simply supported, while for a modal analysis, this did not happen. The double-clamped beam behaved properly independently.

Therefore, as conducted for the d^1 -index, in section 5.2.2, an investigation on the influence of some parameters involved were also analyzed for the d^2 -index.

The variation of the polynomial degree of the damage severity prediction curves is presented in Table 6.6. Meanwhile, the variation of the material of the beam, is presented in Table 6.7.

Other parameters are shown in following Tables 6.8 up to Table 6.13, which present the wavelet mother type and its decomposition level, the load location, mode shapes and the normalization of the curve, respectively.

Table 6.8. Wavelet Mother influence on damage quantification.

Analysis	Beam	Parameter	Function coefficients ($y=ax^3+bx^2+cx$)			
			a	b	c	R
Static	Double-Clamped	coif2	4.024E-5	5.180E-4	1.867E-3	1
		sym8	4.035E-5	5.152E-4	1.875E-3	1
		db5	3.991E-5	5.276E-4	1.839E-3	1
Modal	Double-Clamped	coif2	4.053E-5	5.099E-4	1.89E-3	1
		sym8	4.054E-5	5.097E-4	1.891E-3	1
		db5	4.061E-5	5.078E-4	1.896E-3	1
Static	Simply Supported	coif2	4.123E-5	4.9E-4	1.948E-3	1
		sym8	4.123E-5	4.9E-4	1.948E-3	1
		db5	4.123E-5	4.9E-4	1.948E-3	1
Modal	Simply Supported	coif2	4.087E-5	5.003E-4	1.918E-3	1
		sym8	4.087E-5	5.003E-4	1.918E-3	1
		db5	4.084E-5	5.012E-4	1.916E-3	1
Static	Cantilever	coif2	4.123E-5	4.9E-4	1.948E-3	1
		sym8	4.123E-5	4.9E-4	1.948E-3	1
		db5	4.123E-5	4.9E-4	1.948E-3	1
Modal	Cantilever	coif2	4.120E-5	4.909E-4	1.945E-3	1
		sym8	4.120E-5	4.909E-4	1.945E-3	1
		db5	4.128E-5	4.883E-4	1.964E-3	1

Table 6.9. Decomposition Level influence on damage quantification.

Analysis	Beam	Parameter	Function coefficients ($y=ax^3+bx^2+cx$)			
			a	b	c	R
Static	Double-Clamped	$j=1$ with F51	4.019E-5	5.195E-4	1.862E-3	1
		$j=2$ with F51	4.019E-5	5.195E-4	1.862E-3	1
		$j=3$ with F51	4.019E-5	5.195E-4	1.862E-3	1
		$j=1$ with F77	4.027E-5	5.175E-4	1.868E-3	1
Modal	Double-Clamped	$j=1$ with vibmod1	4.053E-5	5.099E-4	1.890E-3	1
		$j=2$ with vibmod1	4.053E-5	5.099E-4	1.890E-3	1
		$j=3$ with vibmod1	4.053E-5	5.099E-4	1.890E-3	1
		$j=1$ with vibmod2	3.959E-5	5.365E-4	1.813E-3	1
		$j=2$ with vibmod2	3.959E-5	5.365E-4	1.813E-3	1

Table 6.10. Load and Damage Localization influence on damage quantification.

Analysis	Beam	Parameter	Function coefficients ($y=ax^3+bx^2+cx$)			
			a	b	c	R
Static	Double-Clamped	E5N5	3.943E-5	5.411E-4	1.8E-3	1
		E5N25	3.942E-5	5.421E-4	1.798E-3	1
		E5N51	3.941E-5	5.416E-4	1.799E-3	1
		E25N5	4.031E-5	5.163E-4	1.871E-3	1
		E25N25	4.031E-5	5.163E-4	1.873E-3	1
		E25N51	4.019E-5	5.195E-4	1.862E-3	1
	Simply Supported	E5N5	4.123E-5	4.9E-4	1.948E-3	1
		E5N25	4.123E-5	4.9E-4	1.948E-3	1
		E5N51	4.123E-5	4.9E-4	1.948E-3	1
		E25N5	4.123E-5	4.9E-4	1.948E-3	1
		E25N25	4.123E-5	4.9E-4	1.948E-3	1
		E25N51	4.123E-5	4.9E-4	1.948E-3	1
	Cantilever	E5N5	2.379E-2	-1.474	21.84	0.669
		E5N6	4.123E-5	4.9E-4	1.948E-3	1
		E5N51	4.123E-5	4.9E-4	1.948E-3	1
		E5N97	4.123E-5	4.9E-4	1.948E-3	1
		E25N51	4.123E-5	4.9E-4	1.948E-3	1
		E25N97	4.123E-5	4.9E-4	1.948E-3	1

Table 6.11. Function Normalization influence on damage quantification.

Analysis	Beam	Parameter	Function coefficients ($y=ax^3+bx^2+cx$)			
			a	b	c	R
Static	Double-Clamped	coif2	3.636E-22	4.179E-21	1.866E-20	1
		sym8	5.049E-22	5.802E-21	2.591E-20	1
		db5	3.338E-22	3.836E-21	1.713E-20	1
Modal		coif2	9.235E-13	1.252E-12	4.562E-11	1
		sym8	5.867E-13	7.948E-12	2.899E-11	1
		db5	2.455E-13	3.329E-12	1.213E-11	1

Table 6.12. Mode shapes influence on damage quantification.

Analysis	Beam	Parameter	Function coefficients ($y=ax^3+bx^2+cx$)			
			a	b	c	R
Modal	Double-Clamped	mode 1	4.053E-5	5.099E-4	1.890E-3	1
		mode 2	3.959E-5	5.365E-4	1.813E-3	1
		mode 3	3.873E-5	5.610E-4	1.744E-3	1
		mode 4	3.818E-5	5.765E-4	1.7E-3	1
		mode 5	3.896E-5	5.544E-4	1.763E-3	1
		5 modes	3.899E-5	5.534E-4	1.766E-3	1
	Simply Supported	mode 1	4.087E-5	5.003E-4	1.918E-3	1
		mode 2	3.922E-5	5.469E-4	1.784E-3	1
		mode 3	3.881E-5	5.589E-4	1.744E-3	1
		mode 4	3.932E-5	5.441E-4	1.792E-3	1
		mode 5	3.866E-5	5.627E-4	1.739E-3	1
		5 modes	3.882E-5	5.583E-4	1.749E-3	1
	Cantilever	mode 1	4.120E-5	4.909E-4	1.945E-3	1
		mode 2	4.074E-5	5.039E-4	1.907E-3	1
		mode 3	3.981E-5	5.302E-4	1.831E-3	1
		mode 4	3.962E-5	5.357E-4	1.816E-3	1
		mode 5	3.947E-5	5.4E-4	1.803E-3	1
		5 modes	3.982E-5	5.3E-4	1.834E-3	1

Tables 6.8-6.13 show that the variation of the parameters do not influence at all the quantification curve results. Noticed variations are far too small to be considered alterations on the functions. Although, the double-clamped beam showed to be more sensitive to some of these alterations.

From the damage quantification regarding the static analysis data, the cantilever and the simply supported developed the same functions, while the double-clamped produced slightly lower coefficients. Additionally, the only beam sensitive to load location and the wavelet mother was also the double-clamped. From the vibration modes, each beam developed a unique function, while the highest coefficients were observed for the cantilever.

7 CONCLUSION

This research investigated the potential of a DWT-based damage localization and quantification procedure. The proposed approach consists in examining the DWT coefficients of damaged and undamaged beams. Two d-indexes were proposed: d^1 -index for damage localization and d^2 -index for quantification. The indexes were able to detect the probable region of damage and also predict the curve of damage severity.

Three types of beams were studied: simply supported, cantilever and double-clamped beam. The displacement was the function of choice for damage localization on this research, while for the modal analysis were the vibration mode shapes.

Different structures yielded different structural displacement behavior, although the d^1 -index method was able to localize damage on these diverse scenarios. As well as this detail, other parameters which influence damage detection were also studied. This investigation explored the parameters of load location, damage severity, wavelet decomposition level, wavelet mother type and the influence of the beam boundary conditions on damage reading on the near-supports region.

The first parameter analyzed was the Load location. The d^1 -index was able to detect and localize damage on all beam types, with an exception for the cantilever beam at some specific cases due to the bending moment and shear stress. Meanwhile, the use of mode shapes also resulted into a precise damage localization.

The damage severity showed to not influence results, revealing a great sensitiveness to the method. Damage was varied from 5% to 50%. Best quantification results were presented with a maximum severity of 25%. Multiple damaged elements were also investigated. It developed inconclusive results while peaks were not seen proportional to the damage imposed to the element, needing further research.

The wavelet mother type and the decomposition level showed to be very influent on damage detection. The best readings were obtained with $J=1$, since for levels greater than 1, signal dispersion occurs. While for the mother type, best results were observed with the use of the Coiflets 2. The other wavelet types studied were heavily influenced by the near-supports region and hence developed high peaks of coefficients on this areas, harming the results.

The use of a baseline function showed for both localization and quantification it is of significant importance to calculate the wavelet coefficients, while in its absence spurious peaks were observed. Baseline-free results were inconclusive.

For damage localization, both static and dynamic regimes produced precise results. The proposed method showed great potential on damage detection for diverse beam types, with accuracy and not dependent of severe damage appearances, having a great sensitiveness.

Deepening on the Damage Quantification, the polynomial degree of the curve, the beam material and the normalization of the functions were also matter of study. The first, produced the best results with third order degree functions. The elasticity module variation did not influence an inch on results.

The d^2 -index quantification was adimensionalized by the maximum damage severity of 25%. This normalization by the maximum damage created quantification function coefficients very similar independent of the beam analyzed. For various cases, the coefficients were found exactly the same, while for others a slight difference was found on the seventh decimal place. This similarity was also noted for all load types investigated, while producing similar results for both static and dynamic analysis.

The damage functions were observed to be only responsive to the severity degree, while other variables such as load type, load location, analysis type, wavelet mother, wavelet decomposition level and beam material did not influence it. All results were approximated by a third order degree polynomial.

In general, the d^1 -index and the d^2 -index approach produced precise results. Both being able to localize or quantify damage independent of the boundary conditions and the parameters of the investigation. An optimum set was noticed for a specific level of J and mother type, but aside from this, the method works fine independent of any configuration. Notice that the baseline value is mandatory for reliable results.

For the continuation of this research some possibilities are open: furthering the multiple damage analysis to comprehend proportional damage; the quantification curves similarity; 2d and 3d structures; the use of STFT instead of WT; the use of factorial planning; experimental campaign and the addition of noises.

LIST OF REFERENCES

- Allemang, R. J. 2003. "The modal assurance criterion –Twenty years of use and abuse." *Journal of Sound and Vibration*: 14-21.
- Alvandi, A., and Cremona, C. 2006. "Assessment of vibration-based damage identification techniques." *Journal of Sound and Vibration* 292 (1-2): 179-202.
- Amezquita-Sanchez J. P., Garcia-Perez A., Romero, R. J., Osornio, R. A., and Herrera, G. 2013. "High-Resolution Spectral-Analysis for Identifying the Natural Modes of a Truss-Type Structure by Means of Vibrations," *Journal of Vibration and Control*, 19(16): 2347–2356.
- An, H., Youn, B. D., Kim, H. S. 2022. "A methodology for sensor number and placement optimization for vibration-based damage detection of composite structures under model uncertainty". *Composite Structures* (279) 114863.
- Beer, F.P., Johnston, E.R., DeWolf, J.T. and Mazurek, D.F., 2011. *Mecânica dos materiais*. Porto Alegre: Amgh.
- Bendat, J. S., and Piersol, A. G. 1971. *Random data: Analysis and Measurement Procedures*. New York, Wiley-Interscience.
- Beskhyroun, S., Oshima, T., Mikami, S., and Tsubota, Y. 2005. "Structural damage identification algorithm based on changes in power spectral density." *Journal of Applied Mechanics (JSCE)* 8:73-84.
- Beskhyroun, S., Oshima, T., Mikami, S. 2010. "Wavelet-based technique for structural damage detection." *Structural Control and Health Monitoring* 17(5):473-494.
- Chaupal, P. and Rajendran, P., 2023. "A review on recent developments in vibration-based damage identification methods for laminated composite structures: 2010–2022". *Composite Structures*, p.116809.
- Daubechies, I. 1992. *Ten Lectures on wavelets*. Society for industrial and applied mathematics.
- Doebbling, S. W., Farrar, C. R., and Prime, M. B. 1998. "A summary review of vibration based damage identification methods." *Shock and Vibration Digest*, 30(2): 91–105.
- Du, Y., Zhou, S., Jing, X., Peng, Y., Wu, H., Kwok, N. 2019. "Damage detection techniques for wind turbine blades: A review". *Mechanical Systems and Signal Processing*.
- Estrada, E. S. 2008. "Damage detection methods in bridges trough vibration monitoring: evaluation and application." Doc. Thesis, University of Minho.

- Fallahian, M., Ahmadi, E. and Khoshnoudian, F., 2022. "A structural damage detection algorithm based on discrete wavelet transform and ensemble pattern recognition models". *Journal of Civil Structural Health Monitoring*, 12(2), pp.323-338.
- Farrar, C. R., and Doebling, S. W. 1999. *Damage detection II:field applications to large structures*. Modal Analysis and Testing, Nato Science Series. Kluwer Academic Publisher, Dordrecht, the Netherlands.
- Farrar, C. R., and Jauregui, D. A. 1997. "Comparative study of damage identification algorithms applied to a bridge; 2, numerical study." *Smart Materials and Structures* 7: 720-731.
- Farrar, C. R., and Worden, K. 2007. "An introduction to structural health monitoring." *Philosophical Transactions of the Royal Society A: Mathematical, Physical and Engineering Sciences*, 365(1851): 303-315.
- Friswell, M. I., and Penny, J. E. 2002. "Crack modeling for structural health monitoring." *Structural Health Monitoring*, London, 1(2): 139-148.
- Gabor, D. 1946. "Theory of communication." *Journal Electrical Engineers* 93(26): 429-441.
- Gere, J.M., de Castro Paiva, L.F., Bittencourt, M.L. and Zachariadis, D.C., 2009. *Mecânica dos materiais*. Cengage Learning Edições Ltda.
- Gillich, G. R., Maia, N. M., Wahab, M. A., Tufisi, C., Korca, Z. I., Gillich, N., and Pop, M. V. 2021. "Damage detection on a beam with multiple cracks: a simplified method based on relative frequency shifts." *Sensors* 21(15): 5215.
- Gogolewski, D. 2020. "Influence of the edge effect on the wavelet analysis process." *Measurement*, 152: 107314.
- Gomes, G. F., Mendez, Y. A. D., Alexandrino, P. D. S. L., Da Cunha JR, S. S., and Ancelotti JR, A. C. 2018. "The use of intelligent computational tools for damage detection and identification with an emphasis on composites—A review." *Composite Structures* 196: 44-54.
- Grabowska, J., Palacz, M., Krawczuk, M. 2008. "Damage identification by wavelet analysis." *Mechanical Systems and Signal Processing* 22: 1623–1635.
- Grooteman, F. P. 2012. "Damage detection and probability of detection for a SHM system based on optical fibers applied to a stiffened composite panel." *Proceedings of the International Conference on Noise and Vibration Engineering*: 3317-3330.
- Han, J. G., Wei X. R., and Zeng S. S. 2005. "Wavelet packet based damage identification of beam structures." *International journal of solids and structures* 42(26): 6610-6627.

- Hibbeler, R.C., 2010. *Resistência dos materiais*. Pearson Educação.
- Indrusiak, M. L. S., and Moller, S. V. "Wavelet analysis of experimental turbulence time series". *Proceedings of the IV Escola de Primavera de Transição e Turbulência*, Rio Grande do Sul, 2004.
- Inman, D. J., and Singh, R. C. 1994. *Engineering Vibration. Volume 3*. Englewood Cliffs, NJ: Prentice Hall.
- Kaiser, G. 1994. *A Friendly Guide to Wavelets*. Cambridge, MA: Birkhäuser.
- Kam, T. Y., and Lee, T. Y. 1992. "Detection of cracks in structures using modal test data." *Journal of Engineering Fracture Mechanics* 42: 381–387.
- Kankanamge, Y., Hu, Y. and Shao, X., 2020. Application of wavelet transform in structural health monitoring. *Earthquake Engineering and Engineering Vibration*, 19, pp.515-532.
- Katunin, A. 2010. "Identification of multiple cracks in composite beams using discrete wavelet transform." *Scientific Problems of Machines Operation and Maintenance* 45(2): 41-52.
- Katunin, A. 2011. "Damage identification in composite plates using two-dimensional B-spline wavelets." *Mechanical Systems and Signal Processing* 25(8): 3153-3167.
- Katunin, A., Dos Santos, J. V. A., and Lopes, H. 2021. "Damage identification by wavelet analysis of modal rotation differences." *In Structures* 30: 1-10.
- Kim, T. J., Ryu, Y. S., Cho, H. M., and Stubbs, N. 2003. "Damage identification in beam-type structures: frequency-based method vs modeshape-based method." *Engineering Structures* 25,: 57–67.
- Lopes, H. M. R., Dos Santos, A. J. V., Mota, S. C. M., Miranda, G. R. J., and Pires, V. M. A. 2011. "A numerical-experimental method for damage location based on rotation fields spatial differentiation." *Computational Structures* 89(19-20):1754–70.
- Lopes, H. M. R., and Dos Santos, A. J. V. 2012. "Interferometric techniques in structural damage identification." *Shock Vibration* 19: 835-844.
- Machado, M.R., Adhikari, S. and Dos Santos, J.M.C., 2017. "A spectral approach for damage quantification in stochastic dynamic systems". *Mechanical Systems and Signal Processing*, 88, pp.253-273.
- Mallat, S. G. 1989. "A theory for multiresolution signal decomposition: the wavelet representation." *IEEE transactions on pattern analysis and machine intelligence* 11(7): 674-693.

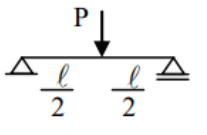
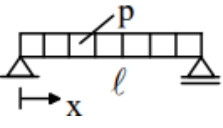
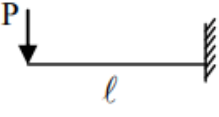
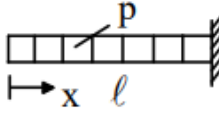
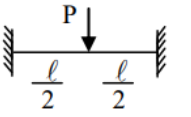
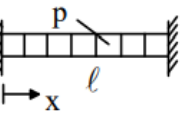
- Misiti, M., Misiti, Y., Oppenheim, G., and Poggi, J. M. 1996. *Wavelet toolbox — user's guide*. Natick, MA: The Math Works Inc.
- Misiti, M., and Poggi, J. M. 2001. *Wavelet toolbox for use with MATLAB*. Natick, MA: The Math Works Inc.
- Nick., H., Aziminejad, A., Hosseini, M. H., and Laknejadi, K. 2021. "Damage identification in steel girder bridges using modal strain energy-based damage index method and artificial neural network." *Engineering Failure Analysis*: 119.
- Okafor, A. C., and Dutta, A. 2000. "Structural damage detection in beams by wavelet transforms." *Smart Materials and Structures* 9: 906-917.
- Ovanesova, A. V. 2000. Applications of Wavelets to Crack Detection in Frame Structures., 2000. University of Puerto Rico.
- Ovanesova, A. V., and Suarez, L. E. 2004. "Applications of wavelet transforms to damage detection in frame structures." *Engineering Structures* 26(1): 39–49.
- Palechor, E. U. L., Silva, R. S. Y. C., Bezerra, L. M., and Bittencourt, T. N. 2014. "Damage Identification in Beams Using Experimental Data." *Key Engineering Materials* 607: 21–29.
- Pandey, A. K., Biswas, M., and Samman, M. M. 1991. "Damage detection from changes in curvature mode shapes." *Journal of Sound and Vibration* 145(2): 321–332.
- Paz, M., Kim, Y. H, 2019. Structural Dynamics, theory and computation. Springer, 6th ed. <https://doi.org/10.1007/978-3-319-94743-3>.
- Percival, D. B., and Walden, A. T. 2000. *Wavelet methods for time series analysis. Volume 4*. Cambridge University Press.
- Polikar, R. 1994. *A Tutorial on Wavelet Transform*. Department of Electrical and Computer Engineering. Rowan University, Glasborro, NJ.
- Quek, S. T., Wang, Q., Zhang, L., and ANG, K. K. 2001. "Sensitivity analysis of crack detection in beams by wavelet technique." *International Journal of Mechanical Sciences* 43: 2899-2910.
- Rytter, A. 1993. "Vibration based inspection of civil engineering structures." Doc., Thesis, Department of Building Technology and Structural Engineering, Aalborg University, Denmark.
- Saadatmorad, M., Talookolaei, R.A.J., Pashaei, M.H., Khatir, S. and Wahab, M.A., 2022. "Pearson correlation and discrete wavelet transform for crack identification in steel beams". *Mathematics*, 10(15), p.2689.

- Salawu, O. S. 1997. "Detection of structural damage through changes in frequency: a review." *Journal of Engineering Structures* 19: 718-723.
- Salgado, R., Cruz, P. J. S., Ramos, L. F., and Lourenco, P. B. 2006. "Comparison between damage detection methods applied to beam structures." *Proceedings of the International Conference on Bridge Maintenance, Safety and Management* 3, Porto, Schnur.
- Santos, J., Morais, M., Machado, M., Silva, R., Palechor, E., Silva, W. 2022. "Beam-like damage detection methodology using wavelet damage ratio and additional roving mass". *Fraterra ed Integrita Strutturale*, 62, p.349-363.
- Saranya, S., Ranjitham, M., Dinesh, A. and Divyapriya, S., 2022. "Structural Health Monitoring Using Sensors with Application of Wavelet Analysis". *Sustainable Materials and Smart Practices: NCSMSP-2021*, 23, p.205.
- SCHIEL, F. Introdução à resistência dos materiais. v.1. 6.ed. São Carlos, Escola de Engenharia de São Carlos, 1976.
- Sifuzzaman, M., Islam, M. R., and Ali, M. Z. 2009. "Application of Wavelet Transform and its Advantages Compared to Fourier Transform," *Journal of Physical Sciences*, 13: 121–134.
- Silva, R. S. Y. R. C. 2015. "Monitoramento e Identificação Numérico e Experimental de Danos em Vigas e Pontes de Aço e Concreto Utilizando Transformadas de Wavelet." Doc., Thesis, Departamento de Engenharia Civil e Ambiental, Universidade de Brasília, Brasília.
- Sohn, H., Farrar, C. R., Hemez, F. M., Shunk, D. D., Stinemates, D. W., Nadler, B. R., and Czarnecki, J. J. 2003. A review of structural health monitoring literature: 1996–2001. *Los Alamos National Laboratory*, USA, 1.
- Solís M, Algaba M, Galvín P. Continuous wavelet analysis of mode shapes differences for damage detection. *Mech Syst Sig Process* 2013;40(2):645–66. <https://doi.org/10.1016/j.ymssp.2013.06.006>.
- Solís M, Ma Q, Galvín P. Damage detection in beams from modal and wavelet analysis using a stationary roving mass and noise estimation. *Strain* 2018;54(2): e12266. <https://doi.org/10.1111/str.12266>.
- Soriano, H. L., 2014. Introdução à dinâmica das estruturas. Elsevier Editora Ltda, 1 ed., Rio de Janeiro, Brasil. ISBN 978-85-352-5153-1.
- Surace, C., Ruotolo, R. 1994. "Crack detection of a beam using the wavelet transform." *In Proceedings of the International Modal Analysis Conference* 1: 1141-1147.
- Umesha, P.K., Ravichandran, R. and Sivasubramanian, K., 2009. "Crack detection and quantification in beams using wavelets". *Computer-Aided Civil and Infrastructure Engineering*, 24(8), pp.593-607.

- Valens, C. 1999. A really friendly guide to wavelets. *Ed. Clemens Valens*.
- Viet, H. N., and Golinval, J.C., 2010. "Damage localization in linear-form structures based on sensitivity investigation for principal component analysis". *Journal of Sound and Vibration*, 329(21), pp.4550-4566.
- Wang, Q., and Deng, X. M. 1999. "Damage detection with spatial wavelets." *International Journal of Solids and Structures* 36: 3443–3468.
- Wang, S., Li, J., Luo, H., and Zhu, H. 2019. "Damage Identification in Underground Tunnel Structures with Wavelet Based Residual Force Vector". *Engineering Structures*, 178: 506–520.
- Weeks, M. 2012. *Processamento Digital de Sinais utilizando MATLAB e WAVELETS. Georgia State University. 2a Edição, LTC. Tradutor e revisor Edson Tanaka. Rio de Janeiro.*
- Yang, Q., and Huang, Y. 2021. "Damage identification method of prestressed concrete beam bridge based on convolutional neural network." *Neural Computing and Applications*, 33(2): 535-545.
- Yu, Z., Xia, H., and Goicolea, J. M. 2016. "Bridge damage identification from moving load induced deflection based on wavelet transform and Lipschitz exponent." *International Journal of Structures and Dynamics* 16(5): 91-105.
- Yu, Y., Wang, C., Gu, X., and Li, J. 2019. "A novel deep learning-based method for damage identification of smart building structures." *Structural Health Monitoring* 18(1): 143-163.
- Yun, G. J., Lee, S. G., Carletta, J., and Nagayama, T. 2011. "Decentralized damage identification using wavelet signal analysis embedded on wireless smart sensors." *Engineering Structures* 33(7): 2162-2172.

APPENDIX A. TABLE OF MAXIMUM DEFLECTION

Table A1. Maximum deflection and elastic line of the investigated beams.

Case	Beam	Load Type	Max Deflection
	Simply Supported	Concentrated	$y = \frac{Pl^3}{48EI}$
		Distributed	$y = \frac{5Pl^4}{384EI}$
	Cantilever	Concentrated	$y = \frac{Pl^3}{3EI}$
		Distributed	$y = \frac{Pl^4}{8EI}$
	Double-Clamped	Concentrated	$y = \frac{Pl^3}{192EI}$
		Distributed	$y = \frac{Pl^4}{384EI}$

* illustrations are an adaptation from Schiel (1976).

APPENDIX B. PUBLISHED PAPERS

The cited papers were produced during the conduction of this research.

Under Review:

Engineering Structures Journal – submitted on 22/09/2023.

Title: Wavelet-based analysis applied to damage localization and quantification in beams using static deflections and mode shapes

Authors: José L. C. R Vila, Eng.; Jhon N. V. Goulart, Ph.D; Sergio H. S Carneiro, Ph.D; Carla T. M Anflor, Ph.D; Ariosto B. Jorge, Ph.D

Published on:

Proceedings of the XIX International Symposium on Dynamic Problems of Mechanics – DINAME 2023

Title: Sensitivity Analysis of Discrete Wavelet (DWT) Based Damage Localization on a Beam-Like Structure

Authors: José Leandro Cardoso Rivera Vila, Jhon Nero Vaz Goulart, Sergio Henrique Carneiro da Silva, Ariosto Bretanha Jorge.

Published on:

Book: On Error Estimators and Bayesian Approaches in Computational Model Validation – 2022 – 1st Edition.

Chapter participation: Chapter 19, On Error Estimators and Bayesian Approaches in Computational Model Validation, pp. 640-673.

Authors: Ariosto B. Jorge*, Sergio H. S. Carneiro, Jhon N. V. Goulart, Marcus V. G. Morais, Guilherme F. Gomes, Carla T. M. Anflor, Jalusa M. S. Ferrari, and José L. C. R. Vila.